A PARAMETRIC STUDY OF FAR-SIDE RESTRAINT MECHANICS

Richard Kent, Jason Forman, David Lessley
Center for Applied Biomechanics, University of Virginia
USA
Kristy Arbogast
Children's Hospital of Philadelphia
USA
Kazuo Higuchi
Takata
Japan
Paper Number 13-0381

ABSTRACT

The goal of this study was to quantify the belt-torso interaction and whole-body kinematics in far-side lateral impacts and how they depend on shoulder-belt geometry, arm position, and belt pre-tensioning. A series of repeated 90-deg far-side impacts on three post-mortem human subjects was performed. A 3-d motion capture system measured skeletal kinematics. Arm position (Down, Slightly Up, Fully Up), D-ring location (Forward, Back, Intermediate), pre-tensioning (Yes, No), and impact severity (8g, 18g) were varied. Maximum lateral head excursion was found to be slightly sensitive to arm position and highly sensitive to D-ring location, pre-tensioning, and impact severity. An interaction between D-ring location and pre-tensioning was found, with the maximum pre-tensioning effect occurring at the Intermediate D-ring position. Limitations of this study include the use of repeated impacts and consideration of a single impact angle. 60-degree far-side oblique impacts are underway to assess the robustness of the conclusions drawn here.

INTRODUCTION

A primary driver of contemporary seatbelt biomechanics research is the challenge of minimizing head excursion and the risk of a head contact with the vehicle interior, while simultaneously limiting belt impingement on the torso and concomitant belt-induced injuries. Many studies have evaluated this tradeoff in frontal impacts, but the topic has not been explored as much in other impact configurations. This tradeoff is particularly important in the far-side impact environment: head strikes are a key injury mechanism (e.g., Gabler et al. 2005) and belt characteristics such as pre-tensioning, D-ring position, and a second shoulder belt (e.g., Rouhana et al. 2006, Bostrom et al. 2008) can have a pronounced influence on head excursion. Several far-side safety countermeasures have been proposed in recent years to address this injury mechanism, including in-board, seat-mounted airbags and deployment of far-side curtain airbags. The literature is lacking, however, a detailed description of the conditions influencing the ability of the standard 3-point seatbelt to restrain a human occupant in a far-side impact exposure. Horsch (1980) evaluated the dynamics of a belted anthromporphic test device (ATD or crash test dummy) in collisions ranging from full frontal to full lateral, but no existing ATD is designed to replicate either the complex ispilateral shoulder mechanics relevent to this situation or the oblique belt loading present on the contralateral lower torso. Efforts to create such an ATD are underway (e.g., the latest generation of the shoulder described by Törnvall 2008 is in evaluation testing now and the THOR dummy is nearing finalization), but post-mortem human subjects (PMHS) remain the most biofidelic model for studying these issues.

METHODS

A series of repeated 90-deg far-side sled impacts was performed using three male post-mortem human subjects (Table 1). The subjects were acquired and prepared in accordance with the UVA Center for Applied Biomechanics Oversight Committee. The subjects were preserved by freezing and confirmed free of infectious diseases including HIV and Hepatitis B and C.

Subject kinematic data were measured using a 1000-Hz Vicon MX™ three-dimensional (3-d) camera-based motion capture system, which tracked the motion of retroreflective spherical markers through a calibrated 3D space within the cameras' collective field of view. The sled test fixture was designed to approximate a vehicle-based restraint environment while providing repeatable and reproducible test conditions and lines of sight for motion capture. The

design objectives of the test fixture included reducing test-to-test variability and increasing measurement capability through the use of simplified boundary conditions. For example, the subjects were positioned on a rigid planar seat with their torsos and heads supported by an adjustable set of plates to approximate a vehicle occupant's seated posture (i.e., the interaction with the seat was unlike that in an actual vehicle) (Figure 1).

Table 1.
Post-Mortem Test Subjects

PMHS	Age	Stature	Weight	Cause of Death	Bone Quality*
551	67	173 cm	83 kg	Stroke	-0.6 (normal)
557	67	175 cm	91 kg	Pulmonary fibrosis	1.5 (above average)
559	60	170 cm	73 kg	Cardiac arrest (NFS)	-1.0 (borderline osteopenia)

*DXA t-score, Total right femur

Restraint was provided by a 3-point shoulder and lap belt with lap-belt anchor positions approximating those in a typical mid-size sedan and a D-ring mount location representing the range present in the field. Four-marker clusters were secured to selected bones and rigid body mechanics was applied to determine the bone's 6-degree-of-freedom motion using a coordinate transformation. This test fixture and kinematic measurement method have been described in detail by Shaw et al. (2010) and Lessley et al. (2011).

Variations in arm position [Down (D), Slightly Up (SU), Fully Up (FU)], D-ring location [Forward (F), Back (B), Intermediate (I)] (Figure 2), pretensioning (PT) (Yes, No), and impact severity (8 g, 18 g) were studied. Every reasonable attempt was made to hold all other parameters constant across tests (e.g., initial position, impact conditions, restraint geometry). The arm position was based on the forward flexion angle of the humerus, with the Fully Up position representing the arms in a steering position. The two impact severities were chosen based on the field analysis reported by Gabler et al. (2005). The low-severity sled pulse, which had a total velocity change (ΔV) of 16 km/h, was based on the median severity of far-side tow-away crashes. The high-severity pulse, which had a ΔV of 34 km/h, was based on the median severity of far-side field crashes in which MAIS 3+ injuries occurred (Figure 3). Repeated low-severity impacts were performed on each subject prior to a single, final high-severity impact. The ribs, spine, and near-side shoulder were palpated for the presence of injury following each impact. The final test matrix included 15 sled tests (Table 2).

Table 2.
Sled Test Matrix

Test	PMHS	Impact Severity	PT	Arm	D-ring
S0077	557	Low	N	SU	B
S0078	557	Low	N	D	B
S0079	557	Low	Y	D	B
S0080	557	Low	Y	SU	B
S0081	557	High	N	D	B
S0082	551	Low	Y	FU	F
S0083	551	Low	Y	D	F
S0084	551	Low	N	FU	F
S0085	551	Low	N	D	F
S0086	551	High	N	D	F
S0087	559	Low	N	D	F
S0088	559	Low	Y	D	F
S0089	559	Low	N	D	I
S0090	559	Low	Y	D	I
S0091	559	High	Y	D	I

Full-body computed tomography (CT) scans were taken of each subject prior to testing to confirm the absence of bony trauma. Dual-energy X-ray absorptiometry (DXA) assessed bone quality. After completion of the entire test battery, another full-body CT scan was taken and a detailed necropsy was performed to document the trauma sustained during the test series.

Instrumentation included tension gages on the shoulder belt near the D-ring and bilaterally near the lap belt mounts. The motion capture marker arrays were mounted to the skull, pelvis, first thoracic vertebra (T1), and both scapulae. Individual markers were adhered to the external surface of the subject from the mid-thoracic spine to the sacro-lumbar and at selected locations on the buck and along the belt webbing. Frontal, overhead, and oblique high-speed video cameras documented the tests at 1000 Hz.

The effects of the variations in test conditions were quantified by comparing sets of tests. For example, the effects of pre-tensioning were observed by comparing tests S0083 and S0085, and the interaction between D-ring position and pre-tensioning were observed by comparing tests S0087-S0090. Selected effects are reported in this paper, with a particular focus on belt loading, head excursion, and whole-body kinematics. The comparisons employ primarily the frontal video view, the tension gages, and reconstructions of the motion of bony structures using the motion capture data.

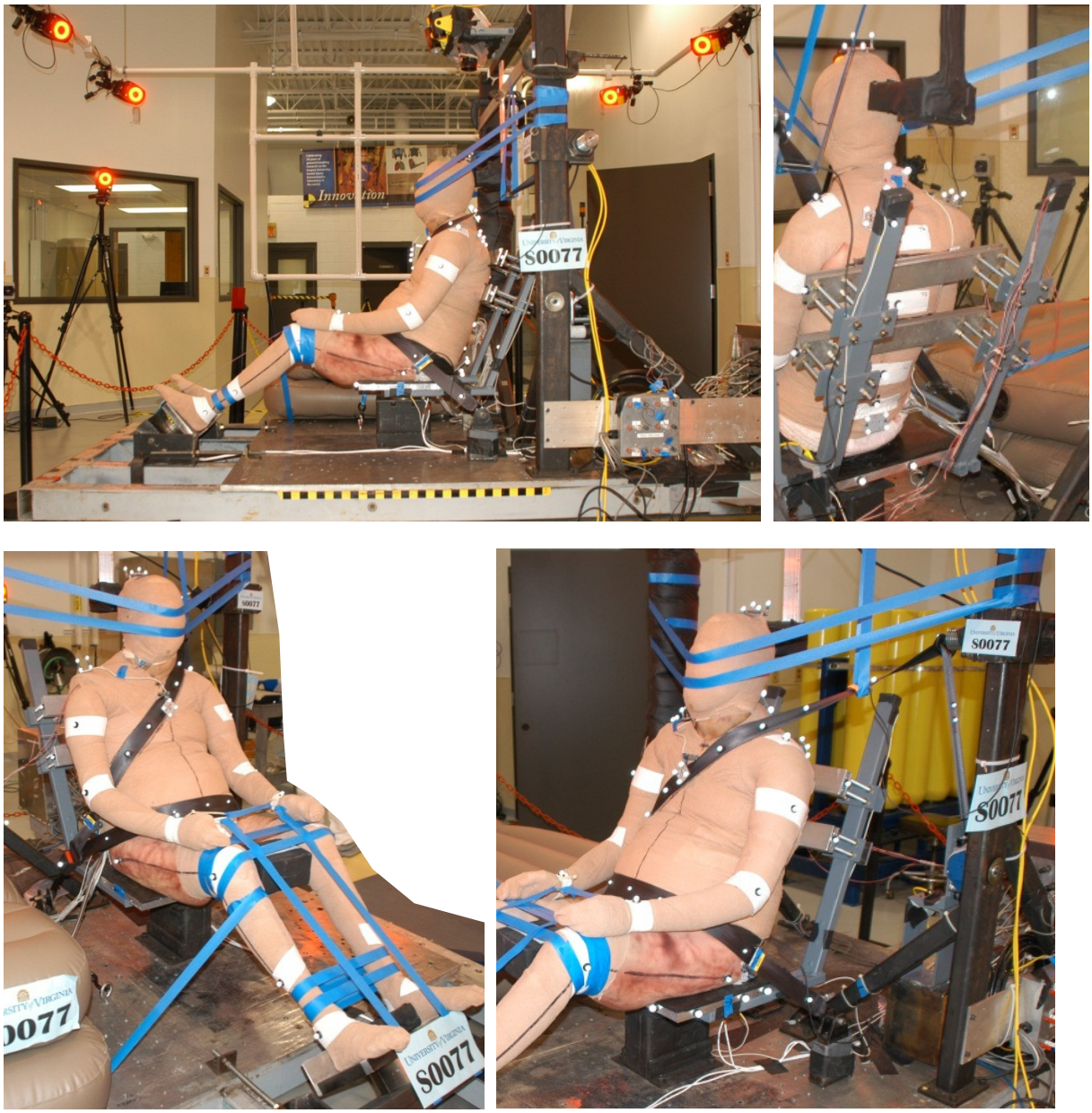

Figure 1. Photographs of the sled test fixture and an occupant positioned for testing. Masking tape used for positioning was partially severed immediately prior to test initiation. Sled motion simulated a far-side impact with the occupant moving right relative to the sled (away from the d-ring). These images depict the "Slight Up" arm position and the "Back" D-ring position.

The frontal video was mounted off-board, so the occupant's motion relative to the buck is not necessarily reflected in the occupant's position within the video frame. There was a vertical frame member on the buck that can be used as a qualitative reference point for excursion in these video views. The horizontal aluminum bars composing the seatback can also be used for this purpose as an occupant's initial positioning on the sled was reproduced in all tests. In the reconstructions of the bony motion, computed tomography (CT) images of the test subjects were used to illustrate the rigid body motion of the head, shoulder girdle, sternum, and pelvis relative to the buck.

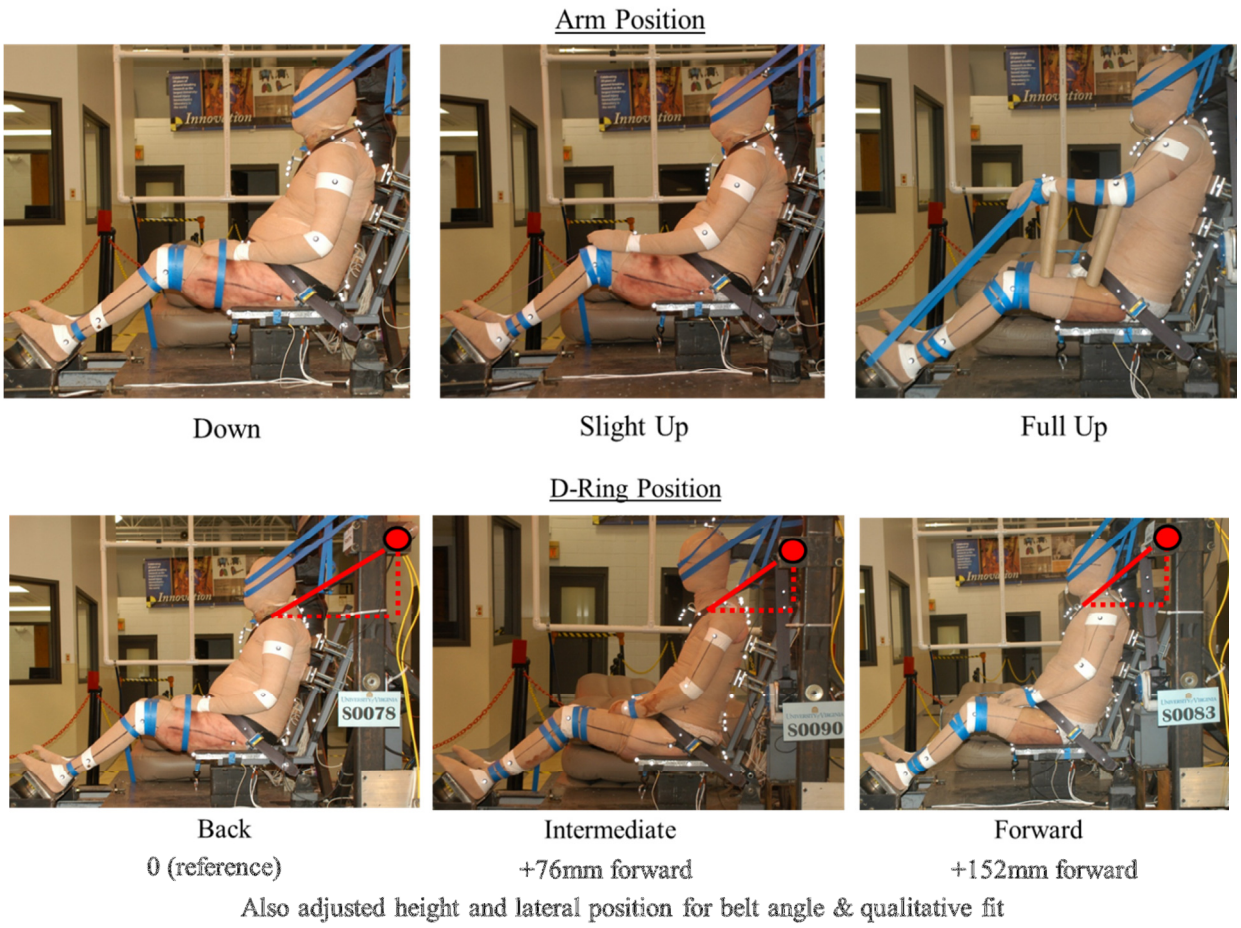

Figure 2. Photographs depicting variation in arm and D-ring position.

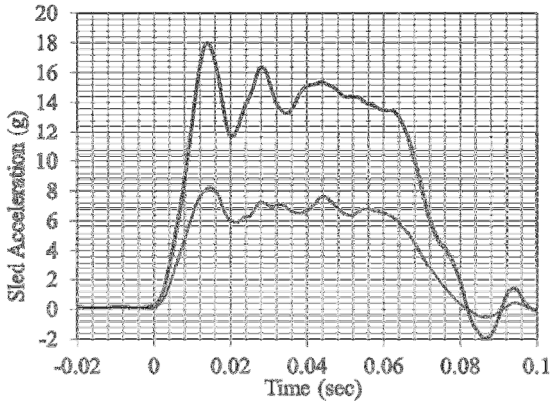

Figure 3. Lateral sled acceleration in low-severity and high-severity tests.

RESULTS

Arm Position

Arm position had the least influence of the parameters studied. Comparison of tests S0084 and S0085, for example, revealed a decrease of only 5.8 mm in the peak lateral excursion of the left acromio-clavicular (AC) joint when the are was Fully Up, which translated into a decrease of only 6.1 mm in peak lateral head excursion. In contrast, pre-tensioning and the fore-aft location of the D-ring substantially affected occupant kinematics, as described in detail below.

Influence of Pre-tensioning

Comparison of S0077 with S0080 shows the influence of pre-tensioning with the D-ring in the back position. The frontal video view illustrates the decreased shoulder motion with the pre-tensioned system and the resulting reduction in lateral head excursion relative to the buck (Figure 4). Reconstruction of the bony motion shows the pronounced reduction in lateral motion of the head, shoulder girdle, and pelvis relative to the buck (Figure 5). The peak values of lateral excursion relative to the buck of the centers-of-gravity of the head, T1, sternum and pelvis, and of the acromio-

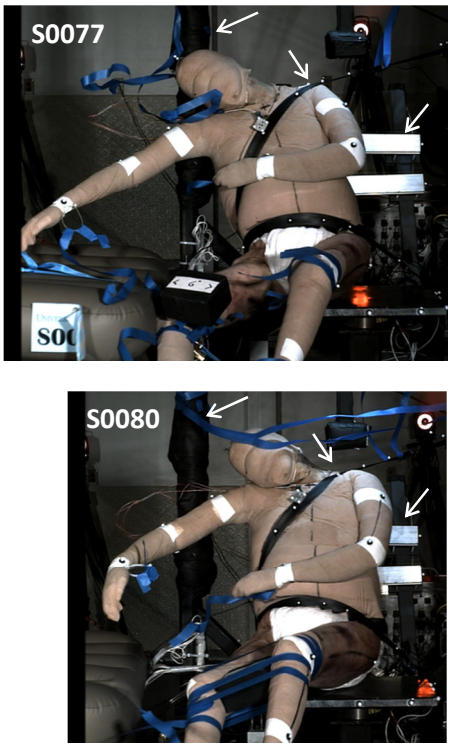

Figure 4. Frontal video views illustrating shoulder retention and head excursion without (S0077, top) and with (S0080, bottom) a pre-tensioner. Arrows point to a vertical rail on the sled and the aluminum bars on the seatback (which provide reference for the excursion) and the shoulder movement relative to the webbing.

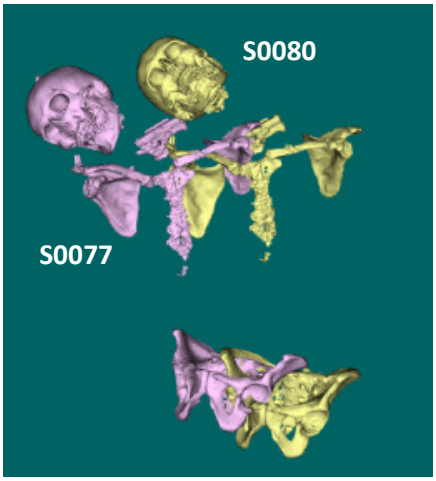

Figure 5. Anterior view of CT reconstructions of the head, shoulder, sternum, and pelvic positions and orientations at the time of peak head excursion relative to the buck. Yellow images are subject 557 in test S0080 (with PT). Purple images are the same subject in test S0077 (no PT).

clavicular joints, are reported in Table 3. The peak lateral excursion of the head was 151.2 mm less in test S0080 than in test S0077, of T1 was 150.1 mm less, of the left AC joint was 147.7 mm less, of the right AC joint was 148.9 mm less, and of the pelvis was 60.4 mm less (Table 3).

The influence of pre-tensioning is apparent in the shoulder-belt tension. Even though the tests were purely lateral, over 2 kN of tension was generated in the shoulder belt and the pre-tensioner reduced the system response time by approximately 40 ms (Figure 6). The peak belt tension was similar with and without pre-tensioning.

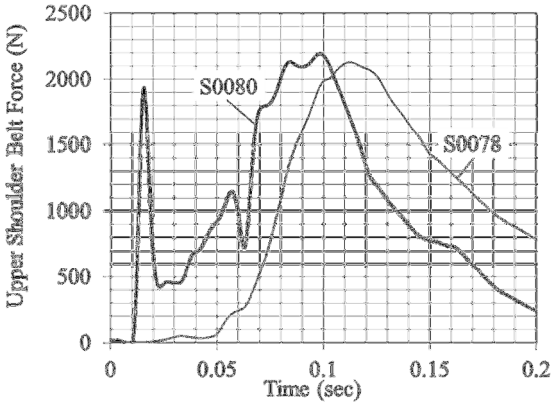

Figure 6. Tension in the shoulder belt in test S0080 (with PT) and test S0077 (no PT).

Influence of D-ring Position

Restraint mechanics were less sensitive to D-ring position than they were to pre-tensioning (Figure 7). Comparison of S0087 with S0089 shows the influence of moving the D-ring 76 mm anteriorly in the absence of pre-tensioning. The peak lateral excursion of the head was 57.4 mm less in test S0089 (Intermediate D-ring position) than in test S0087 (Forward D-ring position), of T1 was 53.0 mm less, of the left AC joint was 67.0 mm less, of the right AC joint was 27.3 mm less, and of the pelvis was 28.2 mm less (Table 3). Comparison of S0088 with S0090 shows the influence of moving the D-ring 76 mm anteriorly with pre-tensioning. The peak lateral excursion of the head was 43.3 mm less in test S0090 (Intermediate D-ring position) than in test S0088 (Forward D-ring position), of T1 was 13.5 mm less, of the left AC joint was 14.4 mm less, of the right AC joint was 10.5 mm less, and of the pelvis was 53.2 mm less (Table 3).

Table 3.
Peak Lateral Excursion*

Test	Head	T1	Pelvis	AC joint (L)	AC joint (R)
S0077	454.4 195	317.4 145	193.0 139	316.7 173	312.1 145
S0078	418.5 179	279.8 140	181.6 138	287.5 146	273.3 138
S0079	302.9 152	179.3 115	152.0 100	180.6 115	175.8 115
S0080	303.2 147	167.3 115	132.6 104	169.0 121	163.2 110
S0081	571.2 126	413.0 110	313.2 115	437.6 120	412.1 115
S0082	251.5 126	160.2 111	146.5 110	146.6 111	160.5 108
S0083	235.8 127	136.5 111	145.8 111	138.5 111	135.9 96
S0084	379.3 173	265.2 140	186.2 133	258.2 169	266.7 131
S0085	373.2 174	240.2 129	160.9 114	264.0 179	238.1 128
S0086	632.8 147	466.8 138	287.1 100	528.6 150	432.1 118
S0087	503.2 268	346.4 284	174.4 132	391.5 284	317.8 284
S0088	264.7 158	143.7 113	120.1 107	141.2 190	144.5 110
S0089	445.9 222	293.4 271	202.6 143	324.5 271	290.5 142
S0090	221.4 143	130.2 112	173.3 115	126.8 101	134.0 104
S0091	494.8 130	325.4 115	287.9 106	342.4 133	336.4 113

*Top number is the peak lateral excursion in mm. Bottom number is the time of peak lateral excursion in ms.

Pre-tensioning and D-ring position

Peak excursion was more influenced by pre-tensioning than by D-ring position, but there were interactions between the two parameters. As shown in Figure 8, the reduction in head excursion associated with pre-tensioning was substantial regardless of D-ring position, but it was more pronouned in the Intermediate D-ring position (50.3%) than in either the Forward (39.3%) or Back (30.5%) positions.

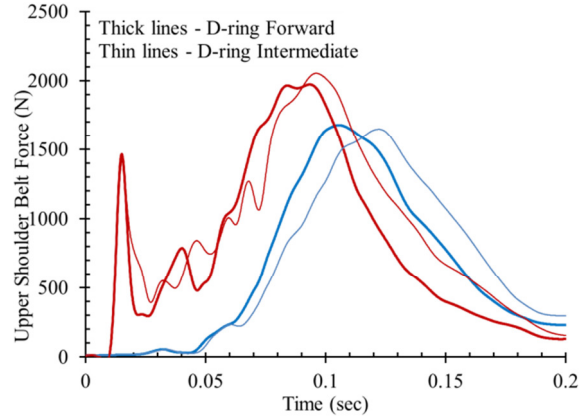

Figure 7. Tension in the shoulder belt in tests S0087 through S0090 illustrating the role of pre-tensioning (red vs. blue lines) and D-ring position (thick vs. thin lines).

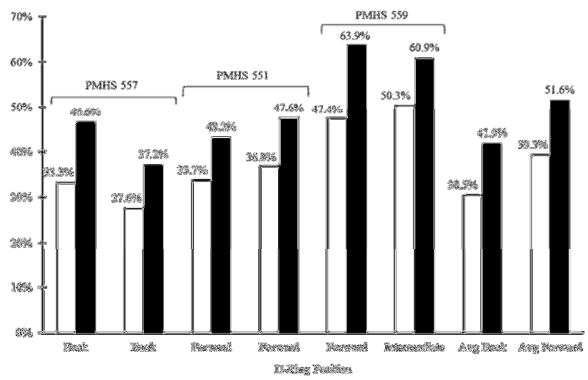

Figure 8. Reduction in peak lateral excursion when a pre-tensioner was used (low-severity tests). White bars are the head. Black bars are the left AC joint.

Comparision of peaks does not fully elucidate these interactions, however, as there is a pronounced difference in the timing of those peaks. It is informative to compare whole-body positions at concurrent time points, as shown in Figure 9. The test with the pre-tensioned belt mounted at the Intermediate D-ring position generated substantially more restraint through the left shoulder as compared to the other test conditions. This resulted in less right-lateral rotation of the torso in addition to the overall reduction in peak head excursion. Furthermore, this peak excursion was attained earlier (143 ms in S0090 vs. 158 ms in S0088, 222 ms in S0089, and 268 ms in S0087).

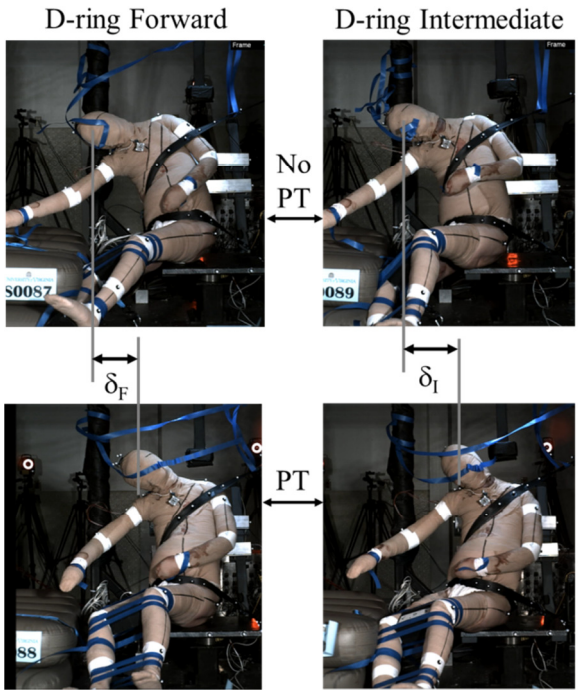

Figure 9. Video frames from tests S0087 through S0090 at peak head excursion illustrating the interaction between D-ring position and pre-tensioning. Note that the effect of pre-tensioning is more pronounced with the Intermediate D-ring position than with the Forward position ($\delta_I > \delta_F$).

High-Severity Impacts and Injury Outcome

The PMHS exhibited distinct patterns of trauma. Subject 559, whose high-severity test involved a pre-tensioned belt with the Intermediate D-ring position, sustained a sternal fracture and 24 fractures on 14 ribs, including a left posterior fracture on rib 11. There was a concentration of fractures in the right lower aspect in the region of heavy shoulder belt loading. Blood was also found in this subject's peritoneal cavity, though no acute laceration was identified. Finally, a fracture of the anterior vertebral body of T9/10 was found in this subject.

Subject 551, whose high-severity test involved no pre-tensioner and the Forward D-ring position, sustained 3 rib fractures, all on the left side and two of which were posterior on ribs 11 and 12. This subject also sustained AIS 2 soft tissue injuries with a facet dislocation on the left aspect of the cervical spine at the level of C6/7. The anterior longitudinal ligament was completely ruptured and soft tissue disruption was identified in the posterior longitudinal ligament, the facet joint capsule, the ligamentum flavum, the interspinous ligament, and the intervertebral disc, which was separated from the vertebra on the left side. Note that all of this trauma was on the left aspect, which was the side put into tension by the restraining forces pulling left on the torso and pelvis and the head's inertia placing the cervical spine into right lateral bending.

Subject 557, whose high-severity impact involved no pre-tensioning and the Back D-ring position, sustained 26 rib fractures, including 4 posterior fractures on the left ribs 7-10. Again, these fractures were concentrated in the lower right quadrant.

DISCUSSION

This study is the first report of PMHS tested in a parametric manner exploring the influence of arm position, D-ring position, and pre-tensioning on restraint mechanics in a far-side 90° exposure. In addition to quantifying the motion of several bony structures, this study reports three key findings.

First, as illustrated in the upper-left image of Figure 9, a 3-point harness applies substantial restraining force to an occupant in a far-side impact, even when the D-ring is in a forward position and there is no pre-tensioning. This restraining force and the resulting kinematics are influenced weakly by the position of the humerus and more strongly by the anterior-posterior position of the D-ring and by the presence of pre-tensioning.

Second, there is an interaction between the position of the D-ring and the effectiveness of the pre-tensioner. In these tests, the Back D-ring position facilitated the development of relatively large restraining force within the shoulder belt regardless of the presence of a pre-tensioner, which reduced the role of pre-tensioning relative to the Intermediate D-ring position. Conversely, with the Forward D-ring position, the shoulder belt was less able to engage the shoulder regardless of the presence of a pre-tensioner. With the Forward D-ring position, the pre-tensioning did not engage the shoulder since the belt angle was such that during pre-tensioning the webbing just translated along a path essentially tangent to the clavicle. In order for belt webbing to generate force normal to its path, it must undergo a change in angle. If the D-ring is positioned such that the webbing changes angle as it passes over the shoulder, then pre-tensioning will apply restraining force to the shoulder. If the D-ring is too far forward for that angle change to occur, then the role of pre-tensioning is limited to pre-loading the lower, contralateral aspect of the torso and the effectiveness of the pre-tensioner as a mitigator of head excursion, while still present, is reduced.

Finally, this study identified a tradeoff between thoracic engagement, head excursion, and injury to the cervical spine. A comparison of the magnitude of injury generated in these PMHS is confounded by the differences in bone quality across subjects, but some general observations can be made. When torso engagement is maximized, there is an increased risk of thoracic injury but a decrease in head excursion. The rib cage is more easily injured by lower, oblique loading than by frontal loading to the superior ribs or loading to the shoulder. While shoulder engagement is an important aspect of restraint in these impacts, a substantial portion of restraining force passes through the lower portion of the contralateral rib cage (Figure 10). Future research should include detailed studies of how the geometry and force-generating characteristics (pre-tensioners, load-limiters, etc.) of a belt system influence the apportionment of loading through the ispilateral shoulder (a strong anatomical load path) and the contralateral torso (less strong), and how that apportionment influences head trajectory. Furthermore, this study showed that effective restraint engagement of the torso can generate lateral bending of the cervical spine sufficient to generate injury from head inertia. These tradeoffs reflect the complex interactions among belt geometry and structural mechanics, whole-body kinematics, and injury mechanisms in far-side crash loading. These interactions are at least as complex as they are in frontal crashes, and significant research will be required to understand them fully. For example, the left posterior rib fractures generated in these tests are unlike the fracture patterns generated in frontal sled tests of restrained cadavers and their mechanism, while unknown, is probably related to the complex rib cage deformations generated by the belt heavily loading the lower-right torso.

The key limitation of this study for application to the in-vehicle environment is the use of simplified boundary conditions. The load paths generated by interaction with the seat pan, seat back, and center console in a vehicle are either understated or ignored completely in this test configuration. The findings should be evaluated in that light.

Subject 557 (26 rib fx) Subject 551 (3 rib fx, c-spine) Subject 559 (24 rib fx, t-spine)

Figure 10. Video frames from tests S0081, S0086, and S0091 (the high-severity tests) at peak head excursion illustrating the interaction between restraint mechanics, whole-body kinematics, and injury mechanisms. Note that the increased torso engagement on subjects 557 (Back D-ring position) and 559 (Pre-tensioned belt) reduced head excursion relative to subject 551 (Forward D-ring, no Pre-tensioner), but was also associated with increased trauma to the torso. Subject 551 sustained less torso trauma, but the reduced torso engagement allowed greater head excursion and the subject sustained cervical spine trauma on the tension side of the neck during lateral bending as the neck arrested the lateral motion of the head.

CONCLUSIONS

This study documented whole-body kinematics and restraint mechanics in a far-side collision. Detailed skeletal measurements and a parametric study design allowed for a detailed assessment of the roles of fore/aft D-ring position, arm position, pre-tensioning, and impact speed. An interaction between D-ring position and pre-tensioning was identified, with the effect of pre-tensioning being greatest at the Intermediate D-ring position. Injury tradeoffs were also identified.

REFERENCES

Bostrom, O., Gabler, H., Digges, K., Fildes, B., Sunnevang, C. (2008) Injury reduction opportunities of far side impact countermeasures. Ann Adv Automot Med 52:289-300.

Gabler, H. C., Fitzharris, M., Scully, J., Fildes, B. N., Digges, K., Sparke, L., (2005). Far side impact injury risk for belted occupants in Australia and the United States. Proceedings of the International Technical Conference on the Enhaced Safety of Vehicles, Paper No.05-0420.

Horsch, J. (1980) Occupant dynamics as a function of impact angle and belt restraint. Paper 801310, Society of Automotive Engineers, Warrendale, PA.

Lessley, D., Shaw, G., Riley, P., Forman, J., Crandall, J. (2011) Assessment and validation of a methodology for measuring anatomical kinematics of restrained occupants during motor vehicle collisions. J Biosens Bioelectron S1:002. doi: 10.4172/2155-6210.S1-002.

Rouhana, S., et al. (2006) Biomechanics of 4-point seat belt systems in farside impacts. Stapp Car Crash J. Vol. 50.

Shaw, G. et al. (2009) Impact response of restrained PMHS in frontal sled tests: Skeletal deformation patterns under seat belt loading. Stapp Car Crash J 53:1-48.

Törnvall, F. (2008) Development of a new shoulder for the THOR dummy intended for oblique collisions. Doctoral thesis, Chalmers University, Göteborg, Sweden.

EFFECT OF INCLUDING A FETUS IN THE UTERUS OF PREGNANT WOMEN OCCUPANT MODEL IN CRASH TEST SIMULATIONS

B Serpil Acar
Moustafa Meric
Memis Acar
Loughborough University
United Kingdom
Paper No: 13-0445

ABSTRACT

Motor vehicle accidents are the largest single cause of accidental death and the leading cause of traumatic injuries for the pregnant occupant and her fetus. Computational pregnant occupant modelling has a role to play in the investigation of the risk of fetal injuries and mortality in crash test simulations. Effective investigation depends on realistic representation of pregnant occupant and her fetus in a virtual environment. However, known pregnant occupant models normally do not include a fetus in the uterus. 'Expecting', the first computational model of a pregnant occupant with a fetus, is used in the current research. The model has a detailed multi-body representation of the fetus as well as a finite element uterus and placenta.

In this paper, the effect of including the fetus in the uterus of the pregnant occupant model is investigated using 'Expecting' in crash test simulations. Previously, drop test simulations with and without a fetus showed that, the presence of fetus in the uterus suggests higher risks to the fetus. Using the pregnant occupant model, 'Expecting', with and without a fetus, provides more realistic simulations to explore the role of including a fetus in the uterus. Five frontal impact speeds, 15, 20, 25 30 and 35 kph with varying levels of restraint system including 'seatbelt and airbag' (ie fully restrained), 'seatbelt only', 'airbag only' and 'no restraint' are used in the simulations. Maximum strains developed in the uteroplacental interface with and without a fetus are compared. The effect of including a fetus in the pregnant occupant model is discussed.

INTRODUCTION

The separation of the placenta from the wall of the uterus due to vehicle accidents is the leading cause of fetal death accounting for 50-70 % of all losses (Pearlman et al., 1990). Pregnant occupant should always wear the three-point safety seatbelt correctly in order to minimize any potential trauma from a car accident. This is a legal requirement in many countries. However, discomfort and the false belief that the seatbelt may put the fetus in danger in case of a crash, lead some pregnant occupants not to wear the seatbelt. This, of course, could cause a serious safety problem for pregnant women and her unborn baby.

Computational modelling and crash test simulations offer an alternative but effective solution to anthropomorphic test devices (ADTs) to investigate occupant safety in motor vehicles. Realistic modelling and simulation of pregnant women in crash tests play a significant role in the investigation of potential injuries to the pregnant occupant and her fetus in vehicle accidents, as realistic pregnant ADTs are not commonly available. The first computational pregnant occupant model with a fetus, 'Expecting', which has a detailed multi-body representation of the fetus as well as finite element uterus and placenta, was developed at Loughborough University.

Previous computational pregnant occupant models were designed without fetus. The decision not to include a fetus in the pregnant occupant model was based on the findings of (Rupp et al. 2001), which concluded that the inclusion of a fetus in the uterus did not make a significant difference. Their research, which included vertical drop simulations of fetus and uterus model onto a rigid flat surface at different angles of orientation, is repeated with the uterus of 'Expecting', the pregnant occupant model, with and without a fetus by Acar et al. (2012). The drop test simulation results showed that the existence of a fetus in the uterus has a significant effect on the strain levels in the uteroplacental interface (UPI), with the exception of 90-degree orientation, where the difference was small.

This study, further investigates the implications of including a fetus in the uterus with the whole 'Expecting' model in crash test simulations. A number of simulations with and without fetus is conducted including 'full restraint', 'airbag only', 'seatbelt only' and 'no restraint' at different crash speeds. The effect of the inclusion of the fetus in the model on the strains generated at the uteroplacental interface is discussed.

METHODOLOGY

The research strategy adopted in this study is to use the current 'Expecting' pregnant occupant model in order to represent a realistic pregnant occupant model, which has a fetus in the uterus. Then, a version of the 'Expecting' model without a fetus, where the uterus is filled with amniotic fluid only, is developed. Both with a fetus in the uterus and its without-fetus version are used to investigate the contribution of the inclusion of a fetus on the strains generated at the uteroplacental interface, in a number of crash test simulations.

'Expecting' is a 5th percentile female in her 38th week of pregnancy. A detailed multi-body representation of a 3.3 kg fetus consisting of 15 rigid bodies and respective joints within a finite element uterus model is integrated into the computational pregnant woman model, which is generated by modifying an existing small female model using the anthropometric pregnant women data. The model was generated in the multi-body/finite element software package MADYMO of TNO Automotive. The development and validation phases of Expecting can be found in Acar and Lopik, (2006). Expecting is illustrated in Figure 1.

In the 'Expecting' witout-fetus model, the entire uterus is filled with the amniotic fluid, which is 98-99% water and hence can be considered as incompressible. In the with-fetus model, the 38 weeks old fetus almost fills the entire volume of the uterus leaving minimal space for the amniotic fluid. The material properties of the uterus, placenta, fat tissue and amniotic fluid, as used by the previous researchers, are given in Table 1.

Table 1. Material properties used in the model

Structure	Material Model	Young's Modulus (kPa)	Density (kg/m□)	Poisson's Ratio
Uterus	Linear elastic	566	1052	0.4
Placenta		63	995	0.45
Fat		47	993	0.49
Amniotic Fluid		20	993	0.49

Simulation Set-up

'Expecting', the pregnant occupant model and its without-fetus version are used in identical crash test simulations. These include (i) 'seatbelt & airbag', representing a properly restraint pregnant driver; (ii) 'seatbelt only' excludes the airbag; (iii) 'airbag only' excludes the seatbelt, but yet the airbag is active; and finally (iv) 'no restraint' excludes all restraints, in other words neither the seat belt is worn nor the airbag is deployed. For each case, tests are run with crash speeds of 15, 20, 25, 30 and 35 kph, and the acceleration pulses applied to the model are half-sine waves with 120 ms duration as shown in Figure 2.

Injury Criteria

Maximum von Mises equivalent strain levels in uterus at placental location (utero-placental interface (UPI)) are determined for with and without fetus models to assess the possibility of placental abruption, which is the main cause of fetal and occasionally maternal fatalities. The threshold strain value for the occurrence of placental abruption is widely accepted to be 0.60 at the UPI (Rupp et al., 2001).

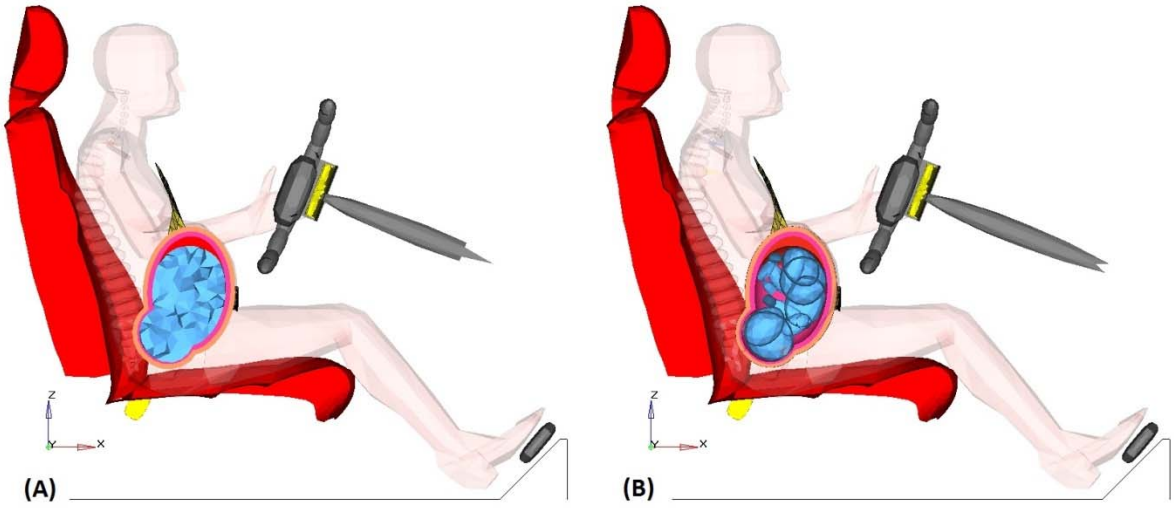

Figure 1. (A) Side view of modified 'Expecting' computational pregnant occupant model without fetus and (B)'Expecting' (with fetus)

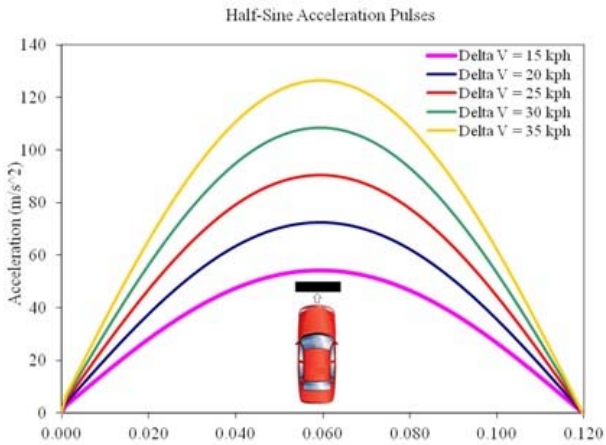

Figure 2. Half-Sine Acceleration Pulses

RESULTS AND DISCUSSIONS

Strains in the uterus at placental location are investigated to highlight the fetal injury risk. Figure 3 depicts visually a typical impact response at 30 kph for the fully restraint ('seatbelt & airbag') occupant with and without a fetus. Figure 3 (a) clearly shows the excessive deformations on the uterus due to fetus loading, whereas the without fetus case shows less severe deformations.

In general, the maximum strain levels at the utero-placental interface increase with crash speed as expected. The maximum strain in the with-fetus model is typically higher than the strains in the without-fetus model, indicating a greater risk of placental abruption.

Figure 4 compares the strain levels for the 'seatbelt & airbag' case for a crash speed range of 15-35 kph. The without-fetus model simulation results show lower strain levels than with-fetus model simulations up to the 35 kph. Figure 4 shows that maximum strains at the UPI for the with- and without-fetus models vary between 0.24 to 0.42 and 0.18 to 0.42 respectively. The increase for without fetus case is gradual and almost linear, whereas for the with fetus case, there is a greater increase in strain from 15 to 20 kph. All strain values at the UPI are considerably below the injury threshold value of 0.60.

The 'seatbelt only' case results for the maximum strains at the UPI are shown in Figure 5, which follows a similar pattern to the strains in the 'seatbelt & airbag' case, but are generally higher. At 35-kph impact, the strain level approaches the placental abruption risk threshold of 0.60 for both cases. The higher strain levels could be attributed to the pressure that the steering wheel applies to the uterus at the anterior edge of the placental location forcing the fetus downwards. However, the lap portion of the three-point seatbelt prevents the occupant moving excessively forward. The placenta is also compressed between the fetus and steering wheel in the with-fetus model and this dynamic motion generates considerably higher strains at the UPI than in the without-fetus model.

Figure 6 shows the maximum strain levels at the UPI for the 'airbag only' case which demonstrates that when the fetus is included in the model, the placental abruption risk emerges at a crash speed of 20 kph, whereas the without-fetus model shows that the placental abruption risk begins at a higher crash speed of 30 kph. Without the seatbelt, it is clear that the contribution of the fetus on the maximum strains at the UPI is much more pronounced and the placental abruption risk is found to be higher. The significant mass of the fetus (3.3 kg) plays a significant role in the behaviour of 'Expecting', the pregnant occupant model. These results clearly demonstrate that the fetus changes the entire dynamic response to impact.

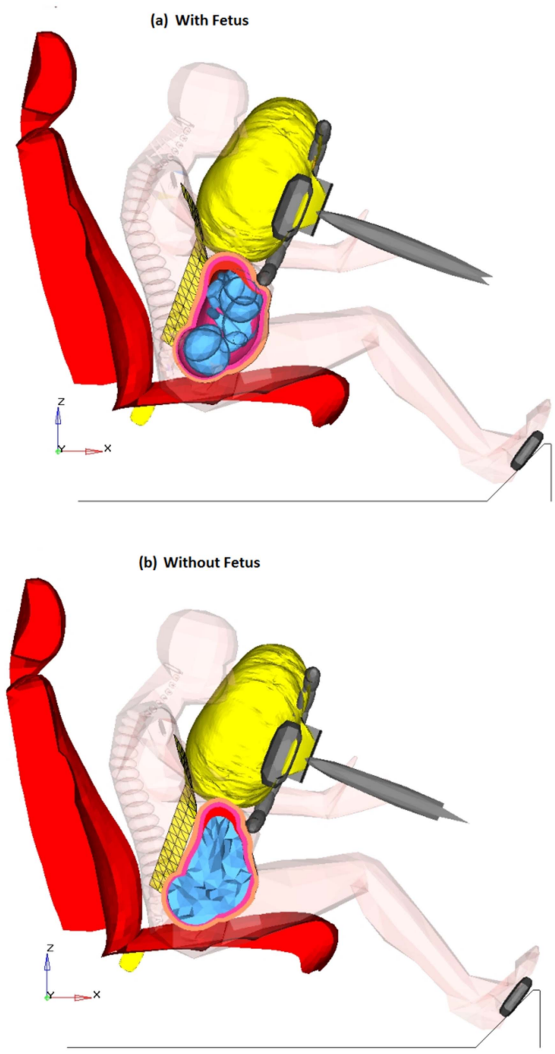

Figure 3. Typical frontal impact responses for 30 kph at 105ms of impact.

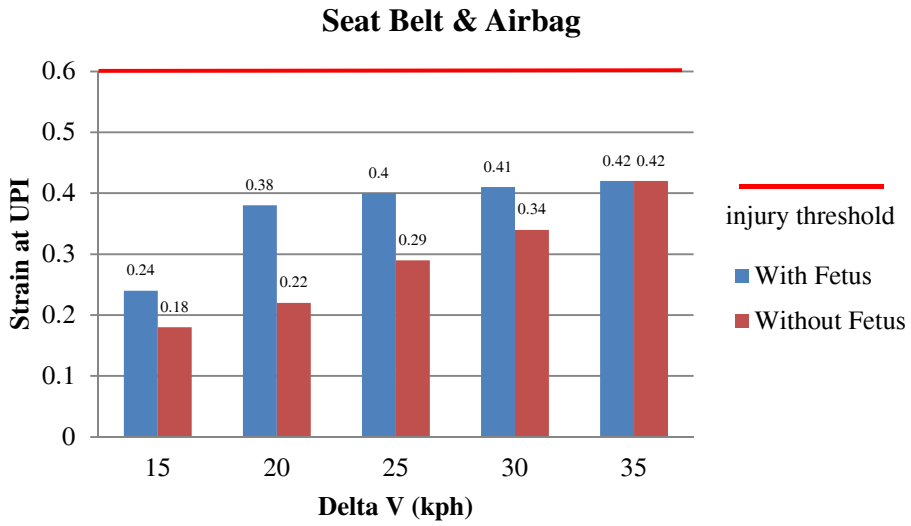

Figure 4. Maximum Von Mises strain at the UPI for the 'seatbelt & airbag' case.

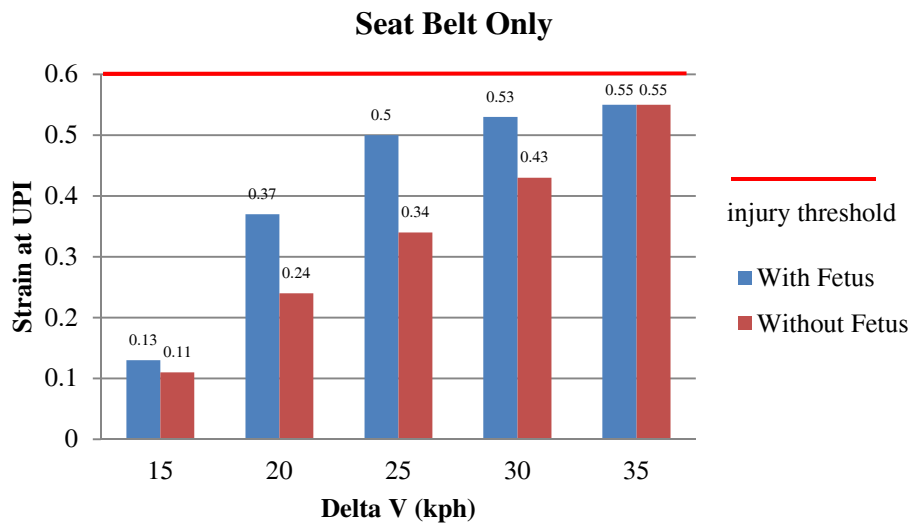

Figure 5. Maximum Von Mises strain at the UPI for the 'seatbelt only' case.

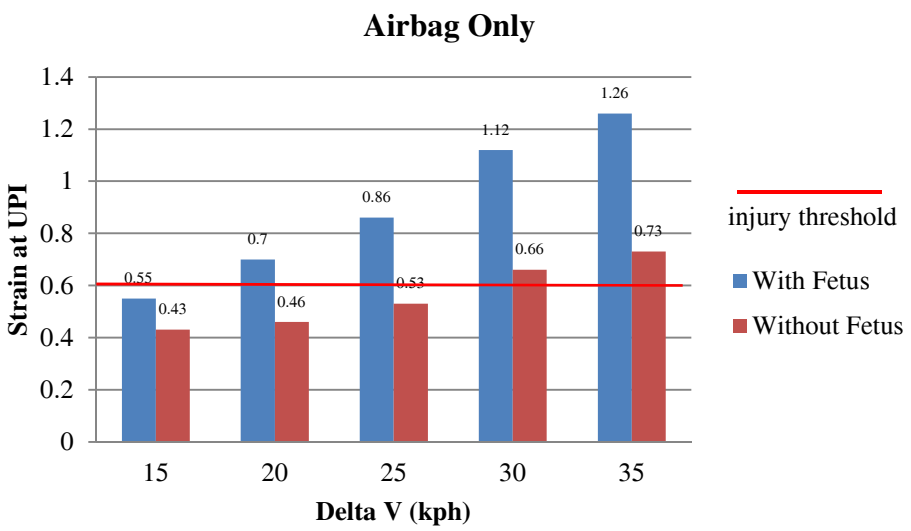

Figure 6. Maximum Von Mises strain at the UPI for the 'airbag only' case.

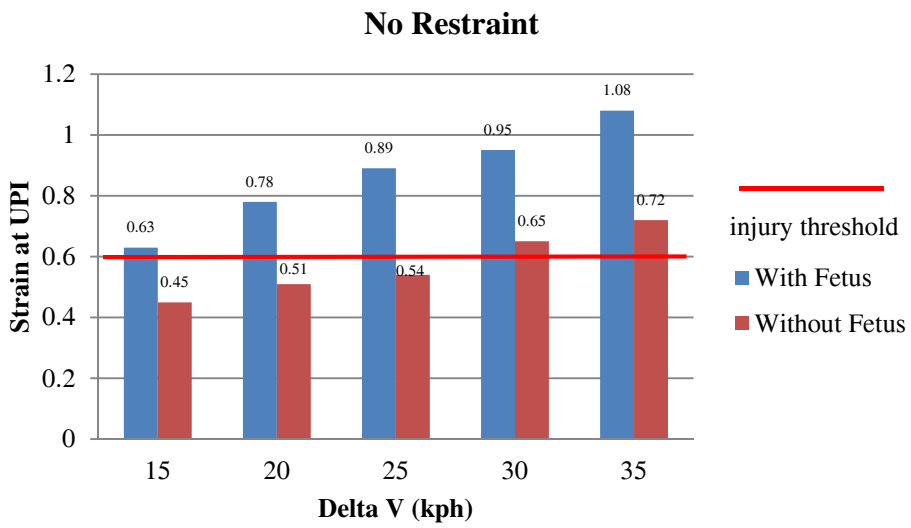

Figure 7. Maximum Von Mises strain at the UPI for the 'no-restraint' case.

For the 'no-restraint' case shown in Figure 7, the with-fetus model, shows placental abruption risk at all speeds considered (15-35 kph), whereas in the without-fetus model, strains at the UPI are below the injury threshold value of 0.60 for at 15, 20, and 25 kph.

The simulation results clearly demonstrate that the use of seatbelt in conjunction with the airbag is essential for the protection of the fetus in vehicle crashes.

CONCLUSIONS

In this research, implications of including a fetus in the uterus of 'Expecting', the pregnant occupant model, are investigated. 'Expecting' with and without fetus model is used to simulate a range of frontal impacts of increasing severity from 15 kph to 35 kph. Four cases of occupant restraint, seat belt and airbag, seat belt only, airbag only and completely unrestraint are investigated. In crash simulations, the loading from the seatbelt, steering wheel and airbag, causes strains to develop in the uterus. When the fetus model is included in the uterus, inertial loading on the uterus due to the motion of the fetus occurs too.

Crash test simulation results from the 'Expecting', the pregnant occupant model, show that the inclusion of the fetus in the model creates a more realistic representation of the pregnant occupant, which changes the dynamic response of the model in crash simulations. Inertial effects on the fetus cause it to move forwards relative to the pregnant occupant. The fetus accelerates towards the anterior wall of the uterus. Consequently, this dynamic motion of fetus generates significantly higher strains at the UPI than without fetus model. Therefore, fetus should be included in the uterus in pregnant woman models for realistic results in crash test simulations.

REFERENCES

Acar, B. S., and van Lopik, D., (2009), "Computational pregnant occupant model, 'Expecting', for crash simulations", *Proc. IMechE Part D: J. Auto Engineering*, 223, pp. 891-902.

Acar, B. S., and Weekes, A. M., (2004), "Designing for safety during pregnancy through a system for automotive engineers", *International Journal of Crashworthiness*, 9(6), pp. 625-631.

Pearlman, M.D., Tintinalli, J.E., and Lorenz, R.P. (1990) "Blunt trauma during pregnancy". *New Eng. J. Med.*, 323(23), 1609-1613.

Rupp, J. D., Schneider, L. W., Klinich, K. D., Moss, S., Zhou, J., and Pearlman, M. D. (2001), "Design, development, and testing of a new pregnant abdomen for the Hybrid III small female crash test dummy", *Report UMTRI-2001-07*, Ann Arbor, Michigan, USA.

Acar, S., Moustafa M., and Acar, M., Implications of including a fetus in the uterus of pregnant woman model, *The Proceedings of ICrash 2012,* July 18-2-. 2012, Milano, Italy

HUMAN FE MODEL TO ESTIMATE HEAD CONTACT TIME FOR PEDESTRIAN PROTECTION

Chinmoy Pal
Okabe Tomosaburo
Nissan Motor Company Ltd.
Japan
Muthanandam Muthukumar
Satheesh Narayanan
RNTBCI
India
Paper Number 13-0376

ABSTRACT

PCA based statistical analysis of NASS-PCDS (National Automotive Sampling System – Pedestrian Crash Data Study) database clearly shows that post-impact pedestrian kinematics is complex and depends on various factors, such as impact speed, height of the pedestrian, front-end profile of the striking vehicle and pedestrian posture, etc. The findings from the NASS-PCDS study were also confirmed and verified with the help of numerical simulations that were performed using two modified JAMA human FE models. An adult model (male, 175cm and 72kg) and a properly scaled child model (6 years old, 120cm and 24.5kg) were effectively utilized to investigate the post-crash kinematics in different conditions. The focus of this study is to investigate those factors that determine the post-crash pedestrian kinematics of children and small adults related to the head impact time (HIT) as specified in Euro-NCAP pedestrian protocol.

INTRODUCTION

Even though the motor vehicle occupant fatalities are decreasing in many countries, the overall percentage of pedestrian casualties is increasing compared to that of vehicle occupants. Annual fatalities, for every 1,000,000 people, are 12.3 in Australia, 15.7 in the EC, 16.4 in the US and 21.8 in Japan. The numbers in developing countries are even higher. Mizuno et al. reported their detailed investigations of pedestrian accident databases from countries including Australia, Germany, Japan and the US (1605 cases, 9463 injuries, include 3305 AIS2+) [1]. According to their reports, in one third of those cases, pedestrians were reported to have suffered injuries to their heads and/or lower extremities. Previous studies on pedestrian crash cases pointed out that the vehicle front geometry, the height and the posture of the pedestrian affect the injury mechanism [2]. Further studies [3, 4] targeting child pedestrians' injury distribution pointed out that anthropometry influences impact kinematics. This study focuses on the leading factors affecting the post-crash pedestrian head trajectory and head impact time with the help of a 6-year old (6YO) human FE model. It is modeled accurately based on anthropometric data and other biomechanical responses such as compression, bending, torsion, and shear characteristics of the spinal joints.

ACCIDENT ANALYSIS

In NASS-PCDS 'Vehicle pedestrian interaction (variable 524)', indicates the post-crash pedestrian kinematics. There are 17 codes to describe the types of interaction [4].

Table 1 PCDS data categorized in 4-types A,B,C,D.

NASS-PCDS (variable 524)	*Type A 35 cases*	*Type B 82 cases*	*Type C 138 cases*	*Type D 20 cases*
Ped. height	158cm	163cm	168cm	172cm
Impact speed (standard dev.)	20 km/h (12.2)	22 km/h (11.2)	41 km/h (19.6)	67 km/h (10.5)
FE analysis (adult& 6YO)				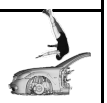

Four of those codes are picked out in accordance with frequencies of occurrences. They are categorized as four main types A-D (Table1). Based on this basic statistical information, human FE model simulations were carried out to verify the kinematics for corresponding types of impact. The range of average impact speed in these four categories matches with the initial input velocities of FE simulations. From the simulation results,

corresponding to four different (Type A-D) kinematical modes, it is observed that:

Type A differs from the other three types in the relative velocity after impact.

The Type A pedestrian is accelerated in the same direction in which the vehicle is traveling. The pedestrian's body is thrown forward in front of the vehicle.

In the other three types, Types B, C and D, the pedestrians are accelerated by the impact, up to a speed not more than the speed of the vehicle. The torso of the pedestrian travels relatively backward with respect to the front end of the vehicle.

Types A and B include children and small adults.

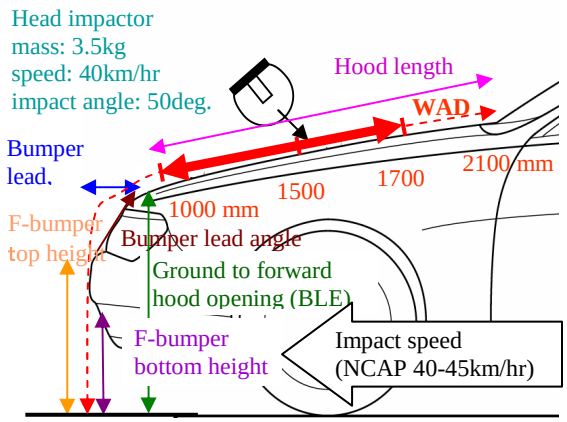

Figure2a. NASS-PCDS database vehicle profile parameters superimposed with Euro-NCAP regulation head impact testing region related to children and small adults.

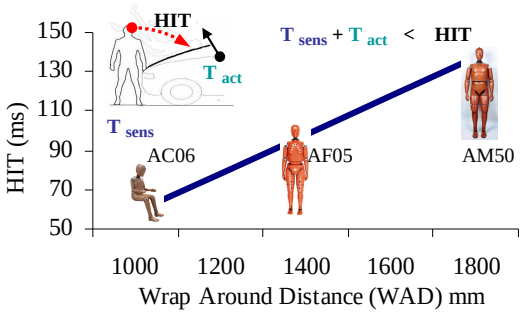

Figure2b. Approximate relationship of Wrap around Distance (WAD) and Head Impact Time (HIT) as defined in EuroNCAP protocol.

The Euro-NCAP pedestrian test protocol procedures specifically indicate the head impact evaluation region for children and small adults as shown in Figure2 for a range of WAD from 1000 to 1700mm. Data related to this region is selected from PCDS and analyzed to find out those factors of the vehicle front-end-profile and pedestrian that have maximum influence on the post-crash kinematics as defined in Euro-NCAP protocol. HIT being directly proportional to WAD, one can assume that a principal component analysis (PCA), using the real world accident data of this region, will be a useful tool in identifying the most influential factors related to HIT. The results of the PCA study are shown in Table2 that clearly reveals the following facts:

Table 2 Results of PCA (refer Figure.3)

Variables of NASS-PCDS *Accidental Year 1994-1998 552 pedestrian crashes 42 cases in WAD 1000-1700 (1,2,3 indicate Component No.)*	Results of first three principal components	
	Child	Child & Small Adult
Ground to forward hood opening (same as Bonnet Leading Edge, BLE)	1	1
F-bumper top height F-bumper bottom height	1 1	1 1
Bumper lead	3	2
Impact speed		1,2,3
Bumper lead angle	1	1
Pedestrian height & weight	1,2	1,2
Pedestrian leg orientation	2	2
Hood length Results based on first 3 principal components	2	2

Figures in gray color indicate less contribution

(i) The BLE height from ground is the most influential factor together with forward bumper top and bottom heights and also the bumper lead angle as they appeared in the 1st principal component (Figure3).

(ii) Pedestrian's height and weight are also important as they contribute maximum in the 2nd principal component. Again, as they appear in the 1st principal component also with lower order of contribution, it may indicate that the inertia (mass x length^2) of the upper part of the pedestrian above BLE may be a key factor.

(iii) The influence of speed of impact is moderate for the pedestrian whose average height is above 155cm (close AF05 size) and very low if the average height is less than 145cm (grown-up child).

(iv) Looking at the detail individual amounts of contribution in PCA results, a part of which is shown in Figure3, one can guess that the relative height of the pedestrian or in other words, the position of its center of gravity (COG) with respect to the BLE of the striking vehicle and to

some extent the bumper lead might be the crucial design parameters of the front end profile of a vehicle to control the value of HIT. The result of sensitivity analysis using 6YO-child FE model is described in detail in the following sections (refer Table3) to confirm the above statement. The sum of sensing-time T_{sens} and actuation-time T_{act} for those vehicles fitted with activated pop-up hood has to meet the present Euro-NCAP requirements ($\mathbf{T_{sens} + T_{act} < HIT}$) based on shortest HIT condition. The HIT is usually lowest for 6YO-child whose weight lies in the range of 19-32kg with an average weight of 24.5kg (refer Figure 8a).

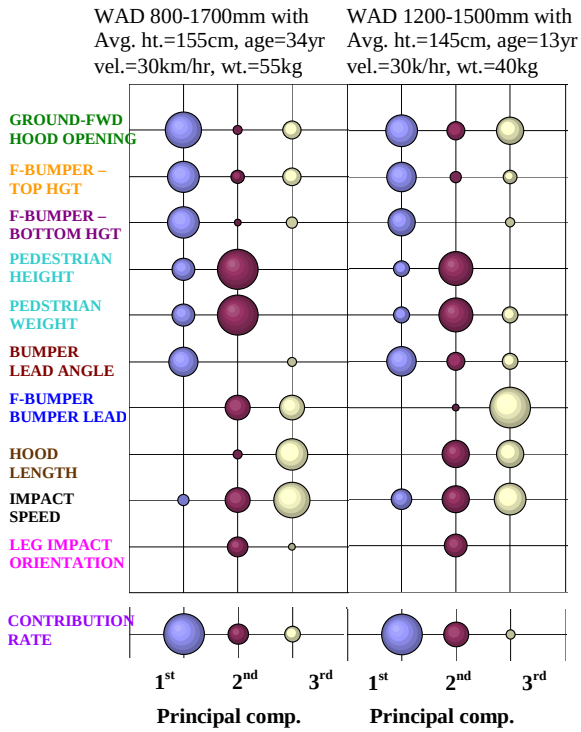

Figure3. Distribution of first three principal components of PCA results for two different WAD regions with approximately 65% (1st: 34%, 2nd: 17%, 3rd:14%) cumulative contribution.

FE ANALYSIS OF HUMAN MODEL

An adult male pedestrian model was developed by JARI (Japan Automobile Research Inst.) under the supervision of JAMA (Japan Automobile Manufacturers Association) in 2010 [7, 8, 10]. The post-crash pedestrian kinematics, including head trajectory, are already validated with PMHS experiments [7,15]. In this paper, the head center of gravity (COG) trajectory of the pedestrian and the head impact time (HIT) with the hood are discussed.

The adult model was modified in-house to create a 50th%ile 6YO-child FE model. The adult 50th%ile adult male model is developed in the JAMA human model consortium. All parts of the 6YO-child FE model are scaled according to the European-children anthropometry data [3, 9].

The two superimposed FE simulation results of overall kinematics of an adult and a child, as shown in Figure 4(a, b), clearly show the influence of the ratio of hood height with respect to pedestrian height "hp" and the vertical position of center of gravity with respect to bonnet leading edge [4].

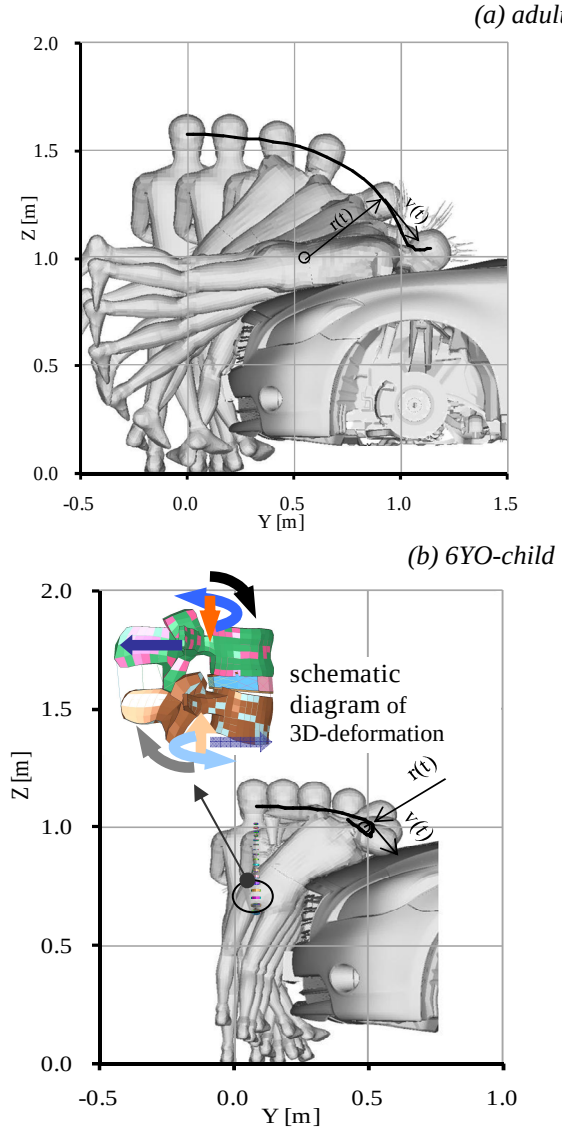

Figure4. Superimposed animations of (a) 50%ile AM50 adult and (b) 6YO-child with a magnified schematic diagram of the 3D-deformation of a typical spine joint.

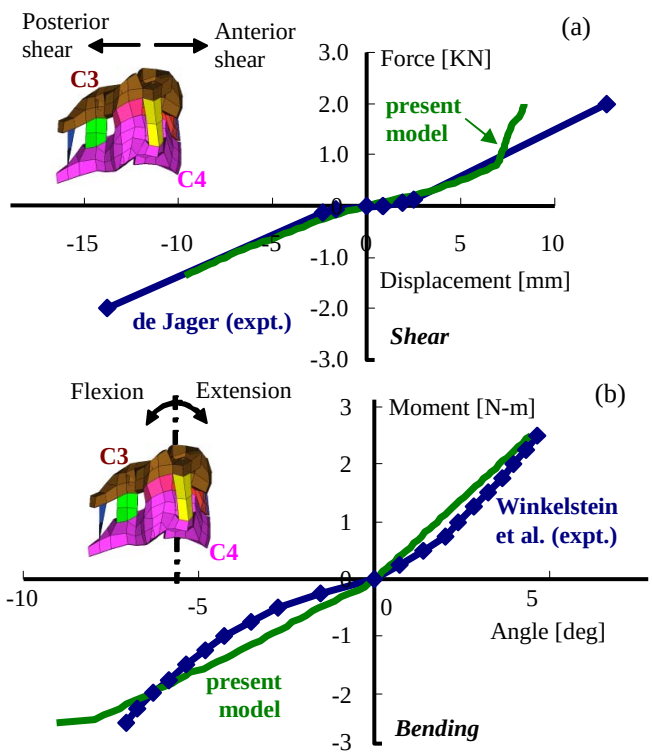

Figure5. Component level responses of upper spine (C3-C4) joint for an adult in shear and bending mode.

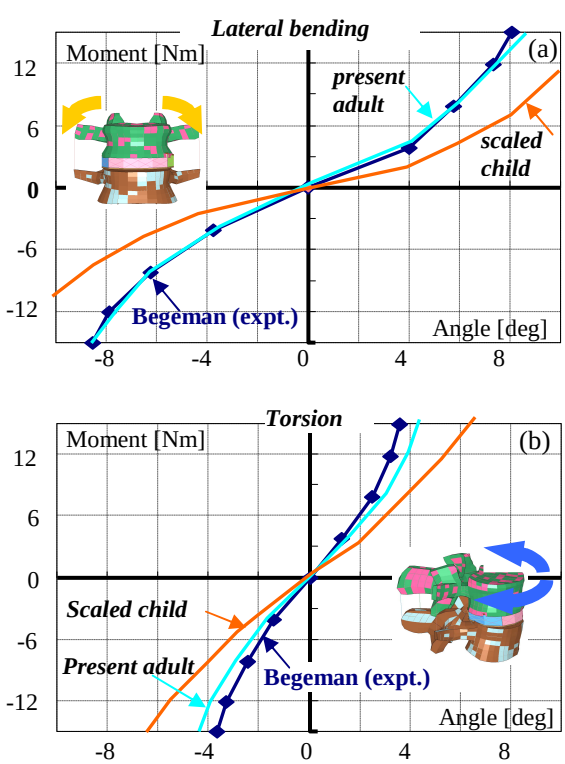

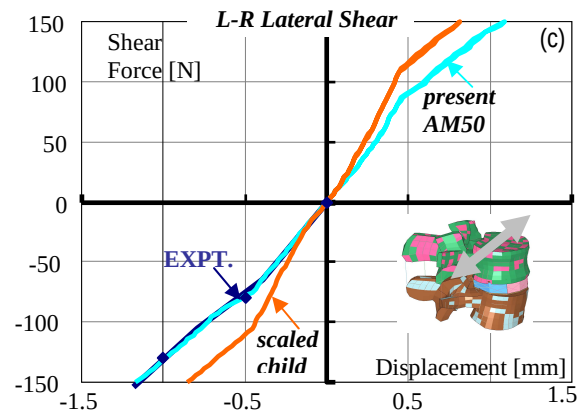

Figure6. Component level responses of lower spine (L3-L4) for adult and geometrical scaled 6YO-child. from AM50 adult, (a) lateral bending, (b) torsion, and (c) lateral shear.

Identification of the overall spine deformation kinematics (especially in lateral bending, torsion and lateral shear mode) of the upper body is important. Deformation pattern of two adjacent vertebrae connected by soft tissues influences the kinematics of the head. Hence, proper identification of load-deformation characteristics at different portions of the entire spine is important. Figure5 shows the quasi-static response identification results of the upper cervical spine (C3-C4) joint for adult in shear and bending. Figure6 shows the quasi-static response identification results of the lower lumbar spine (L3-L4) joint of the present AM50 adult and 6YO-child scaled model [10, 13, 14]. The results of response identification for different modes of deformation of the present simulation model match well with those of biomechanical experiments. Due to geometrical scaling effect, the response of the equivalent 6YO-child, scaled from AM50 adult, will be reduced due to smaller cross-sectional area. However, the response characteristic will be still stiffer in response compared to children as mentioned in a recently published paper [18]. Proper adjustments of material properties, such as, Young's modulus, are necessary to match dynamic response of a child.

HEAD IMPACT TIME

HIT is dependent on various parameters. The task of determining and identifying the factors related to HIT, is an important activity to select the optimum design parameters of the front-end module of the vehicle at the early stage of design. In addition, one has to estimate the shortest possible HIT value with different pedestrian size, varying from adult to

children and the location of impact, as mentioned in Euro-NCAP protocol.

In general, say for typical sedan-type vehicle profiles, the shorter is the height of the pedestrian, the faster is the time of head contact with the hood as mentioned in Figure2b. Different phases of 6YO-child pedestrian kinematics are plotted in Figure 7 to visualize the influences of different factors for a typical sedan.

Phase 0: At the start of impact, the low (center of gravity) of the 6YO-child pedestrian is completely under the bonnet leading edge of the vehicle.

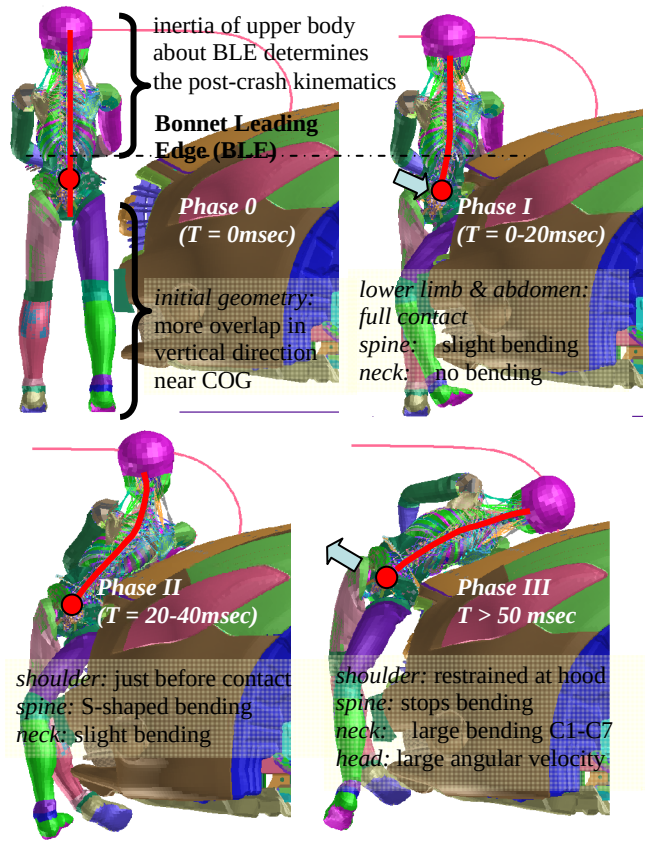

Figure7. Different phases of spinal deformation of a 6YO-child from the start of impact until the head come in contact with the hood.

Phase I: The lower limb and the abdomen are in full contact with the front end of the vehicle. The lower part of the lumbar spine is slightly pushed forward. The portion of spine above the abdomen is almost vertical with head remained straight without any rotational movement.

Phase II: The spine undergoes S-shaped bending. The hip is fully restrained by the hood. With abdomen and chest fully compressed by the bonnet leading edge, the shoulder is about to touch the front end of the vehicle. At this instant of time, the head starts rotating much faster.

Phase III: The head rotates very fast with high angular velocity with shoulder remains fully restrained just before hitting the hood.

Performing a number of simulations with various initial postures, angles and locations of impact of the pedestrian with respect to the vehicle, it is clearly observed that the shoulder and hand interaction, in between the space of the head and the hood of the vehicle, will affect the value of HIT just before the head comes in contact with the hood. Similar result is observed in the PCA study also, as mentioned in Table2 and Figure3, which show some small amount of contribution coming from leg impact orientation.

HIT value is influenced by the impact speed as shown in Figure8.The sensitivity at lower impact speed (V<25km/h) is more than that at higher speed (V>30km/h). It is non-linear and there exits an inflation-point or a change in gradient at this region (25-30km/h). However, it will depend on the type of vehicle and the shape of the front-end profile. Similar result is observed in the PCA study also as mentioned earlier in Figure3, which shows some amount of contributions in 2nd and 3rd principal components. It is to be noted that the effect of impact speed is relatively less estimated in PCA compared to that of the FE analysis. This may be due to the limitation of the PCA based multivariate statistical method, which is effective, efficient and accurate for linearly distributed Gaussian multivariable dataset. In order to verify that one has to reinvestigate in more detail with advanced statistical tools such as non-linear PCA, usually known as Kernel-PCA, before making any general conclusion on the degree of the contribution of speed of impact on WAD or HIT based on real world accident data. However, it is beyond the scope of this present study. The influence of braking and steering on WAD is discussed in detail in earlier publications where it is clearly stated that one has to be careful in selecting the relevant data from real world accident database [4].

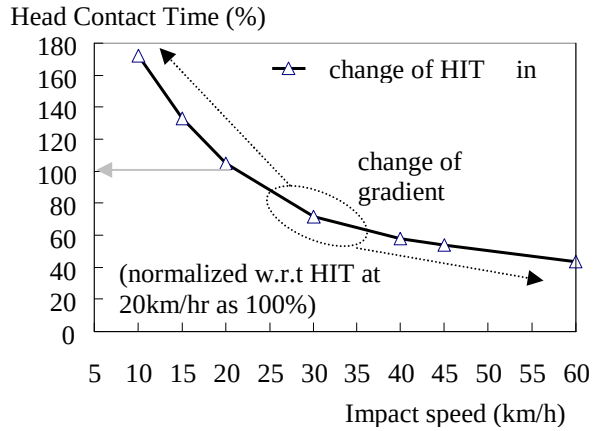

Figure8. Sensitivity of head impact time with respect to speed of impact.

Table3. Sensitivity analysis of different parameters affecting HIT estimation.

Parameter		Degree of influence on HIT at speed 40-45 km/hr
Pedestrian / BLE height: h_p (position COG wart to BLE)		High
Bumper lead and angle		Medium
Location of impact w.r.t. center		High (Min. at CL)
Spine	later bending	medium
	shear	medium
	torsion	low
Ligaments (not spinal)	neck peripheral	low
	thorax-shoulder	low
Upper extremity	interaction of hood-shoulder	medium at center very low at corner
Pedestrian mass (with same COG)	Refer Figure 8	low
Bone fracture	lower-limbs	very low
	upper-limbs	very low
Thorax (chest, abdomen)	compression	Low
Lower extremity	posture	Low

high:> 6%, medium:3-6%, low:2-3%, very low:0-2%

Apart from the impact speed of the vehicle, Table3 shows the "degree of influence" of the other parameters related to 6YO-child FE model, influencing the head contact time as estimated from human FE simulation results. With recent advancement of CAE based FE crash analysis, one can easily capture more accurately the basic trend and the mechanism of complicated post-crash pedestrian kinematics to supplement accident database if sufficient number of simulations are performed by matching the boundary conditions in real world accidents.

Parametric study with FE simulation

The parametric study, as shown in Table3, is carried out to find the effect of geometric scaling of a 6YO-child model, which is accurately scaled from AM50 model.

Effect of mass: 6YO-child 50%ile model compatible to EuroNCAP protocol with stipulated heel-to-heel gap and the ground to pelvis height in standing position. The mass of the present 6YO-child FE model is 24.5kg. The corresponding statistical range of the weight of European 6YO-children is 19-32kg[3]. The influence of the mass of the 6YO-child FE model is simulated by changing the mass without altering the position of the COG of 6YO-child FE model. A 30% increase in weight from the mean value (50%ile 24.5kg → 95%ile 32kg, Figure8b) will lead to an increase in HIT value by a few percent.

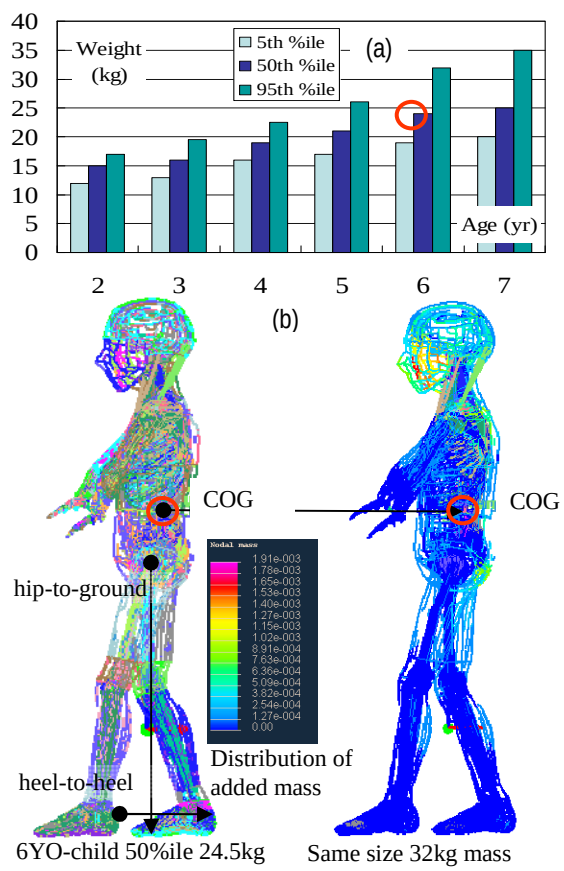

Figure8. (a) Change in weight of child with age (b) Distribution of added mass to convert 6YO-child 50%ile 24.5kg to 32kg mass 6YO-child with same COG.

Effect of COG w.r.t BLE: The change in value of "h_p", i.e., the ratio of pedestrian height with

respect to the height of the bonnet leading edge, has maximum influence. The higher is the value of "h_p" ratio, the longer is the value of HIT. This is due to the increase in inertia with longer lever-arm and larger mass of the free region of the upper body above the BLE of the vehicle.

Effect of spine stiffness: Lateral bending and lateral shear and torsional deformation of the spine also influences the value of HIT to some extent, approximately 2-4%.

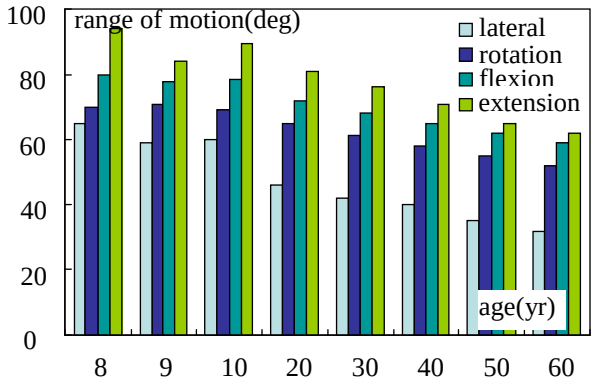

Figure9 Cervical range of motion with age [12].

Effect of upper extremity: Simulation results indicate that the shoulder-hood interaction, the degree of constraint and the timing of the shoulder restraint on the hood, will affect the rotational movement of the head especially at the center of vehicle. However, the degree of shoulder interaction is very low in case of bumper corner impact. This interaction is dependent on the initial posture and the initial angle of impact of the pedestrian that will decide what will be the degree of interaction among the shoulder, arm and head in the final phase of the impact.[4, 17].

Effect of location (centerline vs. corner): From FE simulation, it is observed that, the lateral position or location of impact of the pedestrian at the corner of the vehicle has very large influence on the value of HIT. At the initial phase, the pedestrian hits the bumper causing some initial bumper deformation along with an initial increase in the longitudinal contact force FY acting on the lower part of the pedestrian to make him/her lean laterally towards the hood. In case of corner impact, after sometime (t=15msec), the pedestrian slides along the curvature of the bumper and consequently the longitudinal contact force FY acting on the lower part of the pedestrian becomes constant as shown in Figure 11. Unlike the case of corner impact, for the case of impact at the center-line of the vehicle, the reaction force exerted by the deformed front-end profile of the bumper goes on increasing with lateral contact force FX remains almost zero, causing the upper half of the pedestrian above the BLE, to lean more and faster towards the hood. In all the cases of simulations at different angles of impact (-20deg., -10deg., ref:0deg., +10deg., +20deg.) with respect to the longitudinal direction of the vehicle at different speeds of impact (V=30,35,40,45 km/hr), the estimated HIT values at the center line of the vehicle is always less than those corresponding to the impact cases at the left and right corners of the vehicle. The amount of offset distance of the pedestrian with respect to the center line of the vehicle for corner impact cases, is selected in such a way that the head just touches the corner of the hood as shown in Figure11.

It is also observed that the variation of angle of impact hardly has any influence on the shoulder-hood interaction in case of corner impact. In contrast to that, in case of vehicle center-line impact, the variation of initial angle or the initial orientation of the pedestrian about the vertical axis does show some influence on HIT values.

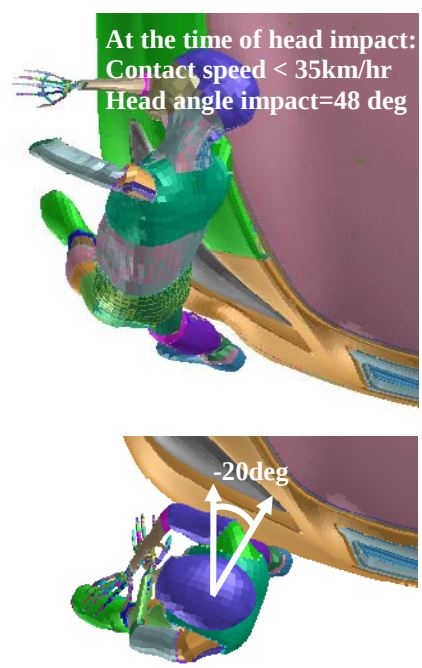

Figure10. Modes of impact at the corner of the vehicle with head contacting just inside the edge of the hood with direction of impact -20deg.

It is also to be noted that at the time when head impacts with hood, for both the locations of impact (at bumper center and corners) the head impact angle of 6YO-child is very close to 50deg. as defined in EuroNCAP test. However, the speed of head contact with the hood is 20-25% less than the initial speed of the striking vehicle. So, one might think of reconsideration of the headform testing speed in accordance with different WAD regions on the hood, based on the results of future research studies for different types of vehicle.

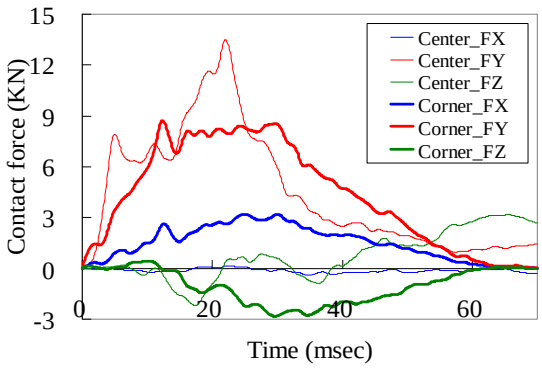

Figure11. Comparison of external contact force in X(lateral), Y(longitudinal), Z(vertical) directions on 6YO-child hit at the center line and at the corner of vehicle at 0-degree angle of impact.

So, reconsideration of testing with the same impactor speed of 40km/hr for different WAD regions may be necessary in future based on the results of more research and studies on different types of vehicle.

CONCLUSIONS

This paper briefly discussed the main factors determining the post-crash pedestrian kinematics based on a detailed study on NASS-PCDS. Those cases are categorized into four types (Type A-D) of post-crash pedestrian kinematics.

The 6YO-child model, developed by accurate scaling of different parts from existing JAMA human adult model is effectively used to identify the main parameters related to head impact time.

Both FE simulation and the PCA of NASS-PCDS data, reveal that the relative position of the bonnet leading edge with respect to the center of gravity of the pedestrian (COG: approx. 55% of the pedestrian height), bumper profile and the speed of impact are the main influential factors in determining the time of contact of head with the hood.

The lateral bending and shear responses of the 6YO-child affects HIT also..

In general, for standard sedan types of vehicle the HIT value for 6YO-child is shortest for the location at the centerline of the vehicle.

It is to be noted that, the range or degree of influence will vary from vehicle to vehicle. However, with respect to an equivalent actual 6YO-child which is more softer and flexible than the present scaled model, the estimated value of HIT calculated by a 6YO-child FE model scaled geometrically from a validated AM50-adult FE human model, will most probably give a conservative or lower-bound estimate of true HIT value.

REFERENCES

[1] Mizuno, Y., “Summary of IHRA Pedestrian Safety WG Activities”, ESV 19, No. 138, 2005

[2] Longhitano, D., et al., “Influence of Vehicle Body Type on Pedestrian Injury Distribution”, SAE World Congress, 2005

[3] Serre, T., et al., “Child pedestrian anthropometry: evaluation of potential impact points during a crash”, Accident Analysis and prevention, Vol. 42, Issue 6, 2010

[4] Kawabe, Y., et al., Different Factors Influencing Post-crash Pedestrian Kinematics, SAE World Congress 2012-01-0271

[5] Okamoto, Y., et al., "Pedestrian Head Impact Conditions Depending on the Vehicle Front Shape and Its Construction - Full Model Simulation", Traffic Injury Prevention, 4: pp74-82, 2003

[6] Dokko, Y., et al., “Validation of the Human Head FE Model against Pedestrian Accident and its Tentative Application to the Examination of Existing Tolerance Curve”, ESV18 No.322, 2003

[7] Takayama S., et al.,”The Clarification of Individual Injury Mechanism Difference in Pedestrian FE Model Utilizing Cadaver Scaling and Posturing Techniques”, ESV22, No.11-0414, 2011

[8] Ejima, S., et al., “Modification and Validation of Human Neck Model under Direct Head Loading”, ESV 18 No. 333 (2003)

[9] Serre, T., et al., “Comparison between New Data on Children Anthropometry and CRS Dimensions”, ESV 21 Paper 09-0484, 2009

[10] Sato, F., et al., “Validation of Segmental Motion Properties of a Human Lumbar Finite Element model" JARI Journal, Dec. 2012.

[11] Yang, J., et al., “Correlation of Different Impact conditions to the Injury Severity of Pedestrian Real World Accidents”, ESV 19 Paper 05-0352, 2005

[12] Caris, T, L, et al., “Cervical Range of Motion Data in Children”, SAE 2006-01-1140, 2006
[13] Schultz, A., B., et al., “Mechanical Properties of Human Lumbar Spine Motion Segments Part-I”, Transactions of the ASME, Vol.101, Feb., 1979
[14] Begeman, P.C., et al., “Visco-elastic Shear Response of the Cadaver Hybrid III Lumbar Spine, SAE World Congress 942205.
[15] Nishimura, R., et al., “Development of the Human FEM Model for Child Pedestrian” JSAE Spring Convention, 2002, 20025504
[16] R. B. Martin et al., “Age and Sex-related Changes in the Structure and Strength of the Human Femoral Shaft”, Journal of Biomechanics, Vol.10, pp.223-31, 1977
[17] Yasuki, T., Yamamae, Y., “Validation of Kinematics and Lower Extremity Injuries Estimated by Total Human Model for Safety in SUV to Pedestrian Impact Test”, J. of Biomechanical Science and Engineering, Vol.5, No.4, pp.340-356, 2010,
[18] Francisco J. Lopez-Valdes, et al., “The Biomechanics of the Pediatric and Adult Human Thoracic Spine”, 55th AAAM Annual Conf. Annals of Advances in Automotive Medicine, Oct. 3-5, 2011.

ACKNOWLEDGENTS

The authors would like to acknowledge the members of the users’ support group of ESI Japan, for PAM-CRASH and the members of JARI for the adult human FE model.

DEVELOPMENT OF A FINITE ELEMENT MODEL OF 5TH PERCENTILE FEMALE WITH MULTIPLE MUSCLES AND ITS APPLICATION TO INVESTIGATION ON IMPACT RESPONSES OF ELDERLY FEMALES

Masami Iwamoto
Yuko Nakahira
Hideyuki Kimpara
Toyota Central R&D Labs. Inc.
Japan
Kyuengbo Min
Tokyo Metropolitan Institute of Medical Science
Japan
Paper Number 13-0366

ABSTRACT

The rates of fatality and injured persons of elderly people are gradually increasing in automotive accidents in Japan. In particular, elderly female occupants are most susceptible to injuries, especially on thorax and head-neck regions, based on previous studies using automotive accident data. This study developed a finite element (FE) model of 5th percentile female (AF05) with multiple muscles, and applied it to investigation on the injury mechanisms of elderly female occupants.

Individual muscle models of whole body with passive and active properties were integrated with an AF05 FE model that we developed previously. Material properties of skeletal parts with low strength of elderly people and smaller physiological cross-sectional area (PCSA) of each muscle of elderly females were obtained from the literature and commercially available image data, and were inputted to the model. Smaller PCSA of each muscle in elderly females would generate less muscular forces than younger males while less stiff bone properties of elderly females would generate more bone fractures than younger males. The developed elderly AF05 model without muscle activation was firstly validated against some cadaver test data on frontal impacts for the thorax and abdomen, and head-neck responses during a low-speed rear-end collision, and were compared with young adult 50th percentile male (AM50) model with multiple muscles that we developed previously. The simulation results of the elderly AF05 model generally showed good agreement with test data.

The elderly AF05 model was secondly used for investigation on effect of muscle activation to thoracic deformation in frontal impact situations with belt and hub loadings, and head-neck response in a low-speed rear impact situation. In the simulations on the thoracic deformation, a bracing condition was assumed and an activation level of 20% was assumed for all muscles in the trunk. Simulation results showed that the maximum thoracic deflections of the elderly AF05 model without muscle activation were two times and three times larger than those of young adult AM50 model with muscle activation in belt and hub loadings, respectively. From comparison between the elderly AF05 model and the young adult AM50 model, lower strength of bones and smaller PSCA of each muscle in the elderly AF05 model could increase thoracic deflection. In the simulation on the head-neck response, activation level of each muscle during a low-speed rear impact was estimated using a controller of multiple muscles with reinforcement learning (RL) that we developed previously. Simulation results showed that the maximum head angular velocity of the elderly AF05 model was larger than that of the young adult AM50 model, especially in considering muscle activation. The elderly AF05 could not prevent the head from rotating rearward due to their weak muscular forces.

Although the elderly AF05 model has some limitations on lack of experimental data for validations and estimation of muscle activation, it has the potential for better understanding of injury mechanisms of elderly female occupants.

INTRODUCTION

In Japan, population rate of elderly people more than 65 years old became over 23 % of total population in 2010 and is estimated to be increased for 40 % in 2060 (National Institute of Population and Social Security Research, 2012). The number of car accidents involving elderly drivers would increase at an accelerated pace with the increase in population of elderly people and elderly drivers' licensees, and is estimated to be beyond 2,100,000 and the social cost is estimated to be about 10 billion dollars 20 years later (The General Insurance Association of Japan, 2004). The Institute for Traffic Accident Research and Data Analysis (ITARDA) in Japan investigated traffic accident data on belted drivers from 2004 to 2006, and showed that fatality and serious injury rates increase with increase of age, and the fatality

rate of elderly drivers was about two times higher than that of younger adult drivers. The primary injury location was thorax and the secondary injury location was head-neck region, and the succeeding injury location was lower extremity in elderly drivers (ITARDA, 2007). Yee et al. (2006) investigated injury pattern of elderly victims more than 65 years old involved in motor vehicle collisions using data from Victorian State in Australia from 2001 to 2003. They reported that the most common injury for elderly victims was thoracic injury including multiple rib fractures and the second most common injury was head or neck injury.

According to NASS-CDS data analysis from 1993 to 2004 performed by Liu et al. (2007), the percentage of driver overall severe injury severity (MAIS4-MAIS6) of elderly females was 1.6 times higher than that of elderly males. The trend seems to be significant in belted front passengers. Based on accident data analysis in Japan performed by Yaguchi et al. (2011), the fatality of belted front passengers of elderly female was 3.6 times higher than that of elderly male while serious injuries of belted front passengers of elderly female was five times higher than that of elderly male. Augenstein et al. (2011) reported that elderly females sustained more severe injuries than elderly males for belted front seat occupants in frontal crashes based on accident data analysis using the 2000-2009 NASS/CDS data. Therefore, elderly female occupants have a tendency to sustain more fatal and severe injuries than elderly male occupants.

Brumbelow et al. (2009) investigated injury patterns in frontal crashes of vehicles based on the NASS-CDS crash data. They showed that occupants of 60 years old or older more often received at least one serious chest injury than a serious head injury, and the opposite was true for occupants younger than 30 years old. Simamura et al. (2003) conducted accident data analysis of a total 246 vehicle occupants using ITARDA data. They reported that elderly occupants frequently experienced rib fractures near the seatbelt line even under lower impact severity while younger occupants appeared not to sustain rib fractures even in higher impact collisions. These accident data analyses on thoracic injury indicate that elderly occupants tend to sustain thoracic injury differently from younger occupants. However, the thoracic injury mechanism of elderly occupants is not clear.

Krafft et al. (2003) investigated difference in the risk of permanent whiplash injury between males and females for different seating positions in rear impacts based on accident data reported to the Swedish insurance company Folksam during 1990-1999. The risk of permanent disability was three times higher for female drivers than male drivers. Similarly, permanent disability was 1.5 times higher for female front seat passengers and more five times higher for female rear seat passengers. Brolin (2003) performed a study of hospital data on neck injuries mainly due to fall and traffic accidents among the elderly in Sweden between 1987 and 1999. They showed that elderly have a death rate for cervical fractures that is three times higher than the death rate for the entire population. The fracture locations were mostly Atlas (C1) and Axis (C2) for elderly while those were mostly C4-C6 for younger population. Malik et al. (2008) analyzed the morbidity, mortality, and outcome of cervical spine injuries in 107 patients over the age of 65 years, which were caused by falls or road traffic accidents. They reported that cervical spine injuries are frequent in the elderly population. The injury patterns in elderly patients are different from those among younger patients. In addition, the injuries have the potential to influence the spinal cord and can result in death and permanent disability. Snyder et al. (1975) investigated basic physical measurements related to susceptibility to cervical hyperextension-hyperflexion injury. They found that the small elderly female was most susceptible to injury since the neck muscles are not strong enough even when fully tensed, to prevent the head from reaching its motion limit. However, the neck injury mechanism of elderly people, especially small elderly females, is not well known.

Many researchers investigated physical and motor functional characteristic features of elderly people. Bone mass or density is lost with age, especially in women after menopause so that bones become more brittle and may break more easily. The trunk becomes shorter as the disks gradually lose fluid and become thinner. The joints become stiffer and less flexible due to loss of fluid and cartilage in the joints (Bougie et al. 2001, Rosen et al. 1999). The physiological cross-sectional areas (PCSA) and strength of muscles decrease with age, and changes in the muscle tissue cause muscles to have less tone and ability to contract, even with regular exercise. In addition, muscle activation latency of elderly people is significantly larger than that of younger adults. Therefore, poor posture stabilization is found in elderly people during standing and sitting, especially in dynamic environments.

There are many studies using computational human body models to investigate mechanism of bone fractures of elderly people during automotive accidents (e.g. Ito et al.2009, El-Jawahri et al., 2010). In most of the studies, only loss of bone density and strength, and changes of bone shape with age were considered in their computational models developed to investigate the mechanism. However, recent studies showed that muscle activity before impacts is not negligible (Begeman et al. 1980, Ejima et al. 2009).

Computational human models are effective tools to

understand the injury mechanisms in automotive crashes. Recently, some human FE models have been developed with active muscles to investigate the muscular effects for human body kinematics. Behr et al. (2006) developed a FE model of the lower limb with 20 independent muscle bundles in the superficial and deep layers and used to investigate the effect of muscle tense on the skeletal injuries of the lower limb. They validated the model for isolated muscle contribution in the direction of fibers and bracing conditions under an emergency braking. Their simulation results indicated that muscle activation in bracing during frontal impacts significantly increased the stress level on the tibial shaft. Authors also developed a finite element model of human whole body with multiple muscles (Iwamoto et al. 2011). Simulation results using the human model showed that muscular forces before impacts could affect injury outcomes significantly. In addition, authors showed that muscle activation and the control have an important role on body posture stabilization in impact situations (Iwamoto et al. 2012). Therefore, the loss in PCSA of each muscle and poor ability of posture stabilization in elderly people are supposed to affect kinematics and injury outcomes of elderly drivers and passengers.

In this study, we newly developed a small female FE model with multiple muscles to investigate how age-related ability in muscular forces could affect injury outcomes of elderly female occupants. The developed model was firstly validated against cadaver test data on thoracic and head-neck responses during impacts. The developed model was secondly used for investigation on effect of muscle activation to thoracic deformation in frontal impact situations, and head-neck response in a low-speed rear impact situation. We investigated effects of loss in muscular forces of elderly people for kinematics and impact responses of the human body. All simulations in this paper were performed using an explicit finite element code LS-DYNA (LSTC, USA).

DEVELOPMENT OF ELDERLY SMALL FEMALE FE MODEL

A human whole body FE model with muscles

In previous studies, we developed muscular FE models of a human whole body and integrated them with a human body FE model called THUMS (Total HUman Model for Safety, Iwamoto et al. 2002) whose size was similar to that of AM50 with a height of 175 cm and a weight of 77 kg (Iwamoto et al. 2011 and 2012). Each muscle model of the AM50 model was scaled down to adjust the size of AF05 (5th percentile female) with a height of 152 cm and a weight of 46 kg, and was incorporated into an AF05 FE model that we developed previously (Kimpara et al. 2005 and Iwamoto et al. 2007). Figure 1 shows a developed small female FE model with multiple muscles. In this figure, the skin was removed to see muscles clearly. The model includes 266 muscles of lower extremities, upper extremities, trunk, and neck such as the Sternocleidmastoid, Trapezius, Rectus Abdominis, Erector Spinae, Pectoralis Major, Deltoid, Biceps Brachii, Triceps, Extensor Digitorum, Flexor Carpi Radialis, Rectus Femoris, Gluteus Maximus, Vastus Medialis, Biceps Femoris, Vastus Lateralis, Tibialis Anterior, Gastrocnemius, and so on. Total number of nodes and elements in the whole body model is about 140,000 and 240,000, respectively.

Each muscle FE model was represented as a hybrid model by combination of solid elements with passive muscle properties and bar elements with active muscle properties. The solid elements were modeled with a rubber-like material model (LS-DYNA: #181, MAT_SIMPLIFIED_RUBBER) to simulate 3D geometry of individual muscles and non-linear passive properties. This material model is based on Ogden model and users can use the model by inputting a single uniaxial non-linear stress-strain curve. Poisson's ratio is set to 0.495. The non-linear passive properties were given using tensile properties of muscles obtained from Yamada (1970). The bar elements were modeled with a Hill type muscle model (LS-DYNA: #156, MAT_MUSCLE) to generate muscular force according to inputted activation levels which are in a range from 0 to 1. Some material properties are needed for the Hill type muscle model. A maximum contraction force per unit cross-sectional area of 5.5 kgf/cm^2 of each muscle was obtained from Gans (1982). The active force-length and active force-velocity curves were obtained from Thelen et al. (2003). Although the passive force-length relations are needed in the Hill

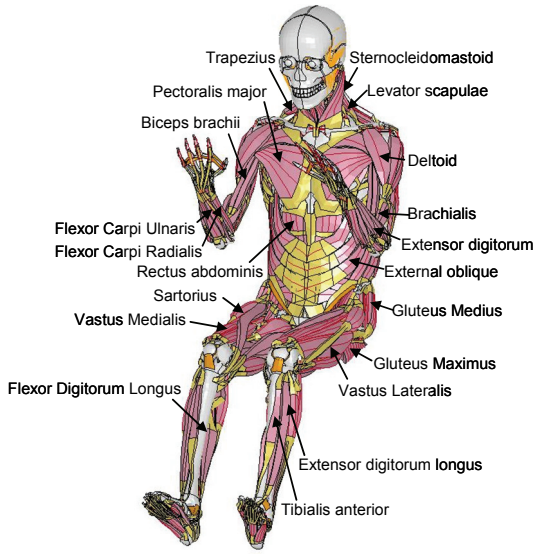

Figure 1. A small female FE model with muscles.

type model, they were not assigned to bar elements because the solid elements have the passive properties. According to anatomical text (Agur et al., 2005), each muscle model was connected to the corresponding bone model through tendon models. The tendons were modeled by using shell or solid elements at both ends of muscles. Material properties of the tendons were obtained from the literature (Pioletti et al., 1998, Carlson et al., 1993). Some sliding contacts were defined to produce the interaction between adjacent two muscles and the interaction between muscles and bones close to the muscles. The skin was modeled using shell elements with elastic material properties obtained from Yamada (1970) while the fat was modeled using solid elements with the rubber-like material model. Sliding interfaces were also defined to produce interaction between the muscles and the skins.

Aging effects in material properties

PCSA data of muscles for elderly people Force generated by a single muscle is proportional to its PCSA. Therefore, the PCSA of each muscle could affect the muscular force significantly. The PCSA of each muscle model was primarily determined based on Winters (1990). The PCSA data of one third of all muscles were determined based on two series of physical slicing data with high resolution of a 38 years old adult male cadaver with a height of 180 cm and a weight of 90 kg, and a 59 years old elderly female cadaver with a height of 167cm and a weight of 72 kg. These image data were obtained from commercially available data (Visible Human Project Data; NIH, USA). Table 1 shows PCSA data of primary muscles in the adult male and the elderly female, and rate of each PCSA of the elderly female against that of the adult male. The obtained PCSA of each muscle in the elderly female was inputted as cross-sectional area of bar elements with active muscle properties of the corresponding muscle in the small female FE model. The muscular PCSAs of the elderly female were smaller than those of the adult male and the rates of muscular PCSAs of the elderly female against those of the adult male were from 13 to 84 % (average value: 51 %).

Material properties of ribcage for elderly people According to accident data analysis described previously (ITARDA 2007, Yee et al. 2006), the primary skeletal injury locations were thorax and lower extremity in elderly occupants. Therefore, we focused on the ribcage and long bones of lower extremity in determining bone properties of the elderly female model. As for aging effect in material properties of the rib, Kemper et al. (2005) measured tensile properties of cortical bones in ribs using six cadavers including three females with 46, 61, and 64 years old and three males with 18, 45, and 67 years old. Figure 2(a) summarizes tensile stress-strain curves of rib cortical bones obtained from Kemper et al.. The elastic moduli of ribs in elderly females were stiffer than those in the youngest male while the failure strains of ribs in elderly females were half as much as those in the youngest male. We inputted the average values of material properties of the elderly females as material properties of ribs in the small female FE model.

Table 1.
PCSA* data of primary muscles in adult male and elderly female

Body Part	Muscle Name	PCSA* A (mm^2)		Ratio
		Young male A_{ym}	Elder female A_{ef}	A_{ef}/A_{ym} (%)
Neck	Sternocleidomastoid	166.00	131.50	79.22
	Longus Colli	39.30	25.90	65.90
	Splenius Capitis	99.00	75.40	76.16
	Semispinalis Capitis	95.20	50.40	52.94
Shoulder	Levator Scapulae	993.00	125.70	12.66
	Trapezius	2323.00	868.50	37.39
	Deltoid	2282.00	1455.40	63.78
	Pectoralis Major	1179.00	872.08	73.97
Upper Arm	Biceps Brachii	319.00	174.67	54.76
	Brachialis	881.00	247.67	28.11
Lower Arm	Flexor Carpi Ulnaris	557.00	129.17	23.19
	Extensor Digitorum	430.00	81.48	18.95
	Flexor Carpi Radialis	310.00	92.59	29.87
Abdomen	Rectus Abdominis	658.00	372.48	56.61
	External Oblique	685.00	439.86	64.21
Hip	Gluteus Medius	1710.00	1308.00	76.49
	Gluteus Maximus	1813.00	1458.00	80.42
Upper Leg	Sartorius	320.00	268.00	83.75
	Vastus Medialis	3237.00	1560.00	48.19
	Vastus Lateralis	4063.00	1648.00	40.56
Lower Leg	Tibialis Anterior	1277.00	848.00	66.41
	Flexor Digitorum Longus	1897.00	586.00	30.89
	Extensor Digitorum Longus	667.00	404.00	60.57

*PCSA: physiological cross-sectional area

As for aging effect in material properties of the rib cartilage, Yamada (1970) reported on tensile stress-strain curves of rib cartilages using 28 cadavers with ages from 20 to 69 years old. Figure 2(b) shows tensile stress-strain curves of rib cartilages obtained from Yamada. The elastic moduli of rib cartilages in elderly persons were less stiff than those in the young adult persons while the failure strains of rib cartilages in elderly persons were half as much as those in the young adult persons. These material properties were inputted into the ribcages in the small female FE model. The thickness of rib cortical bone in the small female FE model was set to the average value of elderly persons including males and females by referring to Kemper et al. (2005).

Material properties of long bones in lower extremities for elderly people As for aging effect in material properties of long bones of lower extremities, Yamada (1970) reported on tensile stress-strain curves of cortical bones of femur and tibia using cadavers with ages from 20 to 39 years old and those with ages from 60 to 69 years old as

shown in Figure 3. These data include male and female cadavers. The stresses in post-yield region and failure strains of elderly people is 20 % and 10 % lower than those of young adults, respectively. These material properties were inputted into the femur and tibia in the small female FE model.

In occupant models, bending mode is estimated to be dominant during frontal impacts because of axial compressive load from foot/ankle under a condition with entrapped knee for the tibia and fibula, and axial compressive load from instrumental panel under a condition with fixed pelvis for the femur. Therefore, we validated the long bone models for static 3-point bending tests of the long bones using 43 male or female cadavers with ages from 20 to 83 years old conducted by Yamada (1970). Figure 4 shows a simulation setup of static 3-point bending for the femur model, which reproduced the test condition.

Figure 5 shows comparison of load-deflection curves of the femur and tibia between simulation results and test data. These figures include simulation results of young adult AM50 model (Iwamoto et al. 2011) and

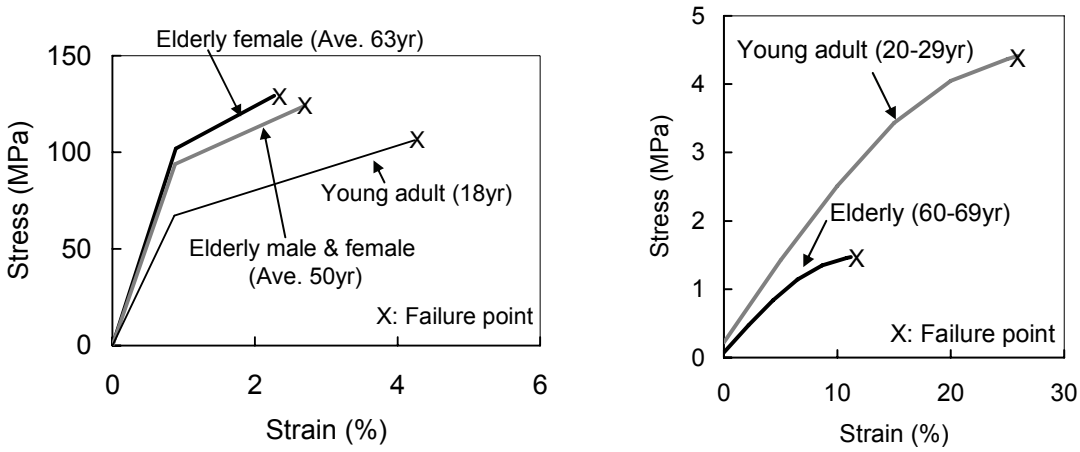

(a) Rib cortical bone (b) Rib cartilage

Figure 2. Tensile properties of rib cortical bone and rib cartilage.

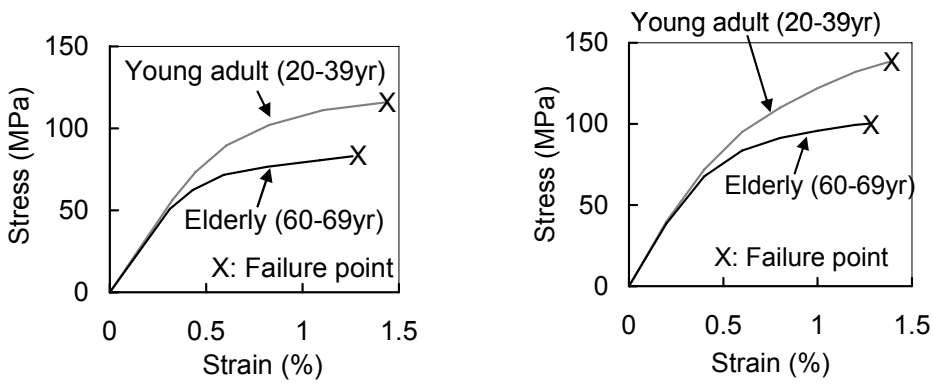

(a) Femur (b) Tibia

Figure 3. Tensile properties of cortical bones of femur and tibia.

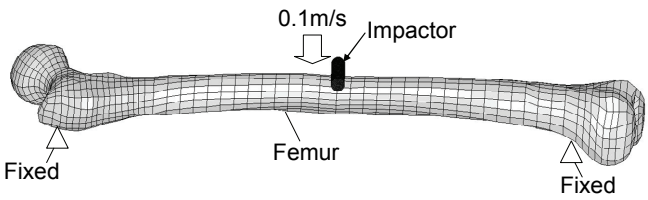

Figure 4. Simulation setup of static 3-point bending for the femur model.

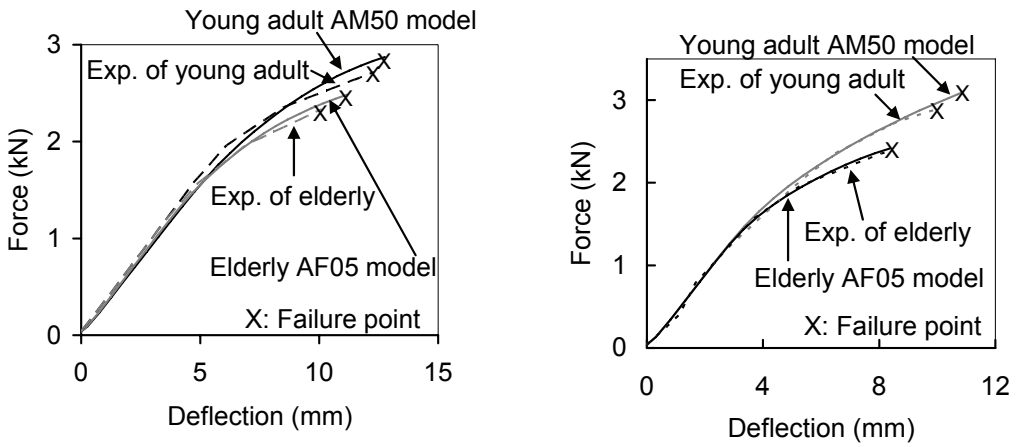

(a) Femur (b) Tibia

Figure 5. Comparison of load-deflection curves in 3-point bending between simulation results and test data.

elderly AF05 model. Simulation results of both models show good agreement test data except the failure deflection. The reason why the deflections at failure were different between simulation results and test data is probably because the material model of cortical bone did not have the anisotropy.

Material properties of cervical vertebral discs for elderly people As for aging effect in material properties of cervical vertebral discs, Yamada (1970) reported on stress-strain curves of wet intervertebral discs in tension. He showed that the elongation at the same stress is a little less in the 40-79 age group than in the 20-39 age group. Therefore, we inputted 1.23 times higher stiffness to C1-C7 discs in elderly AF05 model than in young adult AM50 model. In addition, Brolin (2003) reported on aging effect of mobile segments in cervical spine, and described that C1-C2 motion segment is the most mobile portion of the cervical spine for the normal elderly, as opposed to the C4-C7 motion segment in the younger population. Malik et al. (2008) indicated that the reason of the difference was that the C4-C7 segments would become stiffer with age so that the C1-C2 segment would become the most mobile portion of the cervical spine in elderly people. In this study, we inputted 1.3 times higher stiffness to C4-C7 discs for the elderly AF05 model, which had already had the abovementioned stiffness of cervical discs, to represent cervical spine motion of elderly people.

VALIDATION OF ELDELY SMALL FEMALE FE MODEL

In this study, we validated the elderly AF05 model against some cadaver test data to confirm if the model without muscle activity showed cadaveric responses. The model was validated against four sets of cadaver test data on thoracic and abdominal responses during frontal impacts, and head-neck motions during rear impacts, which were obtained from the literature (Kroell et al.1971, Kent et al. 2004, Nusholtz et al. 1988, White et al. 2009). In simulations of these validations using cadaver test data, muscle activation level of each muscle should be set to 0.0 (0 %) because cadaver has no muscle activity. However, in this study, we set the muscle activation level to values less than 0.01 (1.0%) to ensure computational stability.

Thoracic responses in frontal impacts

The developed elderly AF05 model was validated for frontal impact cadaver test data conducted by Kroell et al. (1971). Kroell et al. conducted a series of cadaver tests on thoracic frontal impacts. Their tests included two cadavers of which the anthropometric data were similar to those of AF05. In simulations, a 23.4 kg hub impactor hit frontal surface of the thorax at two speeds of 6.9 and 9.9 m/s in order to reproduce the experimental set-up (Figure 6(a)). Thoracic deflection was obtained from the distance between the impactor surface and the thoracic posterior surface. Figure 6(b) demonstrates predicted human behaviors in the frontal impact simulations. Figure 7 shows comparison of thoracic force-deflection curves between simulation results and test data at two impact speeds of 6.9 m/s and 9.9 m/s. These figures include two simulation results using young adult AM50 model and elderly AF05 model. Figure 7(a) also includes two elderly female cadaver test data. The simulation results with both impact speeds almost fell within cadaver test corridors. The maximum thoracic deflection of elderly AF05 model was lower than that of young adult AM50 model, and was close to the minimum deflection of the test corridors while the thoracic force until deflection of 30 mm of elderly AF05

model was lower than that of young adult AM50 model. These differences are probably because the body mass and thoracic thickness of the elderly AF05 model were smaller than those of the young adult AM50 model. Figure 8 shows stress distributions of the ribcage with bone fracture locations in the ribs and sternum of elderly AF05 model at the two impact speeds. The model predicted 13 rib fractures and 1 sternum fracture in the case of 6.9 m/s. In the cadaver tests, cadavers from 67 to 80 years old (average of 74.6) sustained 14.6 rib fractures and 1.2 sternum fractures in the case of 6.9 m/s. Therefore, the model has a possibility to predict bone fractures in the ribcages of elderly female occupants.

Kent et al. (2004) presented thoracic response corridors developed using fifteen post-mortem human subjects (PMHS) subjected to four loadings of single and double diagonal belt, distributed, and hub loading on the anterior thorax. Subjects were positioned supine on a table and a hydraulic master-slave cylinder arrangement was used with a high-speed materials testing machine to provide controlled chest deflection at a rate similar to that experienced by restrained PMHS in a 48 km/h sled

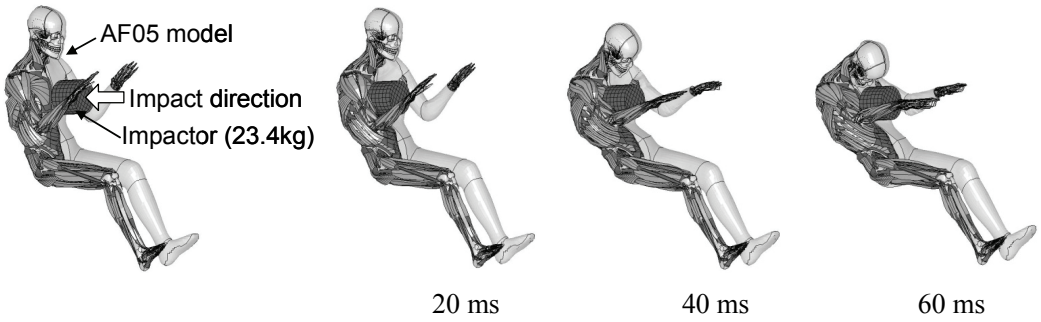

(a) Simulation setup (b) Impact behaviors (impact speed:6.9 m/s)

Figure 6. Hub impact simulation for thorax of elderly AF05 model.

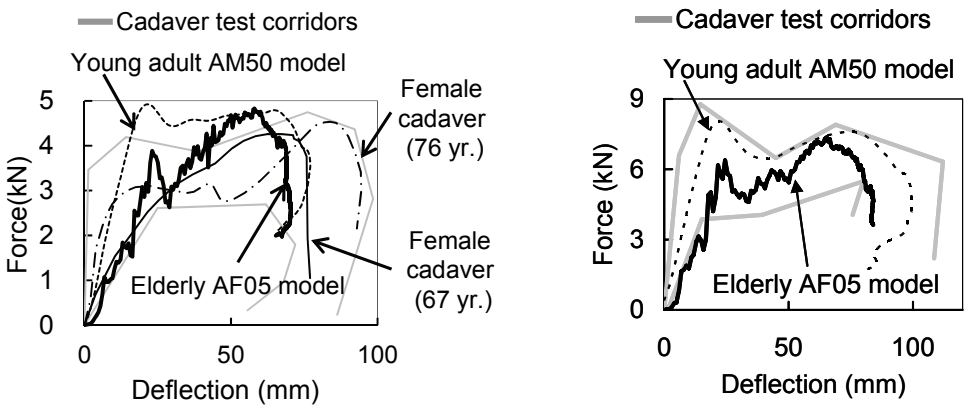

(a) 6.9 m/s (b) 9.9 m/s

Figure 7. Comparison of thoracic force-deflection curves between simulation results and test data.

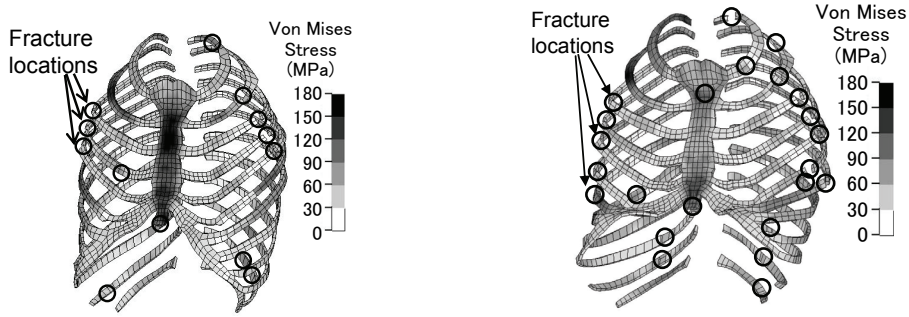

(a) 6.9 m/s (b) 9.9 m/s

Figure 8. Stress distributions of the ribcage with bone fracture locations of elderly AF05 model.

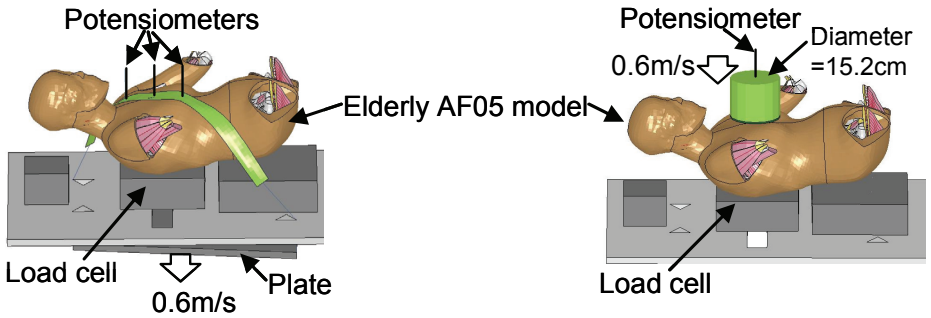

(a) Single shoulder belt (b) Hub impactor

Figure 9. Simulation setups for two cases of hub and single shoulder belt loadings.

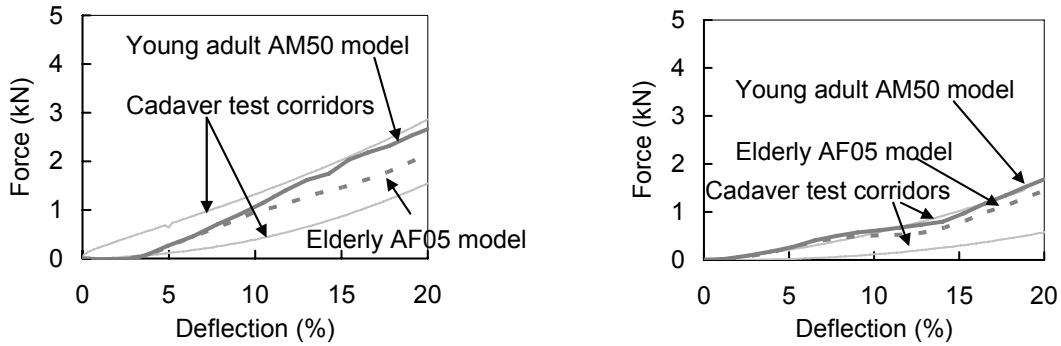

(a) Single shoulder belt (b) Hub impactor

Figure 10. Comparison of force-deflection curves in thorax between simulation results and test data.

test. Thoracic response was characterized using the deflection at the midline of the sternum and a load cell mounted between the subject and the loading table. Simulation setups using the human body FE model carefully reproduced the abovementioned experimental setups. Figure 9 shows simulation setups for the two cases of hub and single shoulder belt loadings. Figure 10 shows simulation results of the posterior reaction forces and chest deflection compared with test corridors. Simulation results generally fell within test corridors in both cases.

Abdominal responses in frontal impacts

Nusholtz et al. (1994) conducted abdominal frontal impact tests using three cadavers of a 63 years old male with a height of 180cm and a weight of 70.1 kg, a 46 years old male with a height of 176 cm and a weight of 50.0 kg, and a 55 years old female with a height of 162 cm and a weight of 70.3 kg. Figure 11(a) shows a simulation setup to reproduce the experimental cadaver tests, in which the impactor simulated a lower half of a steering wheel. In this simulation, the mass and initial velocity of the impactor were set to 18 kg and 10 m/s, respectively. Figure 11 (b) shows comparison of abdominal force-deflection curves between simulation results and test data. Predicted force-deflection curve of the elderly AF05 model was similar to that of the 55 years old female cadaver. The initial slope of the force-deflection curve of the elderly AF05 model was lower than that of young adult AM50 model. These differences are probably because the body mass and abdominal thickness of the elderly AF05 model were smaller than those of the young adult AM50 model.

Head-neck responses during rear impacts

The elderly AF05 model was validated against cadaver test data on head-neck responses during a low-speed rear impact. White et al. (2009) investigated head-neck responses during rear impact with a velocity of 8 km/h using two cadavers of a 41 years old male with a height of 180 cm and a weight of 99 kg and a 64 years old male with a height of 176 cm and a weight of 82 kg. They showed head C.G. (Center of Gravity) angle time histories of the cadavers. Ono et al. (1997) performed a series of volunteer tests to investigate head-neck responses during rear impact with the same velocity of 8 km/h as White et al. and with almost the same experimental conditions. In this study, we performed simulations to predict head-neck responses during the rear impact situation. The accelerations of X direction (posterior-anterior) and Z direction (inferior-superior) at T1 and angle time histories

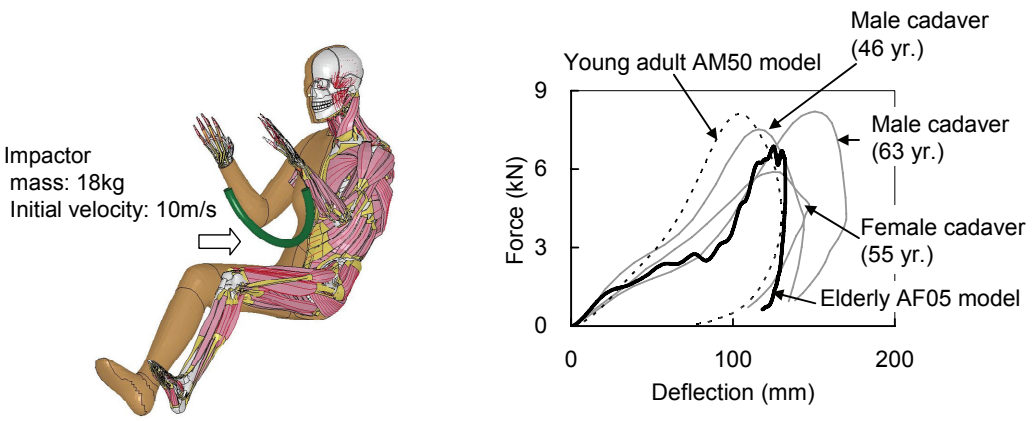

(a) Simulation setup (b) Force-deflection curves

Figure 11. Abdominal impact simulations using an impactor simulating a steering wheel.

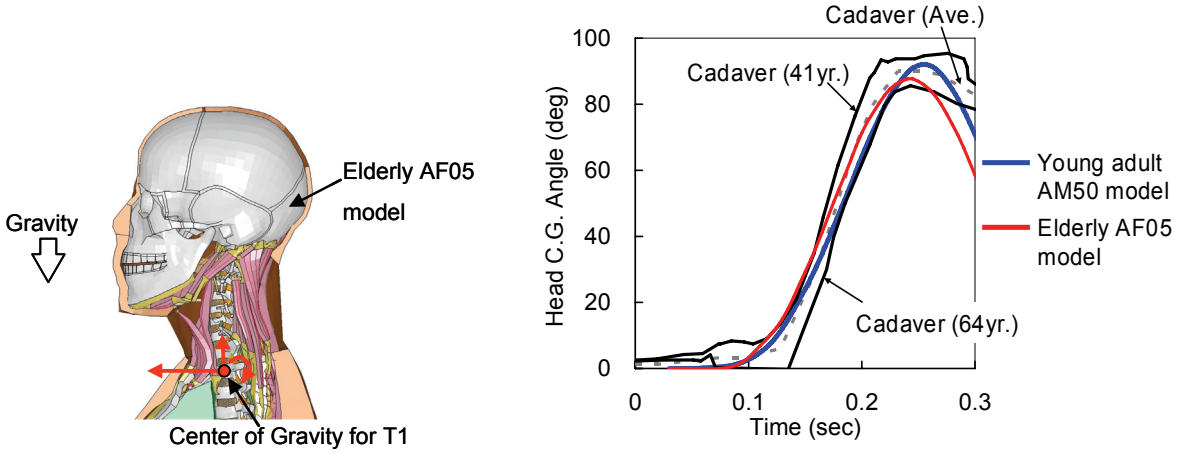

(a) Simulation setup (b) Comparison of head C.G. angle time histories

Figure 12. Low-speed rear impact simulations with a velocity of 8km/h.

around Y axis obtained from the volunteer tests were given to the T1 in two models of young adult AM50 model and elderly AF05 model. Figure 12(a) shows a simulation setup of the low-speed rear impact. Figure 12(b) shows comparison of head C.G. rotational angle between simulation results using the two models and experimental test data. The two simulation results show good agreement with cadaver test data, although there are some differences after peak head C.G. rotational angle. In addition, the peak head C.G angle of the elderly AF05 model was close to that of elderly cadaver (64 years old) while the peak head C.G angle of young adult AM50 model was close to that of the average angle-time history curve of two cadaver tests. Therefore, the elderly AF05 model has a possibility to simulate head-neck motions of elderly occupants during low-speed rear impacts.

AGING EFFECTS OF MUSCULAR FORCES FOR IMPACT RESPONSES

Aging effect of muscular forces for thoracic impacts

In emergency braking before an impact, well-trained drivers do braking by activating agonists and antagonists efficiently while beginner drivers do braking by activating both agonists and antagonists simultaneously. In the latter cases, the activation levels have a tendency to be larger than in the former cases. In this study, we hypothesized that drivers cannot control agonists and antagonists in the worst cases of emergency braking so that the activation levels of agonists and antagonists could be the same. We investigated how muscle activation levels could affect cadaveric impact responses for the thorax under the same simulation conditions conducted by Kent et al. (2004) and Kroell et al. (1971) described previously when drivers took the activation levels in the worst cases of emergency braking. The same muscle activation level was inputted to all agonist and antagonist muscles in the trunk under the same simulation conditions of the thoracic impacts. The

activation level was set to 0.2 (20 %), which was the average of activation levels of the trunk muscles or lower extremity muscles measured in the volunteer tests on driver's bracing that we conducted previously (Iwamoto et al. 2011).

Figure 13 compared thoracic force-deflection curves of simulation results with and without muscle activation under the thoracic impact conditions of Kent et al. (2004). The figure includes simulation results of the young adult AM50 model and the elderly AF05 model. In both models, the slope of force-deflection curve with muscle activation was larger than that without muscle activation. The muscle activation tends to increase the thoracic stiffness. In addition, the thoracic stiffness of the elderly AF05 model was much lower than that of the young adult AM50 model in the case with muscle activation. Figure 14 shows comparison of the maximum thoracic deflection at 1kN loading obtained from the force-deflection curves of Figure 13 between the young adult AM50 model and the elderly AF05 model. The maximum thoracic deflections of the elderly AF05 model without muscle activation was three times and two times larger than those of the young adult AM50 model with muscle activation in the cases of hub impactor loading and single shoulder belt loading, respectively. These results suggest that the elderly female occupants in passenger seats who are not easy to brace their bodies before impacts tend to have more thoracic deflection than young adult males in driver seats who are relatively easy to brace their bodies in frontal impacts. Figure 15(b) shows muscle tensing influence on peak force as a function of the maximum thoracic deflection in hub impactor loadings. The figure includes simulation results with a low-speed of 0.6 m/s for the impact condition of Kent et al. (2004) and a high-speed of 6.9 m/s for the impact condition of Kroell et al. (1971). Thoracic forces for thoracic deflections of 5, 10, 15, 20 % with and without activation were obtained as shown in Figure 15(a) and the percent increase of the force

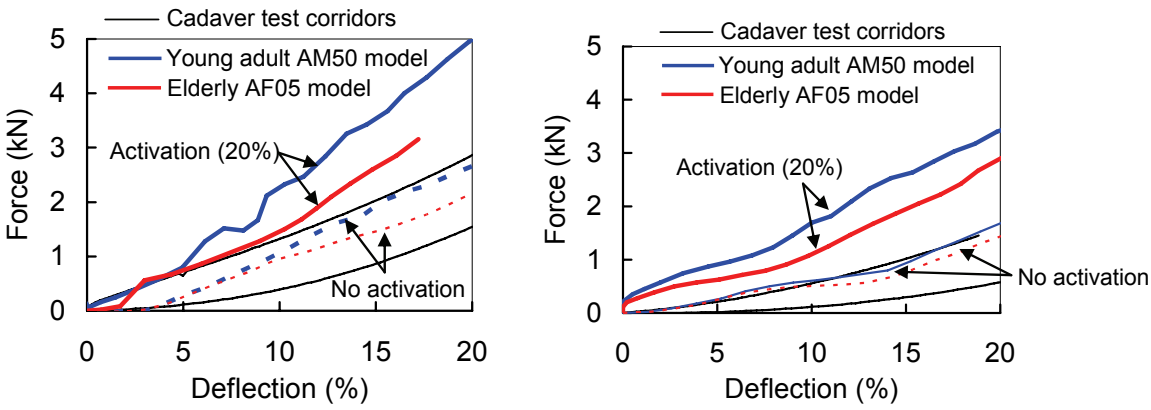

(a) Single shoulder belt (b) Hub impactor

Figure 13. Comparison of thoracic force-deflection curves of simulation results with and without muscle activation in thoracic impacts.

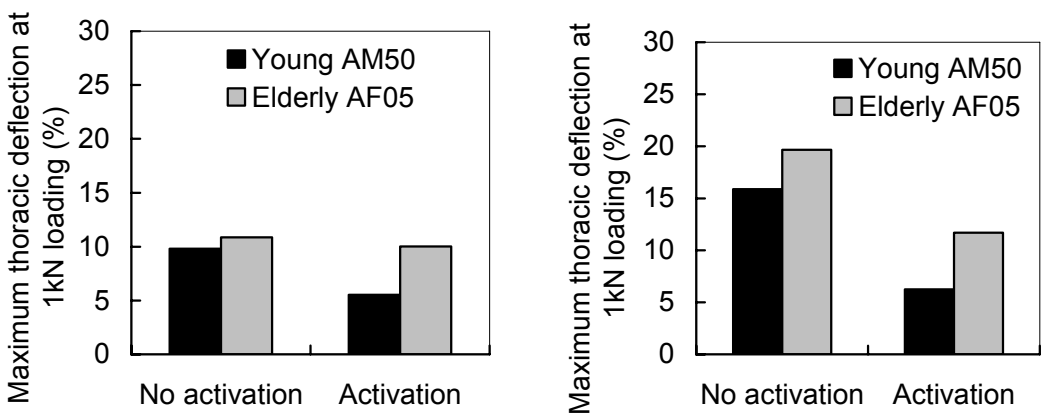

(a) Single shoulder belt (b) Hub impactor

Figure 14. Comparison of the maximum thoracic deflection at 1kN loading between young adult AM50 model and elderly AF05 model.

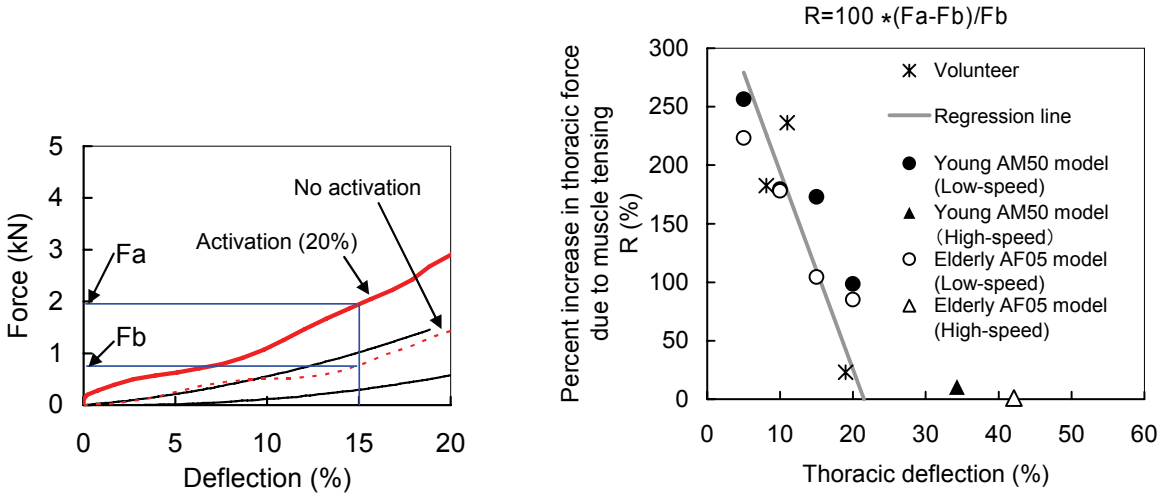

(a) Calculation method of percent increase (b) Comparison of percent increase in thoracic force

Figure 15. Muscle tensing influence on peak force as a function of the maximum thoracic deflection in hub impactor loadings.

with activation for the force without activation was calculated and plotted on the graph of Figure 15(b). The graph also includes human volunteer test data. The original human volunteer test data were obtained from Stalnaker et al. (1973). The percent increases of thoracic force due to muscle tensing predicted by both models of young adult AM50 model and elderly AF05 model were almost along the regression line in low-speed hub impactor loadings while the percent increase of thoracic forces predicted by both models were almost zero in high-speed hub impactor loadings. Therefore, the model has a possibility to estimate muscular effects on the thoracic impact responses.

Aging effect of muscular forces for head-neck responses during rear impacts

In rear impact scenarios of real-world accidents, the occupants are supposed to activate their neck muscles to maintain their postures for impact decelerations inattentively or attentively. Therefore, activation level of each neck muscle should be estimated to predict head-neck responses during rear impacts. In controlling activation level of each muscle to achieve an objective motion or posture, the calculation method such as optimization needs to repeat simulations with try and error. Therefore, computational cost for one cycle simulation should be reduced. We newly developed a musculo-skeletal FE model of elderly AF05 in a simple form that the skeletal parts were modeled by rigid bodies and the articulated joints were modeled with mechanical joints in addition to muscles modeled by only bar elements. The model was created by scaling down a musculo-skeletal FE model of AM50, which we developed previously (Iwamoto et al. 2012), to adjust the size of AF05. The model includes 8 cervical joints including C7-T1 joint and 23 neck muscles such as Longus Colli and Splenius Capitis. Each joint was modeled with a non-linear torque-angle property obtained from the literature (Panjabi et al. 1976). Since Kuhlman et al. (1993) reported that the cervical range of motion in elderly females with ages from 70 to 90 years old was 27 % smaller than that of young adult males with ages from 20 to 30 years old, we changed the non-linear torque angle property of the musculo-skeletal FE model of elderly AF05 to represent the difference. Each muscle was modeled using Hill type muscle material (LS-DYNA Material type 156, MAT_MUSCLE) with the maximum contraction force, passive and active force-elongation curves, and an active force-velocity curve obtained from Thelen et al. (2003). The PCSA of each muscle of the elderly female described in Table 1 was inputted to the corresponding muscle of the musculo-skeletal FE model of elderly AF05. Each muscle was connected with tendons at both sides of the muscle, which formulated muscle paths between the origin and the insertion points. The tendons were modeled with tension only non-linear stress-strain curves (LS-DYNA Material type B01, MAT_SEATBELT). The muscle included only one bar element (actually truss element) while the tendons included multiple seatbelt elements with a via-point on each side to represent muscular alignments and moment arm of the muscle based on anatomical references (Neumann, 2002). As a result, the 23 neck muscles included 90 muscular lines with bar elements and seatbelt elements on right side of head-neck region. For the simplicity of the musculo-skeletal FE model, no other tissues including skin and flesh, which might change the muscle paths and magnitudes of moment arms, were

directly represented in this study, because the musculo-skeletal FE model consisting of skeletal parts, joints, and muscles was supposed to be enough to represent gross motions of human body during impacts. In this study, the head rotational angle can be calculated as a rotational angle change around the head C.G.. The rotational angle corresponds to a rotational angle change of a line through the head C.G. that is parallel to the Frankfurt-plain line connecting infraorbitale to the external auditory meatus.

Authors previously proposed the reinforcement motion learning model with the synergy control policy between multiple muscles, which is modeled on the multiple muscle control function of Corticospinal motoneurons in cerebral cortex (Min et al., 2012). This model can robustly control the motion against external force. Based on this model, the system applied to the whole human body FE model was developed for estimating occupant motions and impact responses in crash situations (Iwamoto et al. 2012). The reinforcement learning (RL) is controlled in basal ganglia, which plays an important role for posture maintenance (Takakusaki et al., 2003). For accurate estimation of occupant postures in various occupant conditions including inattentive and attentive conditions under inertial environments with impact decelerations, the proposed learning model could be useful. Figure 16 shows a muscle control system for head-neck posture stabilization using this learning model. The system was developed using C++ program. The system produces control function of each muscle around a pre-determined articulated joint to hold the posture on a pre-determined target position. Three steps are necessary to perform the muscle control simulations under the inertial environments. Firstly, joint angle range and joint angular velocity range around a pre-determined target joint angle of 0 degree, should be determined, which were set to a range from -80 to 80 degrees and a range from -1600 to 1600 degrees/sec in this paper, respectively. The system provides the head C.G. with a boundary prescribed motion to rotate the head with the range around the head C.G.. Since each vertebra is connected by the associated articulated joints in the head-neck region, each vertebra in the head-neck region can rotate by the rotation around the head C.G.. Then the system creates a database including positions of the skeletal part, the joint, and muscle bar elements within the joint angle range. Secondly, after initial angle is randomly determined among the joint angle range, activation level of each muscle randomly generated by agent of RL is transferred to the muscle of a musculo-skeletal FE model via an interface, and then the musculo-skeletal FE model performs a motion around the joint using LS-DYNA. As a result, the information on the position, joint angle, and velocities of the joint and a target point is transferred to the agent via the interface. Then, the agent estimates the muscle control function as feedback controller, which outputs activation level of the muscle with the motion state consisting of joint angle and joint angular velocity (cf. Figure 16). This routine is repeated until stably controlling the motion for a goal with learning the optimal control policy. Thirdly, under an impact deceleration condition, activation level of each muscle obtained by inputting the current joint angle and joint angular velocity to the optimal control function of the muscle is given to the muscle model so that the human body motion is estimated. The detailed description of this learning model is found in the authors publications (Iwamoto et al.2012, Min et al. 2012).

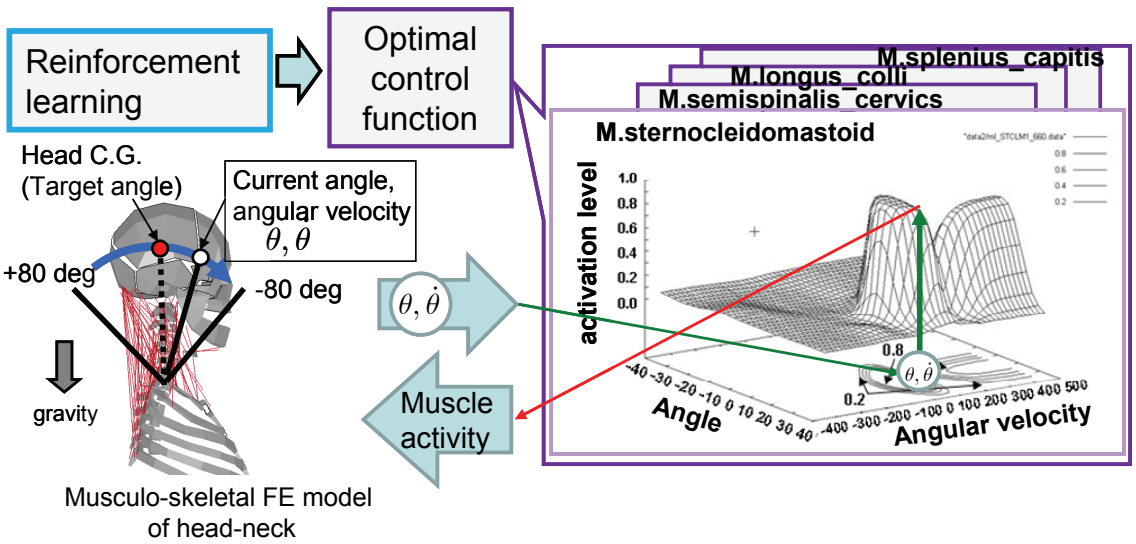

Figure 16. Muscle control system for head-neck posture stabilization using RL

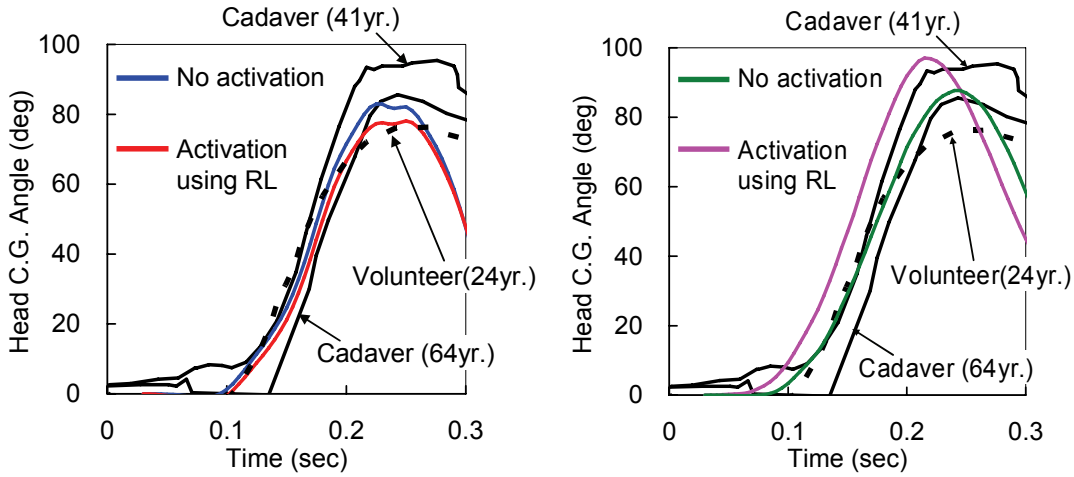

(a) Musculo-skeletal model (b) Muscular solid model

Figure 17. Head C.G. angle time histories in low-speed rear impact simulations using elderly AF05 model with and without muscle activation.

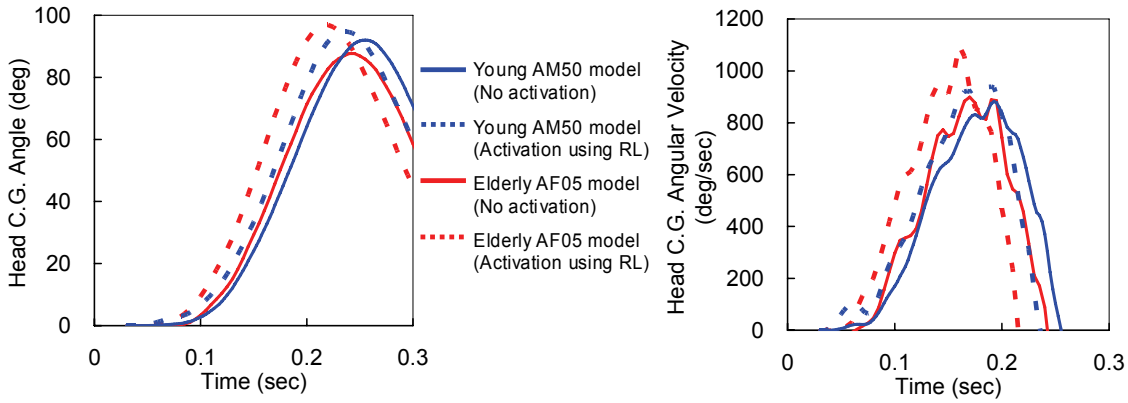

(a) Head C.G. angle (b) Head C.G. angular velocity

Figure 18. Comparison of time histories of head C.G. angle and angular velocity (Muscular solid model).

The musculo-skeletal FE model of elderly AF05 and the muscle controller with the proposed motion learning model were used for estimation of head-neck responses during a rear impact with a velocity of 8km/h as described previously. Figure 17(a) shows comparison of head C.G. rotational angle between simulation results and experimental test data. Figure 17(a) includes simulation results using the elderly AF05 model without activation and with activation levels obtained from the muscle controller.

Figure 17(a) also includes two cadaver test data obtained from White et al. (2009) and one volunteer test data obtained from Ono et al. (1997). The peak head C.G. angle of simulation result without muscle activation was close to that of elderly cadaver test data while the peak head C.G. angle of simulation result with RL was close to that of the volunteer test data. Muscle activation decreased the peak head C.G. angle by 5.0 degrees. The muscle activation level of each muscle obtained from the muscle controller was inputted to the corresponding muscle of the elderly AF05 model with the muscular solid elements shown in Figure 12(a), hereafter called muscular solid model, in the rear impact simulations. The activation level was also inputted to the muscular solid model of young adult AM50 to investigate aging effect of muscular forces for impact responses. Figure 17(b) shows comparison of head C.G. rotational angle between simulation results using the elderly AF05 model with and without activation. The peak head C.G. angle of simulation result of muscular solid model was close to that of musculo-skeletal model in the case without activation. On the other hand, the peak head C.G. angle of muscular solid model was different from that of musculo-skeletal model in the case with activation. This inconsistency is due to difference in modeling muscles and joints between two models of musculo-skeletal model and muscular

solid model. Figure 18 shows comparisons of time histories of head C.G. angle and angular velocity among four simulation results of the elderly AF05 model and the young adult AM50 model with and without activation. The head rotated earlier in the elderly AF05 model with activation than in the young adult AM50 model with activation by 22 msec. This is because the peak head C.G. angular velocity of the elderly AF05 model with activation were the largest among the four simulations, and was larger than the young adult AM50 model with activation by 158 degrees/sec as shown in Figure 18(b). The simulation results suggest that weak muscular forces of the elderly AF05 model with smaller PCSA could rotate the head rearward easily during rear impacts.

CONCLUSIONS

Elderly female occupants are most susceptible to injuries, especially on thorax and head-neck regions, based on previous studies using automotive accident data. This study developed a finite element (FE) model of 5th percentile female (AF05) with multiple muscles, and inputted material properties of elderly people to bones in ribcage and lower extremities, cervical spine discs, muscles of whole body to elucidate injury mechanism of elderly female occupants.

The developed elderly AF05 model was firstly validated against some cadaver test data on thoracic deformation in frontal impacts and head-neck responses in a low-speed rear impact. The model was secondly used for investigation on effect of muscle activation for the impact responses. Several comparisons between the elderly AF05 model and the young adult AM50 model showed that lower strength of bones and smaller PSCA of each muscle in the elderly AF05 could increase thoracic deflection. Those comparisons also suggest that the elderly AF05 could not prevent the head from rotating rearward due to the weak muscular forces compared with the young adult AM50.

Although the elderly AF05 model has some limitation on lack of experimental data for validations and the inconsistency in human body kinematics between the musulo-skeletal FE model and the muscular solid model, it has a promising tool for better understanding of injury mechanisms of elderly female occupants.

REFERENCES

[1] Agur, A.M.R., Dalley II, A.F. 2005. Grant's Atlas of Anatomy; 11th Edition, Lippincott Williams & Wilkins, Baltimore, Maryland.

[2] Begeman, P., King, A.I., Levine, R., Viano, D.C. 1980. "Biodynamic Response of the Musculoskeletal System to Impact Acceleration" Stapp Car Crash Conference, No.801312, 479-509.

[3] Behr, M., Arnoux, P-J., Serre, T., Thollon, L., Brunet, C. 2006. "Tonic Finite Element Model of the Lower Limb" Journal of Biomechanical Engineering, Vol. 128, 223-228.

[4] Bougie, J.D., Morgenthal, A.P. 2001, The Aging Body: conservative care for common neuromusculoskeletal conditions, McGraw-Hill Companies, Inc.

[5] Brolin K. 2003, "Neck injuries among the elderly in Sweden", Injury Control and Safety Promotion, Vol.10, No.3, 155-164.

[6] Brumbelow, M. L., Zuby, D.S. 2009. "Impact and Injury Patterns in Frontal Crashes of Vehicles with Good Ratings for Frontal Crash Protection", 21st ESV Conference, No.09-0257.

[7] Carlson, G.D., Botte, K.J., Josephs, M.S., Newton, P.O., Davis, J.L.W., Woo, S.L-Y. 1993. "Morphologic and biomechanical comparison of tendons used as free grafts", Journal of hand surgery, Vol.18A, No.1, 76-82.

[8] Ejima, S., Zama, Y., Ono, K., Kaneoka, K., Shiina, I., Asada, H. 2009. "Prediction of Pre-Impact Occupant Kinematic Behavior Based on the Muscle Activity during Frontal Collision" 21st ESV Conference, No.09-0913.

[9] El-Jawahri, R.E., Laituri, T.R., Ruan, J.S., Rouhana, S.W., Barbat, S.D. 2010, "Development and Validation of Age-Dependent FE Human Models of a Mid-Sized Male Thorax, Stapp Car Crash Journal, Vol.54, 407-430.

[10] Gans, C. 1982. "Fiber architecture and muscle function" Exercise and Sports Sciences Reviws, 10, 106-107.

[11] Institute for Traffic Accident Research and Data Analysis, 2007, "Accident injury of elderly drivers of four wheel vehicles", ITARDA Information, No.71, (in Japanese)

[12] Ito, O., Dokko, Y., Ohashi, K. 2009, "Development of Adult and Elderly FE Thorax Skeletal Models", SAE Paper, No.2009-01-0381.

[13] Iwamoto, M., Kisanuki, Y., Watanabe, I., Furusu, K., Miki, K., Hasegawa, J. 2002. "Development of a Finite Element Model of the Total Human Model for Safety (THUMS) and Application to Injury Reconstruction" IRCOBI Conference, 31-42.

[14] Iwamoto, M., Nakahira, Y., Tamura, A., Kimpara, H., Watanabe, I., Miki, K. 2007, "Development of Advance Human Models in THUMS", Proc.6th European LS-DYNA Users' Conference. 47-56.

[15] Iwamoto, M., Nakahira, Y., Sugiyama, T. 2011, "Investigation of pre-impact bracing effects for injury outcome using an active human FE model with 3D geometry of muscles, 22nd ESV Conference, No.11-0150.

[16] Iwamoto, M., Nakahira, Y., Kimpara, H., Sugiyama, T., Min, K. 2012, "Development of a

Human Body Finite Element Model with Multiple Muscles and their Controller for Estimating Occupant Motions and Impact Responses in Frontal Crash Situations", Stapp Car Crash Journal, Vol.56, 231-268.
[17] Kemper, A. R., McNally, C., Kennedy, E. A., Manoogian, S. J., Rath, A. L., Ng, T. P., Stitzel, J. D., Smith, E. P., Duma, S. M. 2005, "Material properties of human rib cortical bone from dynamic tension coupon tenting". Stapp Car Crash Journal, vol.49, 199-230.
[18] Kent, R., Lessley, D., Sherwood, C. 2004. "Thoracic Response to Dynamic, Non-Impact Loading from a Hub, Distributed Belt, Diagonal Belt, Double Diagonal Belts" Stapp Car Crash Journal, Vol.48, 495-519.
[19] Kimpara, H., Lee, J.B. Yang, K.H., King, A.I. Iwamoto, M., Watanabe, I., Miki, K. 2005, "Development of a Three-Dimensional Finite Element Chest Model for the 5th Percentile Female", Stapp Car Crash Journal, Vol.49, 251-269.
[20] Krafft, M., Kullgren, A., Lie, A., Tingvall C. 2003, "The risk of whiplash injury in the rear seat compared to the front seat in rear impacts", Traffic Inj. Prev., Vol.4, No.2, 136-140.
[21] Kroell, C. K., Schneider, D. C., and Nahum, M.1971, "Impact Tolerance and Response of the Human Thorax", SAE Paper No. 710851.
[22] Kuhlman, K.A.1993, "Cervical range of motion in the elderly", Arch. Phys. Med. Rehabil. Vol.74, 1071-1079.
[23] Liu,C., Utter, D., Chen. C.-L. 2007, "Characteristics of Crash Injuries Among Young, Middle-Aged, and Older Drivers", NHTSA Technical Report, No. DOT HS 810 857.
[24] Malik, S.A., Murphy, M., Connolly, P., O'Byrne, J. 2008, "Evaluation of morbidity, mortality and outcome following cervical spine injuries in elderly patients", Eur. Spine. J., 17, 585-591.
[25] Min, K., Kimpara, H., Iwamoto, M. 2012, "Load Response Simulation of Human Arm Musculo-Skeletal FE Model with the Learning of Muscle Synergy Control Policy", Neural Networks, submitted, 2012.
[26] National Institute of Population and Social Security Research, 2012, "Population projection for Japan in 2011-2060" (in Japanese)
[27] Neumann, D.A. 2002, Kinesiology of the Musculoskeletal System: Fundations for Physical Rehabilitation, Mosby Inc.
[28] Nusholtz, G., and Kaiker, P. 1994, "Abdominal Response to Steering Wheel Loading", Proc. the 14th ESV Conference, 118-127.
[29] Ono, K., Kaneoka, K., Wittek, A., Kajzer, J. 1997, "Cervical Injury Mechanism Based on the Analysis of Human Cervical Vertebral Motion and Head-Neck-Torso Kinematics during Low Speed Rear Impacts", Proc. of the 41st Stapp Car Crash Conference, 973340, 339-356.
[30] Panjabi, M.M., Brand, R.A., White, A.A.1976, "Mechanical Properties of the Human Thoracic Spine", The Journal of Bone and Joint Surgery, 642-652.
[31] Rosen, C.J., Glowacki, J., Bilezikian, J.P. (eds.) 1999, The Aging Skeleton, Academic Press
[32] Simamura, M., Ohhashi, H., Yamazaki, M. 2003. "The Effects of Occupant Age on Patterns of Rib Fractures to Belt-Restrained Drivers and Front Passengers in Frontal Crashes in Japan" Stapp Car Crash Journal, Vol.47, 349-365.
[33] Snyder, R.G., Chaffin, D.B., Foust, D.R. 1975. "Bioengineering Study of Basic Physical Measurements Related to Susceptibility to Cervical Hyperextension-Hyperflexion Injury, UM-HSRI-BI-75-6.
[34] Stalnaker, R.L., McElhaney, J.H., Roberts, V.L., Trollope, M.L.1973, "Human Torso Response to Blunt Trauma, Human Impact Response, Measurement and Simulation", 181-199, PLENUM PRESS, New York-London.
[35] Takakusaki, K., Habaguchi, T., Ohtinata-Sugimoto, J., Saitoh, K., Sakamoto, T. 2003, "Basal Ganglia Efferents to the Brainstem Centers Controlling Postural Muscle Tone and Locomotion: A New Concept for Understanding Motor Disorders in Basal Ganglia Dysfunction", Neuroscience, 119, 293-308.
[36] The General Insurance Association of Japan, 2004, "Current and future state of automotive accidents involving senior drivers" (in Japanese)
[37] Thelen, D. G. 2003. "Adjustment of Muscle Mechanics Model Parameters to Simulate Dynamic Contractions in Older Adults" Transaction of the ASME, Vol.125.
[38] White, N.A. Begeman, P.C., , Hardy, W.N., Yang, K.H., Ono, K., Sato, F., Kamiji, K., Yasuki, T., Bey, M.J. 2009, "Investigation of Upper Body and Cervical Spine Kinematics of Post Mortem Human Subjects (PMHS) during Low-Speed, Rear-End Impacts", SAE 2009-01-0387.
[39] Winters, J.M. 1990. "Hill-Based Muscle Models" A System Engineering Perspective; Multiple Muscle Systems: Biomechanics and Movement Organization, Winters, J.M. and Woo. S. (eds.), New York, Springer, 69-93 and 726-749.
[40] Yaguchi, M., Omoda, Y., Ono, K., Masuda, M., Onda, K. 2011, "Traffic accident analysis towards the development of an advanced frontal crash test dummy indispensable for further improving vehicle occupant protection performance", 22nd ESV Conference, No. 11-0221.
[41] Yamada, H. 1970. Strength of Biological Materials; Williams & Wilkins Company.
[42] Yee, W.Y., Cameron, P.A., Bailey, M.J. 2006, "Road traffic injuries in the elderly", Emerg. Med., J. 23, 42-46.

EVALUATION OF AN ACTIVE MULTI-BODY HUMAN MODEL FOR BRAKING AND FRONTAL CRASH EVENTS

Riske Meijer
Hala Elrofai
Jeroen Broos
TNO, Netherlands Organisation for Applied Scientific Research
The Netherlands
Edwin van Hassel
TASS, TNO Automotive Safety Solutions B.V.
The Netherlands
Paper Number 13-0163

ABSTRACT

Active safety systems that start to act moments before the crash might be capable of anticipating the occupant's position, either by correcting it, or by taking the out-of-position into account. For the development and evaluation of such active safety systems, recently a run-time efficient multi-directional computer human model that can simulate active as well as passive human behaviour has been developed. The objective of this study was to evaluate this so-called active human model for simulations of braking followed by a frontal crash.
Simulations of published PMHS blunt frontal impact tests on the head, thorax, and abdomen showed that the model is capable of predicting the PMHS peak responses within 20% deviation from the PMHS response corridors. Here, the active behaviour was switched off. Simulations of published 1 g to 15 g full-body frontal impact tests with belted volunteers showed that the model is capable of predicting the volunteer peak responses within 20% deviation from the volunteer response corridors. Here, values for the unknown parameters reaction time and level of bracing in the neck (co-contraction of neck muscles) were assumed.
Also, simulations with the active human model in a car interior to which high severity impacts were applied (pulses from Euro NCAP car-barrier frontal impact tests), with and without preceding braking as well as with active behaviour switched on and switched off were performed. The results of these simulations showed that the model is robust and sensitive to effects of braking and active behaviour, and the effects of braking on the injury values are dominant over the effects of the active behaviour itself. However, the active behaviour is indispensable for correct simulation of the human pre-crash kinematics.
From this study it was concluded that the current active human model is capable of simulating realistic human full-body kinematics as well as realistic injury values for the head and the thorax in one single simulation of braking followed by a frontal crash. As such, the current active human model can be used for evaluating the effectiveness of active safety systems in frontal impacts.

INTRODUCTION

If an occupant is out-of-position (due to e.g. onset of rollover, vehicle dynamics or a secondary human task) just before a car crash, the outcome of the injury may be a lot worse than in a normal driving posture for which the restraint systems were designed [1]. Active safety systems that start to act moments before the crash, might be capable of anticipating the occupant's position, either by correcting it, or by taking the out-of-position into account. As examples, a system accelerating the occupant rearward prior to a frontal collision in combination with a reversible belt pretensioner may result in an optimal position of an occupant at the time the crash occurs [2], and a reactive reversible belt pre-pretensioner that was designed to provide benefit in frontal, rearward and lateral crashes [3].
Thereby, several studies showed that the muscle activation significantly affects the kinematics in low severity impacts or pre-crash car movements. From volunteer sled tests at 2.5 G frontal impact a 47±12% decrease in head forward excursion due to bracing was observed, while it was 36±12% at 5.0 G [4]. In lap-belt only frontal sled tests up to 1.0 G it was shown that being tensed reduces head and neck flexion to nearly zero, while flexion of the lower spine was substantially reduced as well [5]. Based on vehicle driving tests in normal traffic, it was observed that head excursion and head flexion were much smaller when drivers applied the brakes themselves versus surprise autonomous braking [6]. As such, the various states of awareness and reactions of drivers and occupants on the impending crash should be taken into account in the development of active safety systems.
In order to evaluate the effect of an active safety system during the crash, it would be most effective if a human model for pre-crash kinematics could also predict the kinematics as well as the risk of

sustaining injuries during the crash. For this aim, recently, a run-time efficient multi-directional computer human model that can simulate active as well as passive human behaviour has been developed [7]. The objective of this study was to evaluate this so-called active human model for simulations of braking followed by a frontal crash.

METHODS

The Active Human Model

The active human model evaluated in this study is version 1.1 [8] available in the multi-body and finite element software package MADYMO version 7.4.1 [9]. The development of this model, which is based on earlier developed MADYMO whole body human models and human segment models, is described in [7]. A detailed description of this model can be found in [8]. The active human model in a frontal crash simulation is shown in Figure1. Below follows a short description of this model.

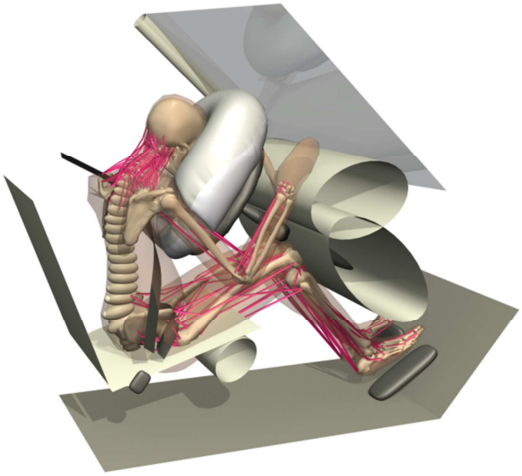

Figure1. MADYMO Active Human Model.

For run-time efficiency and for focussing on kinematics and global injury criteria only multi-body techniques are used in this model. The model consists of 186 bodies (178 rigid bodies and 8 flexible bodies). Inertial properties of the human body segments are represented fully by the inertial properties of the rigid and flexible bodies. The body segments are connected by kinematic joints representing the articular joints in a human body. For modelling the interaction with the environment and for visual representation the outer surface of the whole human body as well as for many bones is represented by meshes of shell-type massless contact elements (further referred to as facets). These facets are connected to the rigid and/or flexible bodies. The ribcage and the hand bones are not represented by facets, and the spinal vertebrae are represented by ellipsoids. The contact force and penetration of the model is calculated from stress-strain functions defined for the facets of the outer surface as well as for the underlying bones in the arms, legs and thorax. Since the bones were defined much stiffer than the outer surface, the penetration is dependent on the location of the contact at these body parts. For the rest of the body parts a combined flesh and bone stress-strain function was defined. The thorax includes flexible bodies for modelling the high deflection that can be seen at the ribcage and abdomen in frontal and side impacts.

For modelling active behaviour Hill-type muscle elements [10] are included in the neck, arms and legs. Because of the complexity of the musculature of the spine, the active behaviour of the spine is modelled by actuators on the vertebral joints. The muscle elements have a realistic curvature that is maintained during movements. Sensors in the model measure the position of the head, elbows, hips and spine. Based on the output of these sensors, control systems determine the activation levels for the various active elements in the model (muscles and actuators) to stabilise to a defined position. The control systems in the active human model are all based on the scheme illustrated in Figure2. Below, this basic control scheme is explained, followed by the implementation and some modifications per body part (neck, elbows, hips, and spine).

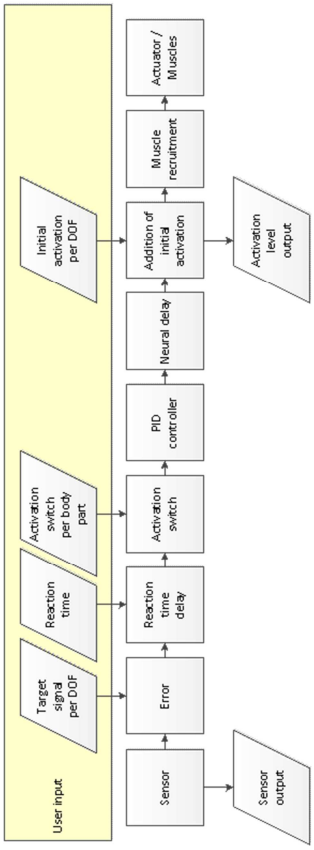

Figure2. Basic control scheme of the active human model.

For each degree of freedom that is controlled, a sensor is defined to measure the motion. Also, a target signal is defined which can be changed (to simulate e.g. voluntary or reflex movement), but which by default is 0 in order to stabilise towards the initial position. The control error is calculated as the difference between the sensor and target signals.
The next step is the reaction time. Here, the reaction time represents the time it takes for the human brain to start responding to any new event. This includes the time needed for sensing, transfer of the signal to the brain, and processing in the brain. The reaction time is implemented such that:
• Control errors related to pure stabilising behaviour, without any new events, cause a direct response;
• New events cause a response with a delay of the reaction time.
New events are automatically detected by the active human model. A new event is defined as any external load causing a control error that is larger than the maximum error occurred in the simulation up to the current time step. If the error remains below the maximum, the signal is transferred directly, but if the error is above the maximum, it is limited to the maximum during the reaction time before it increases further.
For each body part that is controlled the active behaviour can be switched on or off. This is done by multiplying the control signal with the activation parameter, where ‘0’ results in no active behaviour, and ‘1’ results in active behaviour.
Proportional-integral-derivative (PID) controllers aim to reduce the error by calculating a correcting load. The P-action changes the controller action based on the present error. The I-action makes sure the controller will reduce the error to zero by integrating the past errors. To damp out oscillations and reduce future errors the D-action makes the controller action larger, if the error is increasing, and smaller, if the error is decreasing.
After the PID-controller a neural delay is implemented. The neural delay represents the time it takes for the signal transfer from the brain to the muscle and the time it takes for the muscle to convert the signal into a force. This neural delay is defined as (Equation 1):

$$\frac{d(ouput)}{dt} = \frac{(input - output)}{\tau_{delay_time}} \quad (1).$$

For the controllers on the neck muscles τ_{delay_time} is set to 40 ms, for the controllers on the actuators of the spine and on the muscles in the arms to 70 ms, and for the controllers on the muscles in the legs to 100 ms. The neural delay behaves frequency dependent, i.e. signals with lower frequencies are transferred better than signals with higher frequencies.
For initial equilibrium initialisation of the controllers is required. In order to achieve this, initial activation levels need to be defined from the output of a settling simulation in which the model is run with only gravity applied to find an equilibrium. The initial activation levels are added to the controller signals. The last step in the control scheme is different per body part, and explained below.
The neck controller acts in three degrees of freedom, being the three rotations of the head. Depending on the user settings, the head rotations are either calculated relative to the reference space, to keep the head upright, or relative to T1, to keep the neck straight. The muscle recruitment table for the neck was taken from the model of [11]. For the neck the recruitment table is balanced, which means that an error in one degree of freedom results in a torque in only that degree of freedom. Besides the control on the three degrees of freedom of the head, also co-contraction of neck muscles can be defined. Co-contraction is the simultaneous tension of all muscles without giving any resultant torques. Co-contraction will always be present to some extent, and is possibly higher if a person is tensed and/or bracing. In the active human model the co-contraction level can be defined in the initial input as a relative value (0-1) of the maximum possible muscle activation. The co-contraction level is included in the calculation of the muscle recruitment, and is balanced for any pitch angle. For the co-contraction the reaction time and neural delay can be switched off in the user input in order to avoid the co-contraction building up from zero during the first part of the simulation.
The controllers on the left and right elbow each act in only one degree of freedom per side, being the elbow flexion-extension. The muscle recruitment for the elbow divides the muscles in a group of flexors and a group of extensors and activates all muscles in one group to the same extent.
The controllers on the left and right hip each act in three degrees of freedom, being the three rotations of the hip joint, flexion-extension, medial-lateral rotation, and abduction-adduction. The muscle recruitment table for the hip is set up such, that for a specific degree of freedom the muscles that have most effect in that degree of freedom are activated the most.
For the spine no target functions are defined. Hence, the rotation error for the spine is equal to the sensor output. The spine controller acts in three degrees of freedom per vertebra for each of the 5 lumbar and 12 thoracic vertebrae, so 17 vertebrae in total. For each vertebra sensors are defined to measure the angle of the vertebra relative to the sacrum (pelvis). The activation signal for each vertebra is then applied to that vertebra as well as

to the vertebrae below, such that the spine is in a stable position.

Comparison to Human Subjects in Frontal Impact Tests

The active human model's response was tested using almost all the human subject test data that was used for the human and segment models the model is based on, and new tests were added. The test data comprise of blunt impact tests on various body parts as well as full-body impact tests. Frontal, lateral, rear and vertical human subject loading tests at several loading severities and conditions are included. The simulation set-ups of these tests, the human subject responses or response corridors, and the simulation results were put together in an internally developed automated test suite in which the active human model's responses are compared to that of the human subjects. The tests as well as the active human model's responses compared to the human subject responses (or response corridors) are described and shown in a MADYMO Quality Report [12]. The test data are from published post mortem human subject (PMHS) tests as well as from published volunteer tests. In order to simulate the tests in a most biofidelic way, the post mortem human subject tests were simulated with the activation of all controlled body parts switched off (passive model), and the volunteer tests were simulated with the activation of all these body parts switched on (active model). By doing so, the passive behaviour of the model is tested with the PMHS tests, and the combined active and passive behaviour with the volunteer tests.
This study focuses on the evaluation of the active human model's response in braking and frontal impact. Therefore, a number of impact tests that are essential for the evaluation of the response in braking and frontal impact were selected from the test suite for this study. The selected tests comprise of PMHS blunt frontal impact tests on the head, thorax and abdomen at several loading severities (See Table1) as well as volunteer full-body frontal impact tests at several loading severities (See Table2). The 1 g car braking test (See test no 1 in Table2) and the 3.8 g frontal impact sled test (See test no 2 in Table2) are new tests added to the test suite of the active human model.

Table1.
PMHS blunt frontal impact tests

No	Body part	Impactor shape	Impactor mass [kg]	Impact velocity [m/s]	Ref.
1	head	rigid cylinder	23.4	2.0, 5.5	[13]
2	thorax	rigid disk	23.4	3.4, 5.8	[14]
3	thorax	rigid disk	23.4	4.9, 6.9, 9.9	[15], [16], [17]
4	thorax	rigid disk	10.4, 22.2	7.0, 9.9	[18], [19]
5	abdomen	rigid bar	31.4	6.9	[20]

Table2.
Volunteer full-body frontal impact tests

No	Test set-up	Subject position	Peak deceleration [g]	Ref.
1	car braking event	Seating occupant	1 during 1.7 s	[2]
2	sled rigid seat with 3-p belt	seating occupant	3.8	[21], [22]
3	sled rigid seat with 5-p belt	sitting straight-up	15	[23], [24], [25], [26]

Evaluation for Various Frontal Crash Scenarios

In order to evaluate the robustness as well as the sensitivity of the active human model for pre-crash braking followed by a crash, several frontal crash scenarios were simulated. The car interior consists of a seat with conventional 3-point belt (with retractor and load limiter) and airbag. The applied crash pulses were obtained from Euro NCAP 64 km/h 40% offset car-barrier frontal impact tests of three different car types, i.e. a small car with short bonnet, a large car with long bonnet, and a SUV. For confidentiality reasons the car types are not mentioned, and the crash pulses are not shown here.
For evaluating the effect of the active behaviour on the kinematics and the injury values of the model, simulations with the active human model with active behaviour switched on (active model) as well as switched off (passive model) for all body parts were performed. For evaluating the effect of braking on the kinematics and injury values all three simulations with the active model were repeated with a braking phase of 8.0 m/s^2 during 1 s preceding the same crash pulse.
A quantitative evaluation of the risk of injuries was not made, since the injury limits have not yet been validated for the active human model. Thereby, the car interior was not from an existing car, and was the same for all three pulses. However, the seat and

belt parameters were in the range of existing car seats and belts.

RESULTS

Comparison to Human Subjects in Frontal Impact Tests

The force-time responses of the head of the passive model in the blunt frontal head impact tests (See test no 1 in Table1) are compared to the PMHS response corridors in Figure3 and Figure4. Figure3 shows that the peak force as well as the timing of it in the 2 m/s impact are within the peak response corridors. Figure4 shows that the peak force of the head in the 5.5 m/s impact is 4% above the upper corridor, and the peak timing is within the peak response corridors. These simulation results indicate that the passive model's head is capable of predicting realistic forces-time responses of the human head in frontal impacts.

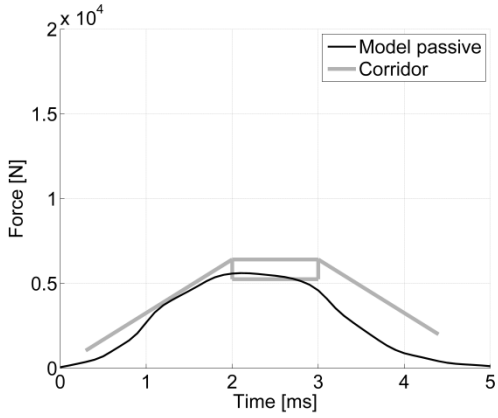

Figure3. PMHS response corridors and active human model (passive) response in blunt frontal head impact with 23.4 kg at 2 m/s.

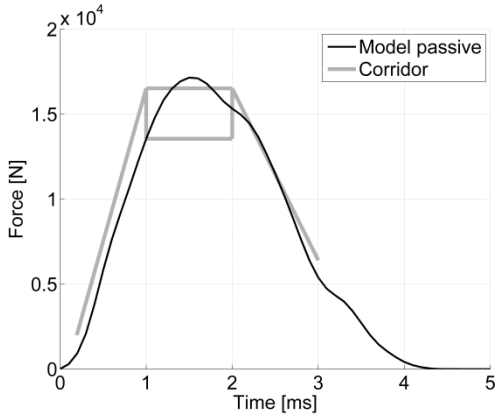

Figure4. PMHS response corridors and active human model (passive) response in blunt frontal head impact with 23.4 kg at 5.5 m/s.

The force-deflection responses of the thorax of the passive model in the blunt frontal thorax impact tests (See test no 2, 3 and 4 in Table1) are compared to the PMHS response corridors in Figure5 to Figure11. These figures show that in five of the seven thorax impact tests the peak force of the passive model is within the response corridors of the PMHS, and in the two most severe impacts (23.4 kg and 22.2 kg at 9.9 m/s) the peak forces are 4% below the peak of the lower corridor. These figures also show that in three impact tests the peak deflection is within the response corridors of the PMHS, in the three most severe impact tests (23.4 kg at 6.9 m/s and 9.9 m/s, and 22.2 kg at 9.9 m/s) the peak deflection is at most 20% above the peak of the upper corridor, and in the impact tests with the lowest mass (10.4 kg at 7 m/s) the peak deflection is 8% below the peak of the lower corridor. The force-deflection responses at the start of the impact are within the corridors for all tests except one (23.4 kg at 5.8 m/s). However, the corridor of this impact test is very narrow compared to that of similar impacts (23.4 kg at 4.6 m/s and 6.9 m/s). These simulation results indicate that the passive model's thorax is capable of predicting realistic force-deflection responses of the human thorax in frontal impacts.

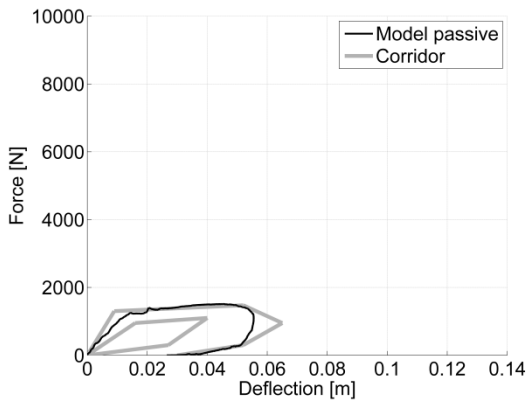

Figure5. PMHS response corridors and active human model (passive) response in blunt frontal thorax impact with 23.4 kg at 3.4 m/s.

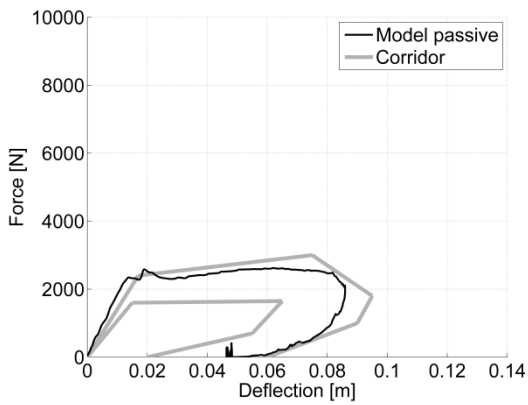

Figure6. PMHS response corridors and active human model (passive) response in blunt frontal thorax impact with 23.4 kg at 5.8 m/s.

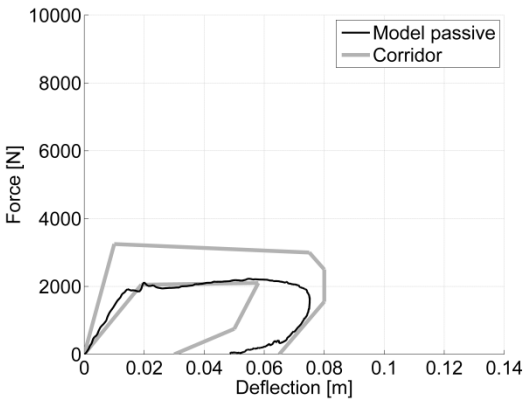

Figure7. PMHS response corridors and active human model (passive) response in blunt frontal thorax impact with 23.4 kg at 4.9 m/s.

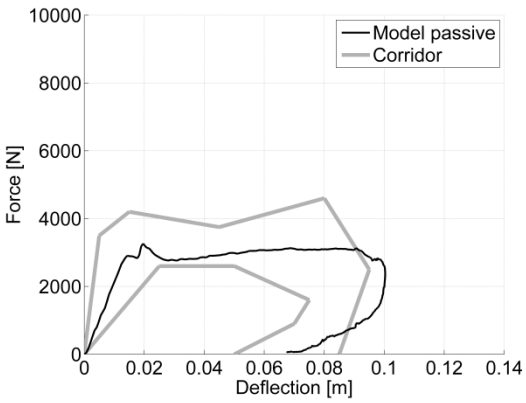

Figure8. PMHS response corridors and active human model (passive) response in blunt frontal thorax impact with 23.4 kg at 6.9 m/s.

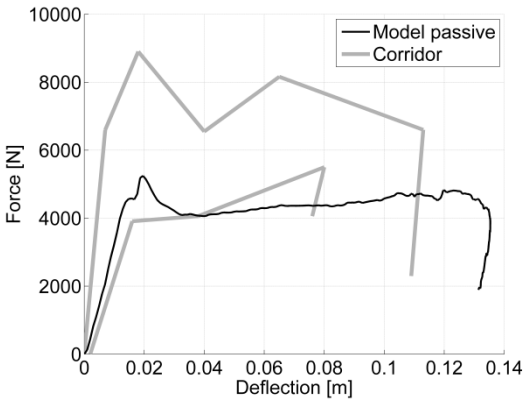

Figure9. PMHS response corridors and active human model (passive) response in blunt frontal thorax impact with 23.4 kg at 9.9 m/s.

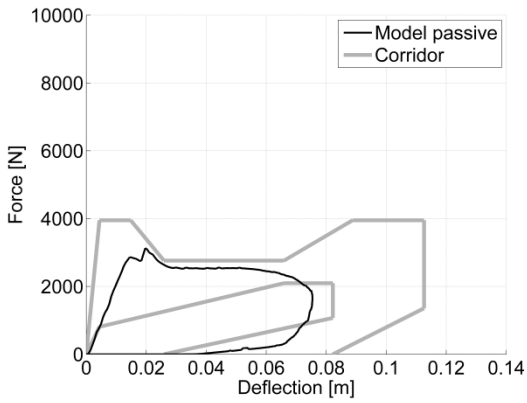

Figure10. PMHS response corridors and active human model (passive) response in blunt frontal thorax impact with 10.4 kg at 7 m/s.

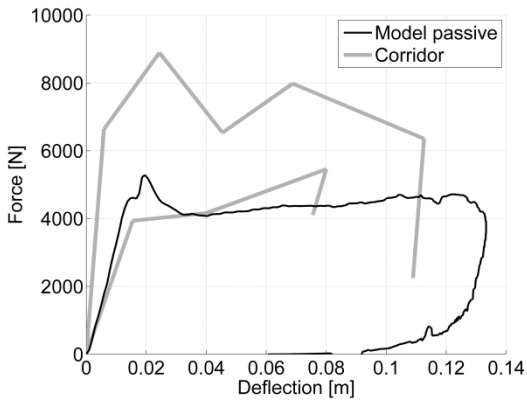

Figure11. PMHS response corridors and active human model (passive) response in blunt frontal thorax impact with 22.2 kg at 9.9 m/s.

The force-deflection response of the passive model in the blunt frontal abdomen impact test (See test no 5 in Table1) is compared to the PMHS response corridors in Figure12. This figure shows that at the start of the impact the force-deflection response is on top of the upper corridor of the PMHS responses. However, the peak force as well as the peak deflection are within the response corridors of the PMHS. This simulation result indicates that the passive model's abdomen is capable of predicting realistic force-deflection responses of the human abdomen in frontal impacts, although it is only evaluated for one impact severity.

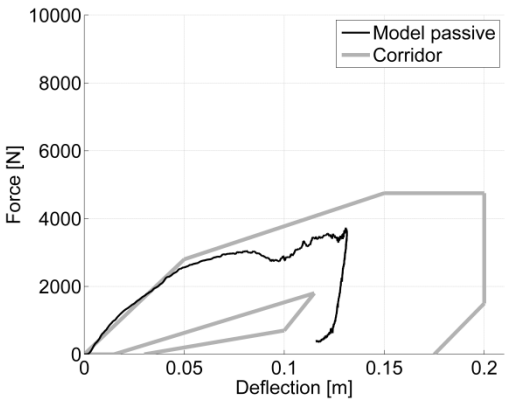

Figure12. PMHS response corridors and active human model (passive) response in blunt frontal abdomen impact 31.4 kg at 6.9 m/s.

The chest and neck horizontal displacements of the active human model in the 1 g car braking test (See test no 1 in Table2) are compared to the volunteer responses in Figure13 and Figure14. These figures were copied from [7] just to show the complete testing of the active model's responses in full-body frontal impact. The chest displacement was measured at the belt, and the neck displacement at a collar around the neck. Various reaction times (RT's) were simulated here. The co-contraction (CCR) was set to 0.5, which was an engineering judgement. However, the co-contraction of the neck muscles hardly affects the neck displacement in this simulation, since the displacement of the spine determines the displacement of the chest and neck most in this case. Figure13 shows that the peak chest displacement of the active model is equal to that of the volunteer with the smallest peak chest displacement. Figure14 shows that the peak neck displacement of the active model is approximately 20% smaller than that of the volunteer with the smallest peak neck displacement. The difference in neck displacement can be explained by the fact that the volunteers were wearing a thick winter coat which was not accounted for in the simulation. This caused the active model to be restrained by the belt a bit earlier than the volunteers, resulting in a smaller neck displacement than the volunteers. These simulation results indicate that the active model is capable of predicting realistic neck and chest displacements in car braking events.

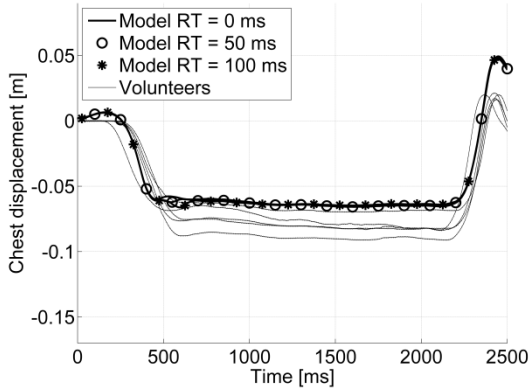

Figure13. Chest displacement of active human model at various RT's and CCR=0.5 and of volunteers in 1 g car braking.

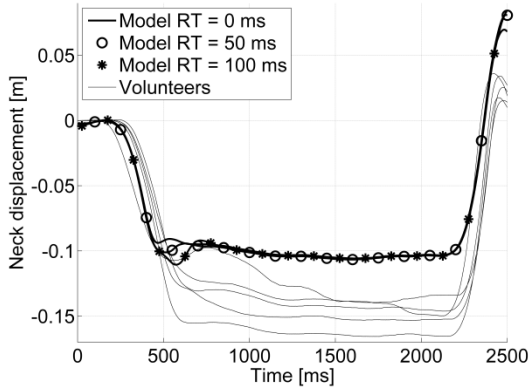

Figure14. Neck displacement of active human model at various RT's and CCR=0.5 and of volunteers in 1 g car braking.

The head, T1 and pelvis horizontal displacements of the active human model in the 3.8 g frontal impact tests (See test no 2 in Table2) are compared to the volunteer response corridors in Figure15 to Figure17. The head horizontal displacement was measured at the top of the head, that of T1 at a position close to T1. The iliac crest was used to measure the horizontal displacement of the pelvis. Various reaction times (RT's) were simulated here. The co-contraction (CCR) was set to 0.5. These figures show that the active model best predicts the volunteers kinematics at RT=25 ms. At this value the active model's head, T1, and pelvis horizontal displacement are completely within the volunteer response corridors. Thereby, Figure15 and Figure16 show that the spread of the volunteer head and T1 horizontal displacements as well as the timing of the peaks can partly be simulated by varying the reaction time. Although, Figure17 shows that the pelvis displacement shows a slightly different movement than that of the volunteers. This was caused by the pelvis sliding a few centimetres over the flesh of the upper legs, which is not modelled in the active human model. These simulation results indicate that the active model is

capable of predicting realistic human full-body kinematics in 3.8 g full-body frontal impact.

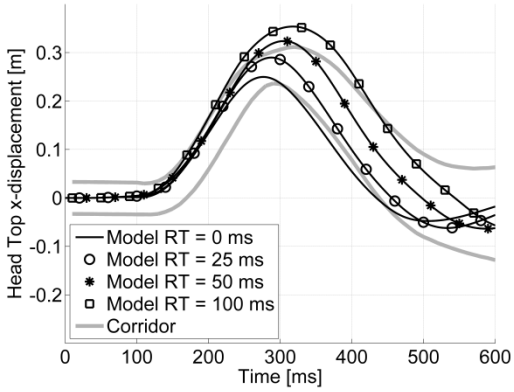

Figure15. Head top x-displacement w.r.t. sled of active human model at various RT's and CCR=0.5 and volunteer response corridors in 3.8 g frontal impact.

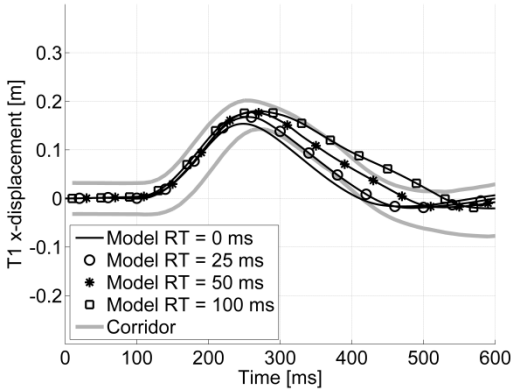

Figure16. T1 x-displacement w.r.t. sled of active human model at various RT's and CCR=0.5 and volunteer response corridors in 3.8 g frontal impact.

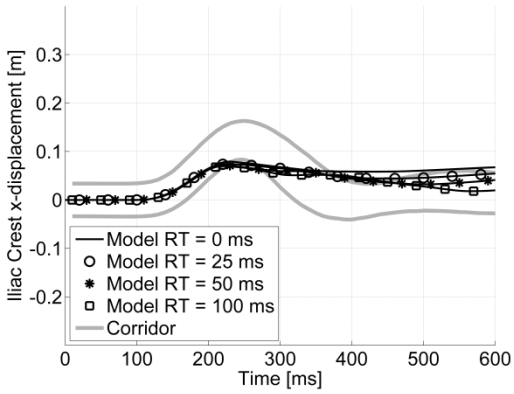

Figure17. Iliac crest x-displacement w.r.t. sled of active human model at various RT's and CCR=0.5 and volunteer response corridors in 3.8 g frontal impact.

The head rotation and head centre of gravity (COG) horizontal displacement of the active model in the 15 g frontal impact test (See test no 3 in Table2) are compared to the volunteer response corridors in Figure18 and Figure19. Various reaction times (RT's) were simulated here. The co-contraction (CCR) was set to 0.5. This test was also simulated in [7] for RT=0, 50 and 100 ms, and various levels of co-contraction. Figure18 and Figure19 show that the active model best predicts the volunteers kinematics at RT=25 ms. These figures show that at RT=25 ms the peak head rotation of the active model is approximately equal to the upper corridor, and the peak head rotation is 5% below the lower corridor. Both responses are almost within the volunteer response corridors, only the timing of the peak head rotation is 15 ms earlier than that of the volunteers. These simulation results indicate that the active model's head-neck complex is capable of predicting realistic human head-neck kinematics in 15 g full-body frontal impact.

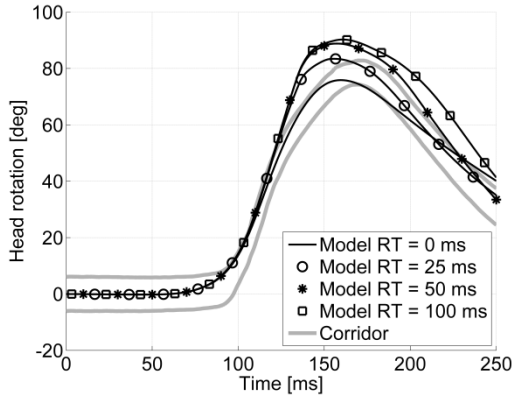

Figure18. Head rotation w.r.t. to sled of active human model at various RT's and CCR=0.5 ms and volunteer response corridors in 15 g frontal impact.

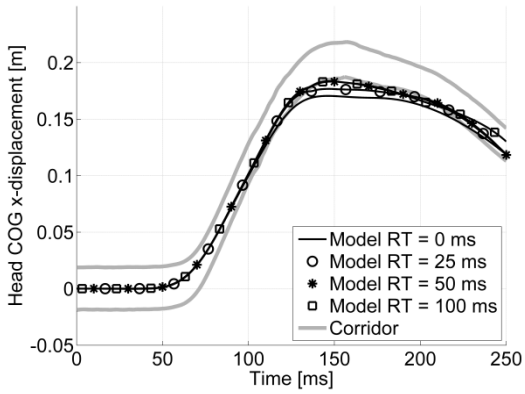

Figure19. Head COG x-displacement w.r.t. sled of active human model at various RT's and CCR=0.5 and volunteer response corridors in 15 g frontal impact.

Evaluation for Various Frontal Crash Scenarios

The position of the active model (red) and passive model (green) at onset of the frontal crash simulation for the small car is shown in Figure20, and at 60 ms (just before contact with airbag) in Figure21. The position of the active model at onset

of the frontal crash simulation for the small car with preceding braking (red) and without preceding braking (blue) is shown in Figure22, and at 1000 ms (prior to start of crash pulse) in Figure23, and at 1060 ms (prior to contact with airbag) in Figure24. The simulations of the other cars showed similar differences between the position of the active model and passive model as well as between with and without preceding braking.
Figure21 shows that the head of the passive model just before contact with the airbag is slightly more upward rotated than that of the active model. Figure23 shows that braking causes the active model to move forward just before the impact. Also, Figure24 shows that due to braking before the crash the active model contacts the airbag earlier than without braking.

Figure20. Position of active (red) and passive (green) model at onset of the frontal impact simulations of the small car.

Figure21. Position of active (red) and passive (green) model at 60 ms of the frontal impact simulations of the small car.

Figure22. Position of the active model with (blue) and without (red) preceding braking at onset of the frontal impact simulations of the small car.

Figure23. Position of the active model with (blue) and without (red) preceding braking at 1000 ms of the frontal impact simulations of the small car.

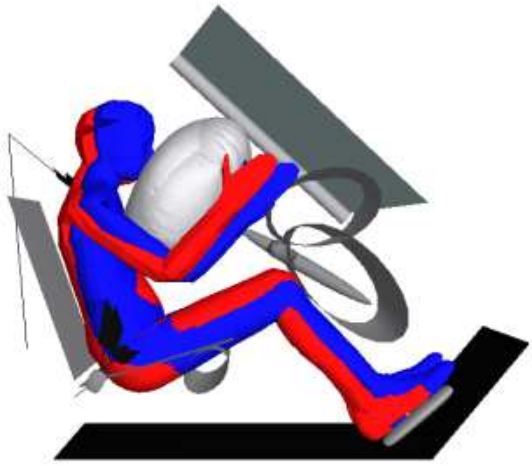

Figure24. Position of the active model with (blue) and without (red) preceding braking at 1060 ms of the frontal impact simulations of the small car.

The resulting HIC_{36ms}, peak upper chest deflection, and peak T1 forward displacement from the simulations of the frontal crash scenarios are shown in Table3.

Table3.
Simulation results of various frontal crash scenarios with active and passive model

Simulation	HIC_{36ms} [-]	Lower chest deflection [m]	T1 x-displacement [m]
Passive model small car	930	0.024	0.361
Active model small car	883	0.026	0.352
Active model small car with braking	620	0.057	0.423
Passive model large car	725	0.023	0.357
Active model large car	733	0.027	0.349
Active model large car with braking	552	0.050	0.419
Passive model SUV	525	0.023	0.338
Active model SUV	477	0.023	0.325
Active model SUV with braking	328	0.050	0.388

Comparing the results of the active model to that of the passive model this table shows that the active behaviour decreases the HIC_{36ms} as well as the peak T1 forward displacement, and increases the peak lower chest deflection for all three crash pulses. This indicates that the active human model robustly predicts effects of active behaviour in frontal crash simulations. Comparing the results of the active model with braking to that without braking this table shows that braking decreases the HIC_{36ms}, and increases the peak T1 forward displacement and peal lower chest deflection for all three crash pulses. This indicates that the active human model robustly predicts effects of braking in frontal crash simulations.
Table3 shows that the active behaviour decreases the HIC_{36ms} by 9% at most, and the braking decreases it by 31% at most. The active behaviour increases the peak lower chest deflection by 14% at most, and the braking increases it by 121% at most. Further, the active behaviour decreases the peak T1 forward displacement with 4% at most, and the braking increases it by 20% at most. So, in these simulations a different position prior to the crash due to braking affects the HIC_{36ms} as well as the chest deflection at least three times more than the active behaviour itself does. Also, the simulation results show that a more forward position prior to the crash, due to the braking, results in approximately twice as high chest deflection. However, in these simulations a shorter distance to the airbag prior to the crash results in a smaller head impact. These results indicate that the active human model is sensitive to effects of braking and active behaviour, and the effects of braking on the injury values are dominant over the effects of active behaviour.

DISCUSSION

The simulation results of the head, thorax and abdomen blunt frontal impact tests showed that the active human model is capable of predicting the PMHS peak responses within 20% deviation from the PMHS response corridors. The maximum deviation from the corridors was found for the peak thorax deflection in the two most severe thorax impact tests. However, the impact severity of these blunt impact tests may be higher than observed in current automotive crashes, due to advances in crashworthiness and restraint systems. It must be noted that the blunt impact test data were all from PMHS. So, only the model's passive thorax and abdomen response could be evaluated.
Nevertheless, for the severity of these blunt impact tests the thorax and abdomen muscle activation is assumed to have a minor effect on the response. For this reason, active behaviour of the ribcage and abdomen are not included in the model. For pre-crash kinematics the active behaviour of the thorax is included in the spine.
The simulation results of the volunteer full-body frontal impact tests showed that the active human model is capable of predicting the volunteer peak responses within 20% deviation from the volunteer response corridors. The maximum deviation from the corridors was found for the peak neck forward displacement in the 1 g car braking test. The simulation results of the two other volunteer full-body frontal impact tests showed a better fit with the volunteer response corridors. These two volunteer tests were performed in a well-defined lab environment, and therefore could be simulated more accurately. For the simulation results of these two tests the best fit with the volunteer response corridors was obtained with the reaction time set to 25 ms, while the co-contraction level of the neck muscles was assumed to be 0.5 (50% of the maximum possible muscle activation).
The simulation results of the various frontal crash scenarios showed that the active human model is robust and sensitive to effects of braking and active behaviour. Also, these simulation results showed that the effects of braking on the injury values are dominant over the effects of the active behaviour itself. However, the active behaviour is indispensable for correct simulation of the pre-crash kinematics.

It must be noted that the active human model has not yet been validated for injury prediction. So, a quantitative evaluation of the effect of active safety systems on the risk of injuries is not possible yet. However, the current model is capable of predicting realistic human head, thorax and abdomen blunt impact responses at several loading severities and conditions, as well as realistic human kinematics in 1 g to 15 g full-body impact. As such, the current active human model can be used for evaluating the effectiveness of active safety systems in frontal impacts.

CONCLUSION

From this study it was concluded that the current active human model is capable of simulating realistic human full-body kinematics as well as realistic injury values for the head and the thorax in one single simulation of braking followed by a frontal crash. As such, this model can be used as a tool in the development process of an active safety system for evaluating its effectiveness in frontal impacts.

REFERENCES

[1] Bose, D., Crandall, J.R., Untaroiu, C.D., Maslen, E.H. 2010. "Influence of Pre-Collision Occupant Parameters on Injury Outcome in a Frontal Collision." Accident Analysis and Prevention, 42, 1398–1407

[2] Woldrich, M. 2010. "Movement in the PRE-Crash Situation - A Simulation Research with a Reversible PRE-SAFE® Pulse System." Abstract for the poster session (P24) Airbag 2010, 10th International Symposium and Exhibition on sophisticated Car Occupant Safety Systems

[3] Mages, M., Seyffert, M., Class, U. 2011. "Analysis of the Pre-Crash Benefit of Reversible Belt Pre-Pretensioning in Different Accident Scenarios." Proceedings of the 22th ESV-Conference, Paper Number 11-0442, Washington DC-US

[4] Beeman, S.M., Kemper, A.R., Madigan, M.L., Duma, S.M. 2011. "Effects of Bracing on Human Kinematics in Low-Speed Frontal Sled Tests." Annals of Biomedical Engineering, Vol 39, No 12, 2998-3011

[5] Ejima, S., Ono, K., Holcombe, S., Kaneoka, K., Fukushima, M. 2007. "A Study on Occupant Kinematics Behaviour and Muscle Activities During Pre-Impact Braking Based on Volunteer Tests." Proceedings of the International Conference on Biomechanics of Impact IRCOBI

[6] Carlsson, S., Davidsson, J. 2011. "Volunteer Occupant Kinematics During Driver Initiated and Autonomous Braking when Driving in Real Traffic Environments.", Proceedings of the International Conference on Biomechanics of Impact IRCOBI, Krakow-Poland

[7] Meijer, R., Hassel, E. van, Broos, J., Elrofai, H., Rooij, L., Hooijdonk, P. 2012. "Development of a Multi-Body Human Model that Predicts Active and Passive Human Behaviour.", Proceedings of the International Conference on Biomechanics of Impact IRCOBI, Dublin-Ireland

[8] MADYMO Human Body Models Manual, 2012. Version 7.4.1., TASS B.V., Rijswijk-The Netherlands

[9] MADYMO Theory Manual, 2012. Version 7.4.1, TASS B.V., Rijswijk-The Netherlands

[10] Winters, J.M. and Stark. L. 1988. "Estimated Mechanical Properties of Synergistic Muscles Involved in Movements of a Variety of Human Joints." Journal of Biomechanics, 21, 1027-1041

[11] Nemirovsky, N., Rooij, L. van, 2010. "A New Methodology for Biofidelic Head-Neck Postural Control." Proceedings of the International Conference on Biomechanics of Impact IRCOBI, Hannover-Germany, 71-84

[12] MADYMO Quality Report Release Update – Active Human 50th Facet Q Model. 2013. Version 1.1 (R7.4.2), Report Number QAHM50FC-130211, TASS B.V., Rijswijk-The Netherlands

[13] Don, B. van, Ratingen, M. van, Bermond, F., Masson, C., Vezin, P., et al. 2003. "Biofidelity Impact Response Requirements for an Advanced Mid-Sized Male Crash Test Dummy." Proceedings of the 18th International Technical Conference on Enhanced Safety of Vehicles, Nagoya-Japan

[14] Bouquet, R., Ramet, M., Bermond, F., Cesari, D. 1994. "Thoracic and Pelvis Human Response to Impact." Proceedings of the 14th International Technical Conference On Enhanced Safety of Vehicles, Munich-Germany, 100-109

[15] Kroell, C.K., Schneider, D.C., Nahum, M. 1971. "Impact Tolerance and Response of the Human Thorax." SAE Paper 710851, Proceedings of the 15th Stapp Car Crash Conference, 163-213

[16] Kroell, C.K., Schneider, D.C., Nahum M. 1974. "Impact Tolerance and Response of the Human Thorax II." SAE Paper 741187, Proceedings of the 18th Stapp Car Crash Conference, 215-253

[17] Kroell, C.K. 1976. "Thoracic Response to Blunt Frontal Loading." SAE Paper 67, 49-77

[18] Nahum, A., Gadd, C., Schneider, D., Kroell, C. 1970. "Deflection of the Human Thorax Under Sternal Impact." SAE Paper 700400, Proceedings of the International Automobile Safety Conference, 797-807

[19] Nahum, A., Schneider, D., Kroell, C. 1975. "Cadaver Skeletal Response to Blunt Thoracic Impact." SAE Paper 751150, Proceedings of the 19th Stapp Car Crash Conference, 259-293
[20] Cavanaugh, J.M., Nyquist, G.W., Goldberg, S.J., King, A.I. 1986. "Lower Abdominal Tolerance and Response." Society of Automotive Engineers, SAE Paper 861878, 41-63
[21] Balasubramanian, S., Seacrist, T., Hopely, T., Sterner, R., Maltese, R.M., Constans, E., Arbogast, B.K. 2009. "Head and Spinal Trajectories in Children and Adults Exposed to Low Speed Frontal Acceleration." Proceedings of the 21st Enhanced Safety of Vehicles Conference, Stuttgart-Germany
[22] Arbogast, K., Balasubramanian, S., Seacrist, T., Maltese, M.R, García-España, J.F., et.al. 2009. "Comparison of Kinematic Responses of the Head and Spine for Children and Adults in Low-Apeed Frontal Sled Tests." Proceedings of the 53rd Stapp Car Crash Conference, Savannah, Georgia-USA
[23] Ewing, C., Thomas, D., Lustick, L., Muzzy, W., Willem, G. et al. 1976. "The Effect of Duration, Rate of Onset, and Peak Sled Acceleration on the Dynamic Response of the Human Head and Neck." Proceedings of the 20th Stapp Car Crash Conference, Dearborn-Michigan, 3-41, Society of Automotive Engineers, SAE Paper 760800
[24] Wismans, J. and Spenny, C. 1984. "Head-Neck Response in Frontal Flexion." SAE Paper 841666, Proceedings of the 28th Stapp Car Crash Conference, Chicago-USA, 161-171
[25] Wismans, J., Oorschot, H. van, Woltring, H. 1986. "Omni-Directional Human Head-Neck Response." SAE Paper 861893, Proceedings of the 30th Stapp Car Crash Conference, San Diego CA-USA, 313-331
[26] Thunnissen, J., Wismans, J., Ewing, C., Thomas, D. 1995. "Human Volunteer Head-Neck Response in Frontal Flexion: A New Analysis." SAE Paper 952721, Proceedings of the 39th Stapp Car Crash Conference, Coronado CA-USA, 439-460

STUDY OF COMPRESSION-RELATED LUMBAR SPINE FRACTURE CRITERIA USING A FULL BODY FE HUMAN MODEL

Ning Zhang
Jay Zhao
Takata (TK Holdings)
United States
Paper Number 13-0288

ABSTRACT

A detailed lumbar spine FE component model (including vertebrae, inter-vertebral discs, all ligaments and facet joints of T12-L5) was built per the Global Human Body Model Consortium (GHBMC) CAD data. The lumbar model was correlated with the Post-Mortem Human Subject (PMHS) lumbar spine tests under flexion, compression and anterior shear loading modes in the physiological ranges (Belwadi, 2008), and was validated with the tests of PMHS functional spine units (FSU) of three adjunct vertebrae in fracture loading conditions (Belwadi, 2008). The lumbar model was integrated into the Takata in-house 50th percentile full human body model. The full body model was validated with the Wayne State University (WSU) PMHS vertical sled tests under +Gz loading in the range of 6G to 10G (Prasad, 1973). Good agreements were found between the test results and the FE model. At the lumbar component levels, stiffness and failure loads along with failure modes were correlated. At the full body level, the seat pan load cell forces, intra-vertebral body force, and the tissue level strains along superior-inferior direction at the anterior vertebral shells were correlated.

Using the validated human model, impactor tests were simulated for a mid-sized human male lying on a table in a vertically sitting posture impacted with a 44kg impactor of 300mmX300mm size onto the buttocks and thigh area at multiple impact speeds from 5.8 m/s to 15 m/s. The simulation results showed that the threshold impactor speeds (or energies) at which the human lumbar vertebrae fractures at the L1 level occurred were in the range of 8.92-10.6m/s (or 1750-2475J impact energy), varying with the fracture type and the test set up conditions.

Physical lab impactor tests in the same test setup configuration were run for the H3 50th%ile dummy at multiple impact speeds in the range of 5.8m/s-7.5m/s. The test data showed that the dummy lumbar load Fz reached 14.5 KN at the 7.5m/s impact.

INTRODUCTION

Compression-related spine fractures are often observed in frontal crashes. Recent studies using the NASS database showed an increase in incidence of thoraco-lumbar fractures in vehicles from later model years. (Pintar, 2012a). Jakobsson et. al. (2006) surveyed 189 vertebral fracture cases from a sub set of 21,034 Volvo car accidents database between 1995 and 2005. The data showed a significantly reduced injury risk for MAIS 2+ cases when comparing the 1995-1999 older cars with 2001-2005 newer cars, however, an insignificant reduction in AIS 2+ vertebral fractures was found between older car groups and newer car groups.

At the lumbar tissue and component test level, there have been numerous published studies on the PMHS lumbar spine response and fracture tolerance under different laboratory test conditions. The tissue test data for the vertebral bodies, ligaments and discs were reported (Yoganandan et al. 1988a). Stiffness and strength of the lumbar spine were experimentally studied using two or three adjacent lumbar vertebrae called the Functional Spine Unit (FSU) (Yoganandan et al. 1988b, Ashton-Miller and Schultz, 1997, A. Belwadi et al., 2008) subjected to a single loading mode such as anterior shear, flexion, and compression, or combined loadings. Whole lumbar spine tests were also performed. (Demetropoulos et al, 1998, A. Belwadi et al, 2008). The reported FSU compression tests showed that the wedge compression fracture (fx) occurred at the failure forces in the range of 2-5KN of the lumbar force, the vertebral body fx observed at 4.3-5.6KN, and the end-plate fx at 5.6-10.2KN.

At the whole PMHS test level, however, there have been relatively few published lumbar injury studies. In earlier 1970s studies whole body PMHS

were applied vertical loading with a vertical sled to simulate pilot ejection forces (King and Vulcan 1971). Recently, a few whole body PMHS were applied underbody loading with a Hyge sled in a high G, short time duration pulse to investigate the blast effect on the lumbar injuries (Pintar, 2012b). Nevertheless, compression-related spine fracture mechanisms of the full human body in various motor vehicle crash conditions were not fully understood. There were no sufficient whole PMHS lumbar testing data for use to derive risk functions of compression-related spine fractures. Also comparative experimental studies for PMHS and Anthropomorphic Test Dummies (ATDs) on the lumbar injury measures and the associated tolerances were rarely seen in literature. Therefore, there was no agreed tolerance for assessment of lumbar spine fractures in motor vehicle safety standards. This situation adversely affected to some extent development of advanced restraints for mitigating risk of the lumbar injuries.

To address this issue, we were motivated firstly to develop a viable lumbar injury assessment tool, and then to develop a simple pendulum impact lab test protocol, to study the lumbar injuries of full human bodies subjected to compression dominated loadings. Such defined physical tests for an ATD like the Hybrid-III 50th%tile dummy, combined with the test simulations using a validated mid-sized human body model, should help us better understand the human lumbar vertebrae fracture tolerances and the corresponding injury measure reference values of the Hybrid-III dummy for the test conditions.

The objectives of this study were

1) to develop the human lumbar fracture criteria of a mid-sized male human model;
2) to determine the threshold impactor speeds (or energies) for an impactor test configuration at which the human lumbar vertebrae fractures at L1 level occurred;
3) to estimate the lumbar fracture research reference values for the H3 50th%ile dummy corresponding to the threshold impactor speeds through comparative study of the lumbar loads between the Hybrid-III 50th%tile dummy and the human model.

METHODS

The first part of this study was to develop a mid-sized male human body model capable of predicting the lumbar injury patterns. Secondly, with this validated model, a series of impactor tests applied to the underbody of the human body were to be simulated. Correspondingly, physical laboratory impactor testing for the Hybrid-III 50th%tile dummy would be run. Finally, analyses were made to define at what threshold impact test conditions injuries to the human lumbar spine would likely occur, and correspondingly what were the corresponding lumbar loads of the Hybrid-III dummy. A lumbar fracture research reference value for the H3 50th%tile dummy could be derived via this approach.

Full human body model upgrade

A previously validated Takata in-house full human body model (Zhao and Narwani, 2007) was further developed for this study. The upgraded model (named as TKHM v4.0) was integrated with the latest developed refined body region models of the thorax, the shoulder and upper extremities, the abdomen, and the pelvis. These body region models were constructed with more accurate anthropometry data and refined meshes of elements with higher standard of meshing quality. The PMHS validation test protocols previously used for these body regions of the human model (Zhao and Narwani, 2007) were re-performed for TKHM v4.0. Additional model validations against recently published component and whole PMHS tests were conducted, which included UVA Rib segment bending tests, isolated rib ring loading tests, point loading to isolated ribcage (Kindig, et al., 2010), and restrained PMHS in frontal sled tests (Shaw, 2009). All the validations demonstrated that the upgrade full body model had improved robustness and kinematics; the refined body region models had better biofidelic responses than the previous version as well.

Modeling of Lumbar spine

Next, a more biofidelic lumbar spine FE component model was developed. A detailed lumbar spine model including vertebrae, inter-vertebral discs, all ligaments and facet joints of T12-L5 was built per GHBMC CAD data representing a healthy young adult male in the driving posture. The vertebrae (body and posterior structure) and inter-vertebral discs were meshed with hexahedra elements of high element quality. Cortical shells wrapped around vertebrae were modeled as shell elements sharing nodes with the surface of solid elements. The anterior longitudinal ligament, the posterior longitudinal ligament, and the interspinous ligament were modeled with membrane elements of specified thickness.

Contacts on facet joints between adjacent vertebrae were defined and surrounding facet capsules were modeled with membrane elements.

Based on the geometrically symmetrical condition, half of spine was built first. It was used for component level validations. The whole lumbar model was built from it using mesh reflection along the symmetric plane. The lumbar model was later assembled into the full human body model (TKHM v4.0) with nodal connections to adjacent connective soft tissue parts (representing muscle and fat).

Material properties of lumbar spine model

Material laws and input parameters for all lumbar components were carefully selected according to the biological tissue's material behavior under both physiological and pathological loadings of laboratory measurements documented in literature. For the trabecular bone inside vertebral body and the cortical bones surrounding the vertebrae, an elastic-plastic material law was selected to consider the fracture failure of tissues under high loading levels (See Table 1 and 2). For the soft tissues, the ligaments were represented as fabric type of material with no resistance for compressive force. The Annulus fibrous was model as elastic, and the nucleus was modeled as fluid type of material with incompressible property (See Table 3 and 4).

Table 1.
Input material parameters for cortical bone

Thickness (mm)	0.36
Density (kg/liter)	1.4
Elastic modulus (GPa)	17.0
Poisson's ratio	0.3
Yield stress (MPa)	133
Strain at failure (%)	0.89
Tangent modulus (MPa)	230

Table 2.
Input material parameters for trabecular bone

Density (kg/liter)	0.9
Elastic modulus (GPa)	0.062
Poisson's ratio	0.3
Yield stress (MPa)	3.2
Strain at failure	24%

Table 3.
Input material parameters for ligaments

Density (kg/liter)	1.1
Elastic modulus (GPa)	0.013
Poisson's ratio	0.4

Table 4.
Input material parameters for inter-vertebral disc

Density (kg/liter)	1.3
Elastic modulus (GPa)	0.029
Poisson's ratio	0.45

Component validations

The lumbar model was subjected to compressive, flexion and anterior shear loading separately according to the laboratory setup using whole lumbar specimens (Demetropoulos, 1998, A. Belwadi, 2008). The loading levels for these tests were within the lumbar spine's physiological loading range without damaging any of the tissues. The loading rate in the simulation was carefully selected to make sure that dynamic effects were negligible.

According to the test setup, the lumbar spine including S1 and T12 was mounted upside down, and vertebra S1 were potted into a fixed jig, and vertebra T12 was potted into a jig whose actuator applied a displacement-controlled loading. A six-axis loadcell was connected to the fixed jig on the S1 side. The model setup followed the test setup, and the aluminum potting cups at both ends were modeled as rigid. Prescribed motion boundary conditions were applied to the cup at the T12 side; the loadcell at the S1 side was modeled using a zero beam loadcell element to output the forces and moments. Table 5 shows the loading level for each loading mode. Figure 1 shows the model setup.

Table 5.
Applied loading type and jig motion

Loading type	**Jig motion**
Compressive	3.5 mm
Anterior shear	18 mm
Flexion	9 degrees

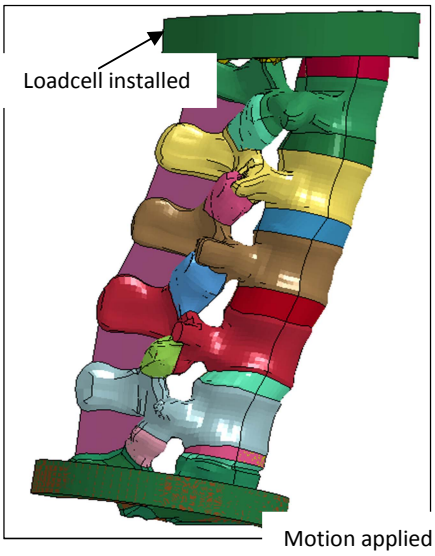

Figure 1. Lumbar spine static loading model setup.

A three segment FSU model including L4, L5, and S1 (See Figure 2) was studied at the component level to verify the material failure criteria for both vertebral cortical shell and trabecular bone exceeding the fracture loading level. Two loading modes: a 10mm compressive displacement, and a combined loading consisting of 15mm shear and 9 degrees of flexion (Belwadi, 2008) were simulated and the failure load was reported and compared with the reported laboratory tests.

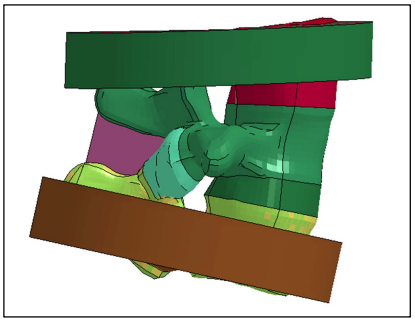

Figure 2. Lumbar functional spine unit (FSU) failure test model setup.

Full body model validation under vertical sled loading

The full body model integrated with the validated lumbar sub-model was further validated against the PMHS tests in a vertical sled system (King and Vulcan, 1971). Figure 3 shows the model setup. The human model was positioned in a vertical sitting posture and restrained with a four point seat belt system with an 180N pretension load. Several vertical acceleration pulses were applied to the seat and foot rest experienced peak acceleration levels varied from 6g to 10g according to the tests. The seat pan-pelvis contact force, lumbar loadcell output, and strain outputs on the anterior vertebral body at the L1 and L3 level were correlated with PMHS test results. Since the instrumentation was different for every test, 3 cases were selected and listed in Table 6.

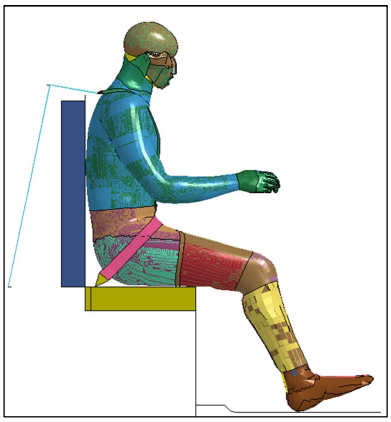

Figure 3. Full body human model validation setup according to test protocol from King and Vulcan, (1971).

Table 6.
Cases used to validate the full human body model

Source of data	Peak G Sled pulse	Instrumentation
King and Vulcan,1971	10G	L1, L3 strain gage
Prasad,1973	8G	Lumbar vertebral load cell
Prasad,1973	6G	Seat pan load cell

Human body underbody impact tests simulation

A linear impactor test configuration for the underbody of the human body was defined, as shown in Figure 4. The validated full human body model was positioned lying on a wood table in a vertically sitting posture. A foam block of small weight (109g) was put underneath his head to hold the head initial position. The height of the impactor was positioned aligned with the center of pelvis of human model. The weight of impactor was 44kg, and the dimension was 300mmx300mm square with a D-shape cross section on the impact side.

Eleven test simulations (Table 7) were initially simulated, with an initial pendulum impact velocity starting at 5.8m/s which was gradually increased to 15m/s step by step to find the velocity level at which the lumbar vertebrae would start to fail.

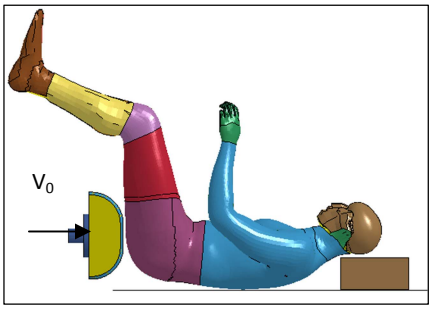

Figure 4. Linear Impactor test setup for the full human body model.

Table 7.
Lists of cases of the human model impactor simulations.

Case #	Impactor Velocity (m/s)	Impactor kinetic energy (J)
1	5.8	740
2	6.5	929
3	7.5	1237
4	8.3	1500
5	9.5	2000
6	10.6	2500
7	11.7	3000
8	12.6	3500
9	13.5	4000
10	14.3	4500
11	15	5000

Hybrid III 50th underbody linear impactor testing

A laboratory study using a Hybrid-III 50th percentile dummy was conducted following the same impactor test configuration for the full human body model. The dummy was instrumented with a 6-axis lumbar spine load cell (model 4609JTF, Humanetics, Plymouth, MI) with a capacity of 20KN for force and 600Nm for moment measurement. Due to the limitation of the linear impactor system, the maximum velocity the system could achieve was 7.5m/s. Several dummy positions were tested to investigate the effect of the pelvis/lumbar angle. Table 8 showed the test matrix. Figure 5 showed the test setup. The dummy output included: head acceleration, chest acceleration, pelvis acceleration, and lumbar forces and moments. All signals were processed according to the SAE J211 standard.

Table 8.
Test matrix of H3 50% laboratory linear impactor test.

Test number	Impactor velocity (m/s)	Pelvis angle (degrees)
1	5.8	0
2	5.8	15
3	5.8	20
4	5.8	25
5	6.5	0
6	6.5	25
7	7.5	0
8	7.5	25

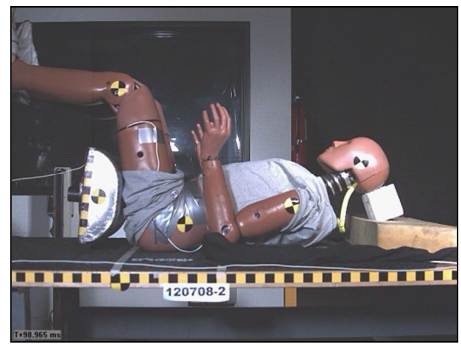

Figure 5. Linear impactor setup for the H3 50th%tile dummy

RESULTS

Results of lumbar model under physiological range of static loading

The load-deflection curves were plotted and linear curve fitting was used to calculate the stiffness of the lumbar model under compression, anterior shear and flexion. Figure 6 (a-c) show the model predictions against the test results for the PMHS lumbar spine specimens. For all three loading modes, lumbar stiffness predictions were within the range of test data variations.

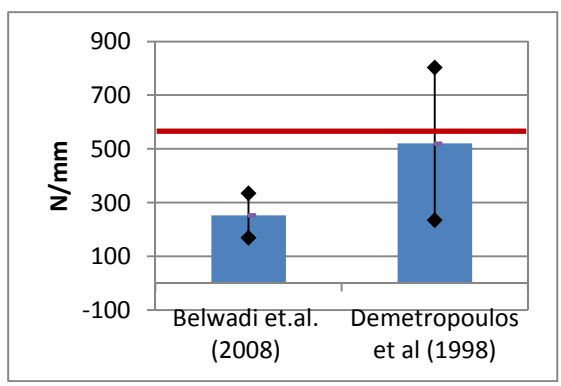

Figure 6(a). Compressive stiffness of lumbar spine (L1-L5), flat red line was the model prediction.

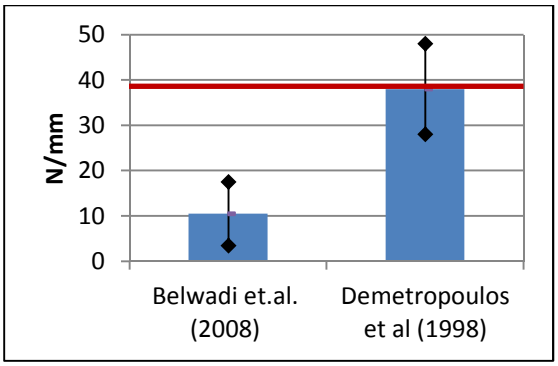

Figure 6(b). Anterior shear stiffness of lumbar spine (L1-L5), flat red line was the model prediction.

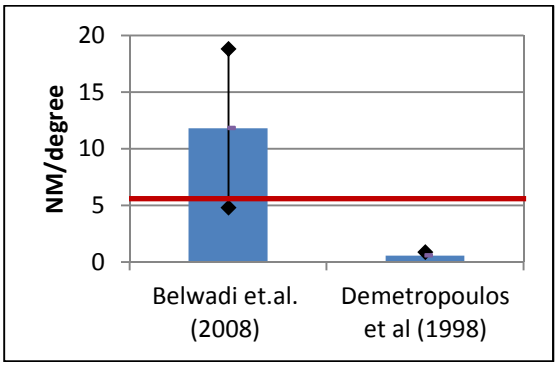

Figure 6(c). Flexion stiffness of lumbar spine (L1-L5), flat red line was the model prediction.

Results of failure loading cases with FSU model

When the pure compressive force was applied to the FSU model, a compression fracture of the vertebral body was predicted (Figure 7). The predicted failure force was 6.3 KN. Figure 8 compares the model predicted compressive failure force with the data of FSU tests under the pure compression conducted by Baudrit (2005) et al. The tests showed that a failure force of 10.2±1.71KN for young specimens (age: 22-46, male) and 5.58±1.64 KN for elderly specimens (age: 46+, male and female), the result from this study was within the range of the elderly group. When the combined shear and flexion load was applied, a posterior structure failure was predicted for the vertebrae (Figure 9). The failure force vs. failure moment (Figure 10) were plotted and compared with the PMHS tests conducted by Belwadi et al (2008). The failure load predicted by the current model was in line with the test results.

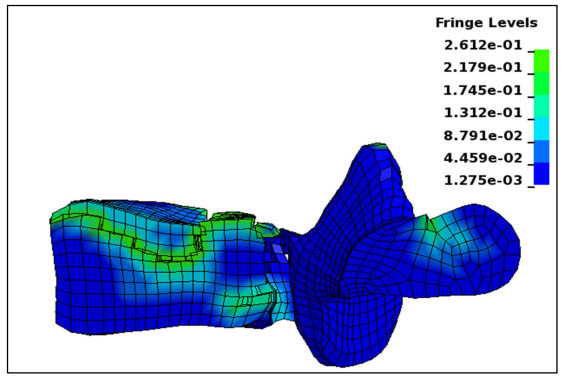

Figure 7. Predicted failure mode (compression type) for the FSU model under pure compressive force; the contour shows the effective strain.

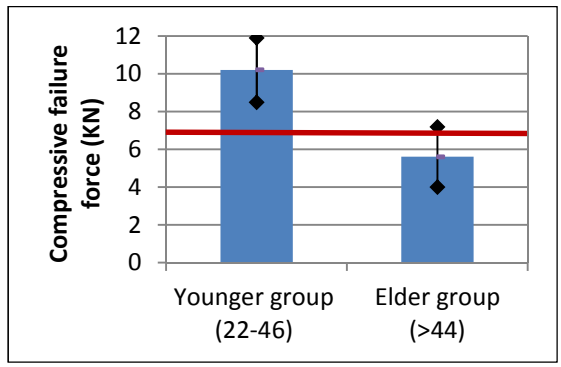

Figure 8. Predicted compressive failure compared with test data conducted by Baudrit et al. (2005). Flat red line was the model prediction.

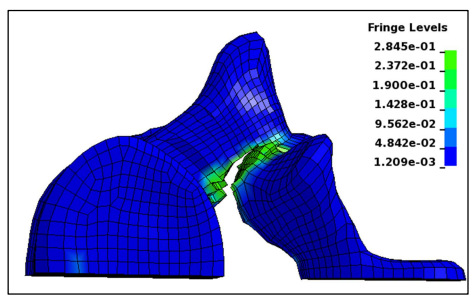

Figure 9. Predicted failure mode (posterior structure failure) for the FSU model under shear force and flexion moment (the contour shows the effective strain).

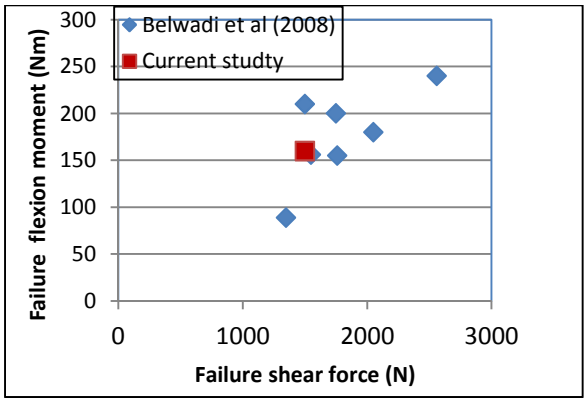

Figure 10. Predicted failure force and moment for the FSU model under shear force and flexion moment.

Results of full body validation under vertical sled loading

Good correlation was found between the model prediction and the test data (King and Vulcan, 1971) for seat pan pelvis contact force (See Figure 11). The current model slightly (13%) under-predicted the spine load Fz (See Figure 12). For the strain outputs at the anterior surface along the superior-inferior direction, the current model had good correlation for the L1 surface strain, but slightly under-predicted the first spike for the L3 vertebra (See figure 13 and 14).

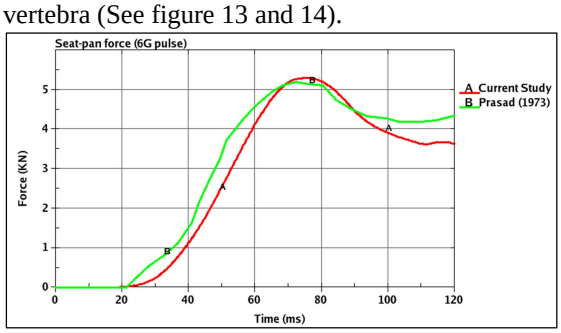

Figure 11. Comparison between the PMHS test and the simulation for seat-pan contact force.

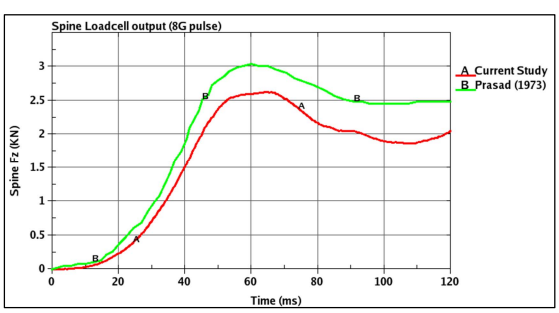

Figure 12. Comparison between the PMHS spine Fz.

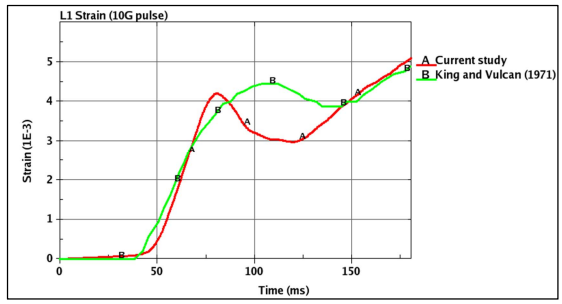

Figure 13. Comparison between the PMHS test and the simulation for strains at the L1 level.

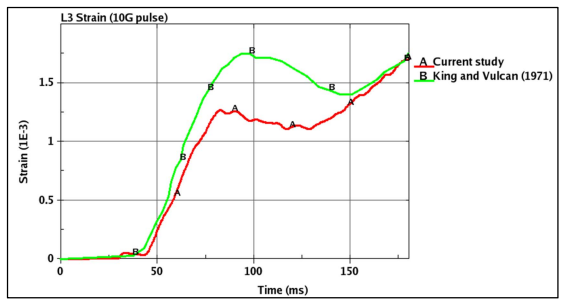

Figure 14. Comparison between the PMHS test and the simulation for strains at the L3 level.

Results of human body underbody impact tests simulations

The impact loading on the pelvis yields a dominant compressive force on the lumbar vertebrae. As a result, the L1 vertebra reported highest strain among the five lumbar vertebrae, due to the curvature of the spine (Lordosis in lumbar region). With an increase in impact velocity, both peak lumbar Fz and peak vertebral strains increased (see Table 9). At the impact speed of 10.6m/s (2475J), a wedge type fracture was observed at the L1 level (Figure 15).

Table 9.
The human model impactor simulation Results: the peak lumbar Fz, the peak vertebral strain and wedge type fracture observation.

Case #	Velocity (m/s)	Peak lumbar Fz (KN)	Peak vertebral strain (%)	Fractures observed
1	5.8	2.85	0.38	No
2	6.5	3.46	0.45	No
3	7.5	3.98	0.52	No
4	8.3	4.87	0.58	No
5	9.5	5.43	0.69	No
6	10.6	6.26	0.73	Yes
7	11.7	7.1	0.73	Yes

8	12.6	7.7	0.73	Yes
9	13.5	8.4	0.73	Yes
10	14.3	8.9	0.73	Yes
11	15	9.26	0.74	Yes

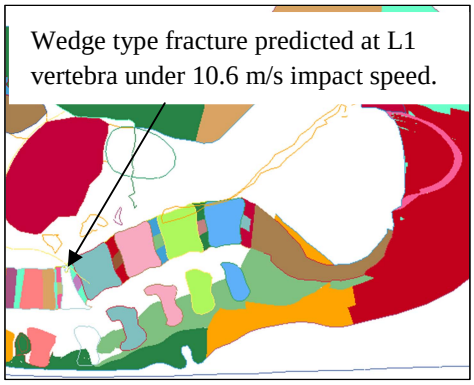

Figure 15. Cross section cut showed wedge type fracture at the L1 level for the 10.6m/s impactor simulation.

Results of Hybrid III 50th underbody linear impactor testing

Eight impacts were conducted for a H3 50th percentile dummy. Table 10 shows the measured peak lumbar Fz, My and pelvis acceleration Gz. Overall the peak lumbar Fz increased when the impact velocity increased (see Figure 16). However, the lumbar flexion moment My (positive My) was not sensitive to an impact velocity change (see Figure 17). When the dummy pelvis angle increased from 0 degree to 25 degrees, a decrease in the lumbar Fz and an increase in the lumbar extension My were observed (see Figure 18 and 19).

Table 10.
The HB3 50th%tile dummy test results: the peak values of lumbar Fz, My and pelvis Gz.

	Pelvis angle	Velocity (m/s)	Lumbar Fz (N)	Lumbar My(Nm)	Pelvis Gz (G)
1	0	5.8	8689	53	255
2	15	5.8	6229	57	136
3	20	5.8	6050	65	238
4	25	5.8	6624	52	139
5	0	6.5	12,640	44	652
6	20	6.5	6988	70	350
7	0	7.5	14,530	60	659
8	20	7.5	8785	67	533

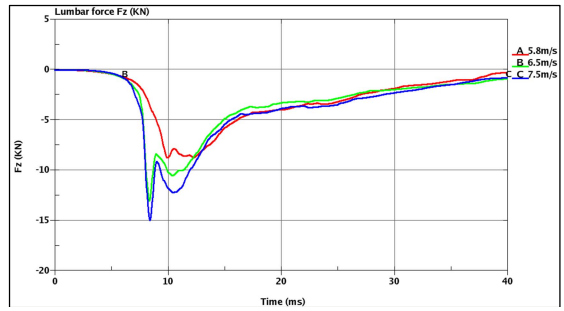

Figure 16. Comparison of the lumbar Fz forces from the tests with different impact velocities (pelvis angle was 0 for all cases).

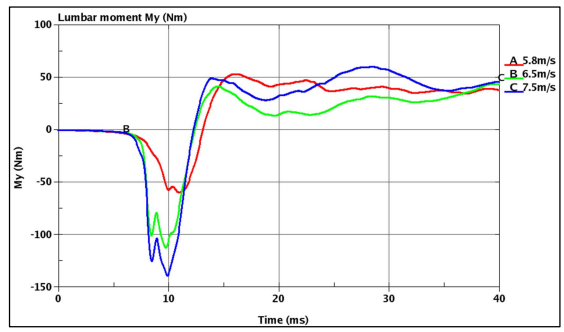

Figure 17. Comparison of the lumbar flexion moments My from the tests with different impact velocities (pelvis angle was 0 for all cases).

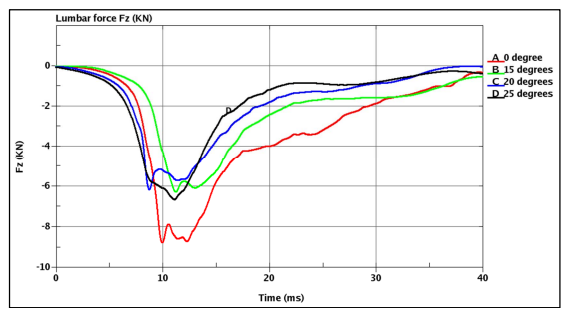

Figure 18. Comparison of the lumbar forces Fz from the tests with different pelvis angles (impact velocity was 5.8m/s for all cases).

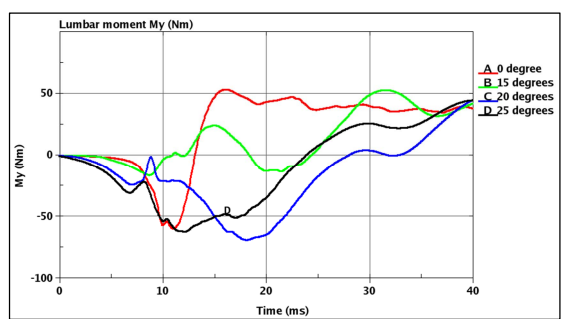

Figure 19. Comparison of the lumbar flexion moments My from the tests with different pelvis angles (impact velocity was 5.8m/s for all cases).

DISCUSSIONS

On results of component validation

For compressive and shear stiffness of the lumbar spine, the current model prediction was closer to the test data from Demetropoulos et al. (1998) than the data from Belwadi et al (2008). When looking into the PMHS' age and sex (Table 11), the specimens from Demetropoulos et al. (1998)'s study were closer to what the current model represented, which was a middle aged 50th percentile male subject. For flexion stiffness, since the testing was sensitive to initial spine positions, larger variations were observed between the two groups and the current model prediction were within the range of data reported from the above two studies.

Table 11.
PMHS statistics for lumbar spine stiffness data from literature [Demetropoulos et al. 1998, Belwadi et al 2008]

	Demetropoulos et al. 1998	Belwadi et. al. 2008
Number of specimens	10	7
Male/Female	8/2	6/1
Range of age	54-65	48-83
Average age	60	68
Average weight (kg)	73	75

On vertebral fracture pattern prediction

The fracture type and pattern of the vertebrae depend on the forces and moments applied to the spine (Nahum and Melvin, 1993). Compression fractures are due to the vertebrae subjected to pure compressive forces which cause the endplate to collapse and the vertebral body to compress. The failure pattern for the FSU model of the current study under the compressive force matched this type of fracture pattern. The mechanism of posterior fracture is due to excessive flexion moments causing failure of the posterior structures or ligaments and discs. The failure pattern predicted by the FSU under flexion and anterior shear matched this type of fracture. A combination of flexion and axial compression causing excessive compression at the anterior site of the vertebral body results in anterior wedge fractures. The loading of the full human body when subjected to underbody impactor loading was a compression dominated force with additional flexion moment caused by the spine curvature around the lumbar and thoracic spine transition zone. Therefore, the wedge fracture predicted from the full body impactor model is reasonable.

On Hybrid III 50th percentile dummy lumbar fracture research reference value and bio-fidelity

The test data (Table 10) showed that the dummy lumbar load Fz reached 14.5 KN at the 7.5m/s impact. A simple linear aggression and interpolation of the data set could be made. It was estimated that about 15-16KN of the dummy lumbar load Fz could be generated at the threshold impact speed of 8.92m/s (see next discussion). The lumbar fracture research reference value for the H3 50th%ile dummy subjected to compressive dominant impact loadings could be in this range. This needs further experimental verification.

Hybrid III family dummies (Backaitis and Mertz, 1994) are widely used for automotive safety design and biomechanical research. However, there are several limitations to directly apply the H3 dummy as a surrogate for lumbar spine injury study and prevention. First, the curvature or the lumbar spine of the H3 dummy is in Kyphosis instead of Lordosis which is the characteristic of the human spine. The curvature differences make the moment measurement at the lumbar spine loadcell less accurate compared with the moment sustained by the human spine. Figure 20 shows a direct comparison of the lumbar moment output at 7.5 m/s impact speed between the human model prediction and the Hybrid III dummy. The dummy exhibited an extension moment at the beginning of the impact, which didn't present in the human model. Further investigations are required to explain why this extension/flexion pattern was observed in the physical dummy. Also the current study showed that an increase in impactor speed for the dummy didn't significantly increase the peak flexion moment of the dummy lumbar spine. Based on the above observations, the lumbar flexion moment might not be a good indicator to predict lumbar spine fractures when a H3 dummy used. Secondly, due to the stiffer H3 dummy pelvis design, the impact force and the measured Fz force from the lumbar loadcell were significantly higher than that from the human model and the failure criteria reported from different groups (See Figures. 21a and 21b). A totally redesigned surrogate with better biofidelity of the lumbar and pelvis regions could be more suitable for automotive safety design involving lumbar spine injury prevention.

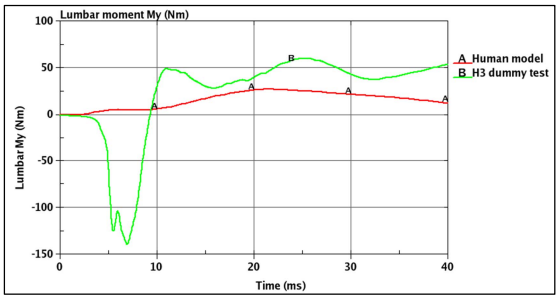

Figure 20. Comparison of the lumbar flexion moment My between human model prediction and the H3 dummy test (impact velocity was 7.5m/s).

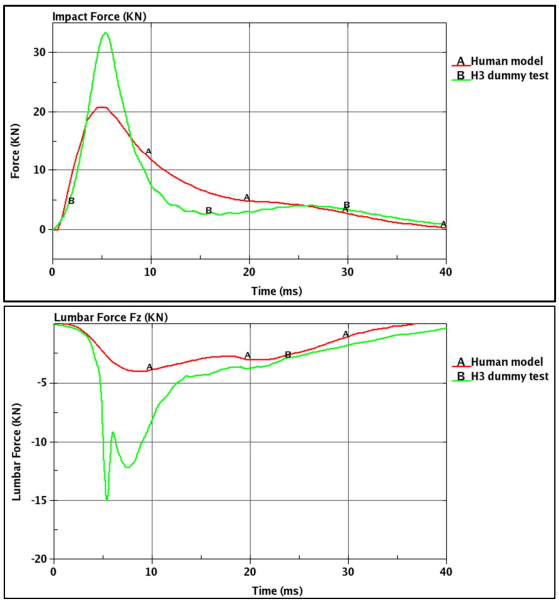

Figure 21. Comparison of the impactor force (a) and the lumbar force Fz (b) between the human model prediction and the H3 dummy test (impact velocity was 7.5m/s).

On the human lumbar fracture threshold impact speed or energy estimation

The element strain based criteria for the lumbar vertebra fractures (see Table 1-2) were validated in this study. However, the definition of "vertebral body fractures" or type of the fractures will affect the threshold impact speed or energy estimation.

For example, from case #6 (Table 9) simulations, we observed that the fractures started from a few cortical bone shell element failure (deletion) and followed sequentially by more cortical shells and trabecular solids failures. Finally the L1 vertebral body collapsed at 15ms and the wedge type fracture was observed (Figure 22 left plot). We repeated the case#6 run but changed only the impact speed to 9.7 m/s. For this run we observed only a few cortical shell and trabecular solid failures, and no wedge type fracture collapse or large deformation occurred, as shown in Figure 22 on the right plot. If we consider a lumbar fracture as any indication of localized failure of the vertebral body cortical shell(s), the threshold impact speed for the case setup (Figure 4) could be as low as 9.7m/s (or equivalent impact energy of 2070J).

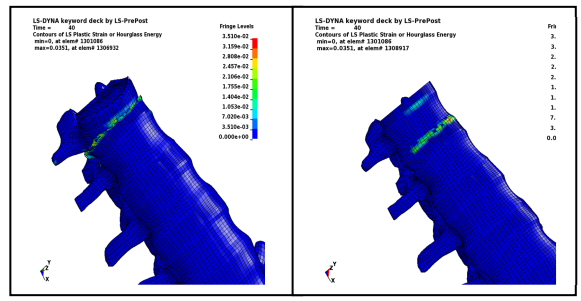

Figure 22. Comparison of the L1 fracture patterns: Left: wedge type fracture at L1 at 10.6m/s impact speed; Right: initial cortical shell failures at L1 at 9.7 m/s impact speed.

Also, in actual impactor testing (Figure 4), the variation of the test configurations or conditions, such as the body supporter block shape and weight, the table material or friction coefficients, and the human body initial positioning, etc., might have influence on the threshold impact speed or energy estimation. We ran additional human body impact test simulations as part of a parametric study on these factors. Table 12 summarizes the simulated test conditions and our observation for initial cortical shell failure at L1 from each of the cases. The two considered human body supporter shapes in these cases were the block that was used in the previous simulation matrix (Table 7, Figure 4) and a wedge shape body supporter shown in Figure 23.

As seen in Table 12, the model predicted that initial cortical shell failure at L1 could occur at a threshold impact speed as low as 8.92m/s (or 1753J impact energy). The most influential factor to affect the threshold impact speed was the body supporter shape or the way we initially positioned the human model. Comparison of run#9 with run#7 showed that the threshold impact speed for L1 cortical shell failure decreased from 9.77 m/s to 8.92 m/s if the body supporter changed from the block to the wedge. The results also indicated that the friction coefficients and the wedge weight under the considered range of 0.92-2.07kg had no

significant effect on the threshold impact speed or energy.

Table 12.
Additional human body impact test simulation cases and results

run#	Pendulum mass(kg)	Impact speed (m/s)	Impact energy (J)	Supporter Shape	Supporter weight (kg)	Wedge/Table Friction Coef.	Local Cortical shell failure?
0	44.05	9.30	1905.1	Wedge	2.073	0.30	YES
1	44.05	9.04	1800.1	Wedge	2.073	0.30	YES
2	44.05	8.92	1752.6	Wedge	2.073	0.30	YES
3	44.05	8.79	1701.9	Wedge	2.073	0.30	NO
4	44.05	8.79	1701.9	Wedge	0.924	0.80	NO
4b	44.05	8.92	1752.6	Wedge	0.924	0.80	YES
5	44.05	8.79	1701.9	Wedge	0.924	0.55	NO
6	44.05	8.79	1701.9	Wedge	0.924	0.30	NO
7	44.05	8.92	1752.6	Wedge	0.924	0.30	YES
8	44.05	9.05	1804.1	Wedge	0.924	0.30	YES
9	44.05	9.77	2102.6	Block	0.924	0.30	YES
10	44.05	9.05	1804.1	Block	0.924	0.30	NO

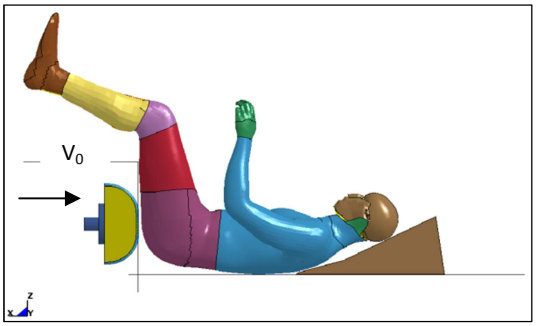

Figure 23. Alternate Linear Impactor test setup for the full human body model.

CONCLUSIONS

A full body human model with a detailed representation of the anatomical structures of the lumbar spine, and with the validated tissue-level injury criteria for the lumbar vertebral fractures under compressive-dominated loadings has been developed.

A linear impactor test configuration shown in Figure 4 was used for comparative study of lumbar loads response between the human full body model and the Hybrid-III 50th%tile dummy. The results showed that the threshold impactor velocities at which the lumbar vertebrae fracture at L1 occurred were in the range of 8.92-10.6m/s of impact speeds (or 1750-2475J of impact energies). Localized cortical shell failures were observed starting from the lower threshold impact velocity of 8.92 m/s. The wedge type vertebrae fractures at the L1 level occurred at 10.6m/s. The human body supporter shape in this test setup was found to have the most significant effect on the threshold impact velocity or energy.

Physical lab impactor tests in the same test setup configuration were run for the Hybrid-III 50th%tile dummy at multiple impact speeds in the range of 5.5m/s-7.5m/s. The test data showed that the dummy lumbar load Fz reached 14.5 KN at the 7.5m/s impact. Differences of the lumbar loads between the human body and the H3 50th%tile dummy have been identified from this study.

ACKNOWLEGEMENT

The authors would like to gratefully acknowledge to Richard Kent, Damien Subit and Zuoping Li of University of Virginia for their support in development work of Takata Human Model v4.0 used in this study. Also thanks to Albert King of Wayne State University for his providing us information of the PMHS vertical sled test data for the model correlation.

REFERENCES

Ashton-Miller and Schultz, "Biomechanics of Human Spine", Basic Orthopaedic Biomechanics, 2nd ed. edited by VC. Mow and WC Hayes. Lippincott-Raven, Philadelphia, PA, pp. 353-394, 1997.

Backaitis SH and Mertz HJ., "Hybrid III: The First Human-Like Crash Test Dummy" SAE, Warrendale, PA, 1994.

Baudrit, P. et al., "Cadaver and Dummy Investigation of Injury Risk with Anti-Sliding System In Case of Static Deployment" ESV paper #05-0399, 2005.

Belwadi, A. and Yang, K.H., "Cadaveric Lumbar Spine Responses to Flexion with and without Anterior Shear Displacement", IRCOBI Conference, Bern, Switzerland, 2008.

Demetropoulos, C.K., Yang, K.H., Grimm, M.J., Khalil, T.B., King, A.I.; "Mechanical Properties of the Cadaveric and Hybrid III Lumbar Spines", 42nd Stapp Car Crash Conference, Paper No. 983160, 1998.

F. Pintar, "Thoraco-Lumbar Spine fractures in Frontal Impacts", 2012 CIREN Conference Presentation, 2012a.

F. Pintar, "Spine and Pelvis Fractures in Axial Z-Acceleration", 40th International Workshop on

Human Subjects for Biomechanics Research", 2012b.

Jakobsson L, Bergman T, and Johansson L., "Identifying Thoracic and Lumbar Spinal Injuries in Car Accidents", IRCOBI Conference, Madrid, Spain, p61-71, 2006.

King AI., and Vulcan AP., "Elastic Deformation Characteristics of the Spine" J. Biomech. Vol 4. pp. 413-429, 1971.

Matthew W. Kindig, et al., "Structural Response of Cadaveric Ribcages Under a Localized Loading: Stiffness and Kinematic Trends", Stapp 2010-22-0015, 2010.

Nahum AM and Melvin JW, "Accidental Injury, Biomechanics and Prevention." Springer-Verlag, New York, USA, 1993.

Prasad P., "The Dynamic Response of the Spine During +Gz (Eyeballs Down) Acceleration." Ph. D. dissertation, Wayne State University, Detroit, MI, 1973.

Greg Shaw, et al, "Impact Response of Restrained PMHS in Frontal Sled Tests: Skeletal Deformation Patterns under Seat Belt Loading", Stapp Car Crash Journal, 2009-22-0001, 2009.

Yoganandan, N., Myklebust, J.B., Cusick, J.F., Wilson, C.R., Sances, A.; "Functional biomechanics of the thoracolumbar vertebral cortex", Clinical Biomechanics, 3:11-18, 1988a.

Yoganandan, N., Pintar, F., Sances, A. Jr., Maiman, D., Myklebust, J., Harris, G., Ray, G.; "Biomechanical Investigations of the Human Thoracolumbar Spine", SAE Technical Paper 881331, 1988b.

Zhao, Jay and Narwani, G., "Biomechanical Analysis of Hard Tissue Responses and Injuries with Finite Element Full Human Body Model." ESV 07-0354, 2007.

CHEST INJURY CRITERION: AN UPDATE OF THE EQUIVALENT DEFLECTION (DEQ)

Xavier Trosseille, Eric Song
LAB PSA Peugeot-Citroën Renault
France
Audrey Petitjean
CEESAR
France
Paper Number 13-0342

ABSTRACT

The rodpot chest deflection measured on the HIII dummy does not discriminate the contributions of the belt and the airbag in crashes. The risks associated to the deflection being different for these two kinds of devices, the assessment of the risk with the rodpot deflection is erroneous for combined restraining systems. Combined restraints known to be efficient in protecting the thorax are consequently penalized. In 2003, the equivalent deflection (Deq) criterion based on the HIII rodpot deflection and the shoulder belt force and applicable to belt, airbag as well as combined restraints was proposed. It has since been evaluated and reviewed by users providing some requests for improvements such as the sensitivity to changes in the pelvic restraint. The objective of this study was to update the Deq criterion to address as much as possible the feedbacks from the users and better predict chest injuries.
New data from HIII 50th percentile tests performed under conditions more representative of the loading encountered with current restraints were collected from the literature. It allowed to better define the relationship between the shoulder load and the deflection caused by the belt. The Deq formulation was updated in order to increase its sensitivity, particularly to airbag loading. Additional paired dummy and PMHS (Post-Mortem Human Subject) tests allowed increasing the size of the sample used to validate the principle of the Deq criterion. The validation of the new formulation was also conducted through simulations with human and HIII models. Then, the biomechanical data were re-processed with currently recommended statistical methods (based on survival analysis) to build a thoracic injury risk curve for the HIII 50th dummy. Finally, a thoracic injury risk curve was provided for the HIII 5th female.
This paper provides the set of data (dummy, PMHS and numerical simulations) used to define and validate the criterion, as well as the equations of the thoracic injury risk curves as a function of the Deq resulting from their processing. The feedbacks from the users as well as the related improvements of the criterion are presented. The effect of the rodpot deflection and the upper shoulder belt force on the Deq is described.
The aim of the Deq criterion is to improve the thoracic protection in frontal crash in the short term, therefore using the currently used HIII dummy. As such, this criterion enhances the prediction of the risk associated with combined restraints compared to the HIII rodpot deflection. However, it does not fully compensate the error introduced by the use of the rodpot deflection.

INTRODUCTION

For several years now, car manufacturers have made significant efforts in the field of thoracic protection. After first limiting the forces in the shoulder belt to 6 kN, these forces are now usually limited to 4 kN, with airbags intentionally designed to absorb the surplus of energy. If this technology is rewarded by a considerable improvement in safety on the road, it remains penalized by the usual biomechanical criteria, when calculated on the Hybrid III and if applied to all restraint systems.
To remedy this problem, a new criterion, valid in all the current restraint configurations (belt, airbag only or airbag and belt) was proposed by Petitjean et al. (2003).

The principle of the thoracic criterion proposed is the following:

The risks associated to a belt and to an airbag are different in terms of deflection. Therefore, the deflections due to a belt or due to an airbag must be evaluated separately.
The risk due to a belt loading can be calculated using the maximal deflection caused by the belt. This localized deflection is evaluated from the shoulder belt force, resolving the differential Equation 1. The stiffness used to calculate this deflection comes from belt-only tests.

$$F_{belt}(t)=k1.dl(t)+c1.vl(t) \quad \textbf{Eq.1}$$

Where k1 and c1 are the linear stiffness and the damping and dl(t) and vl(t) are the deflection and the rate of deflection respectively.

The risk due to an airbag can be calculated using the maximal deflection caused by the airbag. This distributed deflection is calculated subtracting the

localized deflection from the total deflection, as the deflections are supposed to be added.

The localized and distributed deflections are then combined in order to take into account the different risks associated to each restraint and the interaction between them.

However, before, they have to be normalized so that the same value of each deflection produces the same risk. For this reason, the distributed deflection is scaled by the factor Fn.
Finally, the localized deflection and the scaled distributed deflection can be combined to form the Deq (Equivalent Deflection).

This criterion, developed in 2003, was updated in order to take into account more recent restraint systems, PMHS testing performed since 2003 as well as other statistical methods to build the injury risk curves.

METHODS

The principle of the Deq is described in the original paper (Petitjean et al., 2003) and remains the same. The following items were reviewed and updated:

- relationship between the shoulder belt force and the deflection
- Deq formulation
- Validation sample
- Injury Risk Curves (IRCs)

The Deq was evaluated against the validation sample and HIII/HBM simulations.
Test results were analyzed to scale the Deq to the HIII 5th and provide IRCs.

RESULTS

Relationship between the shoulder belt force and the deflection

Localized Deflection Calculation
The upper shoulder belt load was used to determine the deflection caused by the localized loading. Belt only tests with HIII were collected in order to determine the relationship between the upper shoulder belt load and the deflection caused by the localized loading.

The limitations of the belt only tests used in 2003 are that the belt restraints used did not correspond to up-to-date restraint (dual stage load limiter for example) and present shoulder belt force much higher than the load limitation used nowadays (up to 12.7 kN). Additional belt only tests were therefore collected to investigate the relationship between the upper shoulder belt load and the stiffness for belt restraints closer to those currently used in the vehicles. Belt only tests are not easy to collect as most of the restraints include the combination of a belt and of an airbag. A lot of tests were collected in the NHTSA Biomechanics Test Database. The number of belt only tests used was 49 compared to 21 in the 2003 version. The range of maximum upper shoulder belt load was from 2.7 to 12.7 kN with a median equal to 6.2 kN (the median for the belt only sample used in the 2003 version was 8.6 kN).

The stiffness to be used to calculate the maximum localized deflection was chosen to be the one representing the mean **minus** one standard deviation using all the tests included which are shown in Figure 1. The stiffness calculated is described in Equation 2.

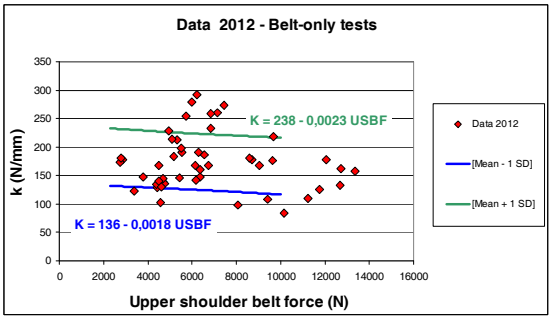

Figure 1. Relationship between the upper shoulder belt load and the stiffness.

k_l = -0.0018*F belt max + 136 **Eq. 2**
with k_l in N/mm and Fbelt in N

The belt only tests were also used to determine the relationship between the linear stiffness and the linear damping, provided in Equation 3 and represented in Figure 2.

c1= 0.0185*kl -0.2357 **Eq. 3**
with k_l in N/mm and c in N.s/mm, R^2=0.31

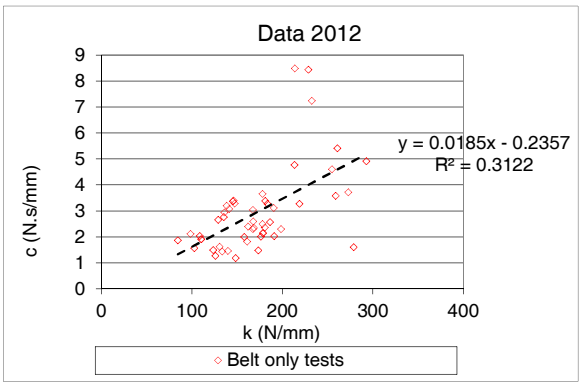

Figure 2. Relationship between the damping and the stiffness to be used for the calculation of the deflection due to localized loading and due to the distributed loading.

The localized deflection was calculated from the upper shoulder belt load using Equation 1, Equation 2 and Equation 3.

Distributed Deflection Calculation

The deflection caused by the distributed loading such as an airbag is calculated subtracting the localized deflection from the total deflection, as described in Equation 4.

$d_{dist}(t) = d_{rodpot}(t) - d_{lr}(t)$ **Eq. 4**

$d_{dist}(t)$: deflection caused by the distributed loading

$d_{rodpot}(t)$: rodpot deflection

$d_{lr}(t)$: localized deflection at the rodpot location

However, the total deflection is only known at the rodpot location. Therefore, this is the localized deflection at the rodpot location that must be removed from the total deflection measured at the rodpot location. The maximum localized deflection as defined in the previous section cannot be used because it does not correspond to the localized deflection at the rodpot location.

To account for this drawback, the stiffness to be used in the calculation of the distributed deflection was chosen to be the one representing the mean **plus** one standard deviation using all the tests included in Figure 1. The stiffness calculated is described in Equation 5.

$k_{lr} = -0.0023 * F\ belt\ max + 238$ **Eq. 5**

with k_{lr} in N/mm and Fbelt in N

It must be noted that the localized deflection used to calculate the distributed deflection is more likely to be underestimated than the one in the 2003 version. It means that the distributed deflection is more likely to be overestimated. This allows having a conservative limit for the Deq.

Statistical method to calculate Injury Risk Curves

Petitjean and Trosseille (2011) evaluated the different methods to construct injury risk curves using statistical simulations. The parameters evaluated were the theoretical distribution of the tolerance (normal, Weibull), the distribution of the points relative to this theoretical distribution (lower end, upper end, centered loosely, centered tightly), the size of the sample (from 10 to 50) and the proportion of exact data (no exact data, 10%, 25% and 50% of exact data). The conclusion is that the survival analysis is recommended to be used to construct injury risk curves for biomechanical samples over the other methods.

In the 2012 updates, all the injury risk curves were built using the survival analysis with the Weibull distribution. As the survival analysis is a parametric method, the age of the PMHS was included as a co-variable in the analysis.

Calculation of the normalization factor for distributed loading

Once the deflection caused by a localized and a distributed loading are calculated, they are combined in the Deq such that the difference of tolerance due to a localized and a distributed loading is taken into account. A normalization factor allowing to have the same risk for a given value of localized or distributed loading was then determined.

For this purpose, two samples – one with localized loadings and one with distributed loadings – were combined and analyzed together to characterize their difference.

Sample with localized loading only

As the Foret-Bruno sample (Foret-Bruno et al., 1998) was close in terms of upper shoulder belt force to more recent restraints and as the size of this sample was much more important than the one of the APR sample (used in 2003), it was chosen to use it to build the injury risk curve as a function of the localized loading. The maximum upper shoulder belt load is the only measure available from the original Foret-Bruno sample. It was then needed to convert the maximum upper shoulder belt load into maximum localized deflection.

First, the relationship between the maximum upper shoulder belt force and the upper shoulder belt force at the time of the maximum deflection was determined using the tests provided in Figure 1. This relationship is provided in Equation 6 and illustrated in Figure 3.

$F\ belt\ d\ l\ max = 0.8373 * F\ belt\ max$ **Eq. 6**

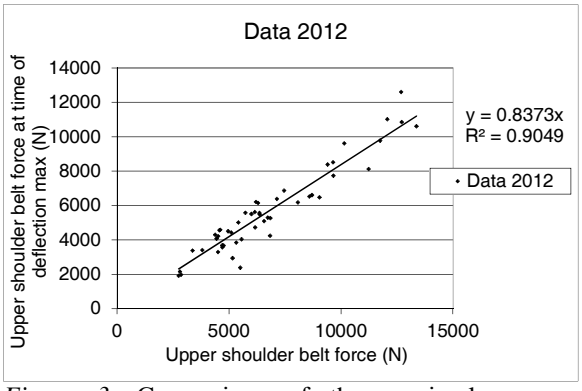

Figure 3. Comparison of the maximal upper shoulder belt load and of the upper shoulder belt load at the time of maximal deflection.

The combination of Equation 1 and Equation 6 then leads to the relationship between the maximum upper shoulder belt force and the maximum localized deflection (Equation 7).

F belt max = (kl/0.8373) dl max **Eq. 7**
With Fbelt max in N, k1 in N/mm and d1 max in mm

The maximal upper shoulder belt loads from Foret-Bruno accident cases were, in this way, converted to dummy maximal localized deflection.

Sample with distributed loading only
Impactor tests performed by Kroell et al. (1971, 1974) were used to characterize the distributed loading. The tests performed with a mass significantly lower than 23 kg were not used for the construction of the injury risk curves. The sample selected to build the injury risk curve is presented in annex (Table A 1).

Definition of the normalization factor
A survival analysis was performed including the sample providing the localized deflection calculated for the Foret-Bruno sample and the sample providing the distributed deflection calculated for the impactor tests. The severity considered was AIS3+ for the Foret-Bruno sample and a number of rib fractures equal or higher than 6 for the Kroell sample. The co-variables were the deflection (localized or distributed), the age of the occupant or PMHS and the type of loading (belt or impactor). This method allowed calculating a single normalization factor, independent from the age and the level of risk.
The results of the survival analysis are presented in Equation 8.

$$Risk_{50th}(AIS3+) = 1 - \exp\left[-\exp\left(\frac{\ln(deflection) - 4.886 - 0.016 \times age + 0.176 \times loading}{0.23}\right)\right]$$

Eq. 8

The normalization factor was found to be 0.84.

Deq formulation

The original Deq was the resultant of the belt deflection and the airbag deflection (Deq quadratic, Equation 9). However, it was not demonstrated that this form was the best one. For this reason, a linear combination of the belt deflection and the airbag deflection (Equation10) was investigated.

Deq quad = max (SQRT{dbelt (t)^2 + (Fn * dairbag (t))^2}) **Eq. 9**

Deq Lin = max (dbelt (t) + Fn * dairbag (t)) **Eq. 10**

In addition, a Deq calculated from the lower shoulder belt force was evaluated. The use of this belt force was suggested because it is less influenced by the belt force limitation and is more likely to show the effects of the pelvis restraint.

Validation sample

The Deq was validated against tests including different types of restraints such as belt, combined belt and airbag and airbag only tests.
The PMHS sample used in 2003 was reviewed and some tests were excluded. As the effect of the liquid injected into the PMHS remains uncertain, the PMHS included in the sample were fresh or frozen. The list of PMHS tests used in the 2012 update is included in annex (Table A 2). Tests with more up-to-date restraints were included compared to the 2003 version, such as dual stage pretensioner or low load limiter. These tests are a selection from Forman et al. (2006 and 2009), Humos (2000), Petitjean et al. (2002), Kent at al. (2001) and Lebarbé et al. (2005).

To assess the performance of the different criteria, IRCs were constructed with this validation sample, using a survival analysis. The quality of the curves was compared by means of statistical index.

The Akaike Information Criterion (AIC) assesses the likelihood of a model and takes into account the number of variables used in the model (AIC= -2*log likelihood+2*number of variables). The lowest AIC indicated the best fit of the model with the test data.

For the validation sample, the AIC is the highest for the injury risk curve built as a function of the rodpot deflection (Table 1). This means that the fit of the injury risk curves as a function of the Deq whatever the option considered is always better than the one for the rodpot deflection.
Among the different options, the lowest AIC values are found for the Deq based on the lower shoulder belt load compared to the Deq based on the upper shoulder belt load. This measurement is sometimes measured during crash tests. However, depending on the seat geometry and belt anchorages, it is not always easy to measure. The Deq based on the upper shoulder belt load would be easier to measure and would still show a better performance than the rodpot deflection.
There is no significant difference between the quadratic and the linear combination of the localized and distributed deflection regarding the fit of the data for the whole validation sample for Deq based on upper shoulder belt load. The AIC

based on the quadratic combination of the localized and distributed deflection is lower than the one based on the linear combination, when based on the lower shoulder belt load.

Table 1.
AIC values and c index for the injury risk curves built using the validation sample

	Rodpot defl. (mm)	Deq			
		Lower shoulder belt		Upper shoulder belt	
		Quad	Linear	Quad	Linear
AIC values	49.6	31.3	35.4	37.2	39.2
C index	0.747	0.92	0.885	0.874	0.864

The appropriateness of a criterion to predict a risk can be assessed by constructing a risk curve as a function of this criterion and calculating the percentage of concordance and discordance and the c statistic index.
A c statistic value equal to 0.5 indicates an inappropriate criterion to predict the risk while a c value equal to 1 indicates a perfect appropriateness. The higher the c value is, the better the criterion predicts the risk.
The injury risk curve as a function of the Deq based on the lower shoulder belt load and the quadratic combination offered the best prediction (Table 1). The other options of Deq have similar c index values. The injury risk curves as a function of the Deq present a better c index value than the rodpot deflection.

Finally, based on the same validation sample, the quality index, as defined by Petitjean and Trosseille (2011) were found to be better for the Deq than for the Rodpot deflection (Table 2).

Table 2.
Quality index based on the size of the 95% confidence interval for Rodpot and Deq

Risk	5%	25%	50%
Deq	Unaccept.	Fair	Fair
Rodpot	Unaccept.	Unaccept.	Unaccept.

HIII/HBM simulations

Simulations were run with Humos2Lab (Song et al. 2011) and Hybrid III models in the same conditions. The restraints were based on lap and shoulder belt and airbag. The contribution of the belt and of the airbag varied, lowering the belt load limiter and increasing the airbag power such that the excursion of the models were kept identical for each combination of belt and airbag restraint. The Deq was found to increase with the increase of injuries on Humos2Lab human body model (Table 3). On the contrary, the rodpot deflection was not found to increase with the increase of injuries. This is due to the fact that the tolerance limit is different in terms of rodpot deflection for localized and distributed loading.

Table 3.
Humos2Lab injuries and HIII measurements at ISO excursion of T8

	Number of Rib Fractures (45 y/o)	Number of Rib Fractures (65 y/o)	Drodpot (mm)	Deq quadratic based on upper shoulder belt load	Deq linear based on upper shoulder belt load
2kN + 90% AB	0	3	35.3	27	37.4
4kN + 55% AB	0	6	40.6	36.1	50
6.5 kN	4	8	35.2	50.7	56.4

Another series of simulations were run with different kinds of restraining systems, in order to verify their effect on the prediction of fractures using either the rodpot or the Deq. Simulations included hub and airbag tests, belt-only or combined airbag and belt sled tests. All configurations were conducted at different severities leading to different injury outcomes.
The effect of the restraining system (shown in Figure 4) confirmed the observations made by Kent et al. (2003) on the relationship between the rodpot deflection and the number of fractures. On the contrary, Deq LIN was very efficient to reduce the effect of loading type.

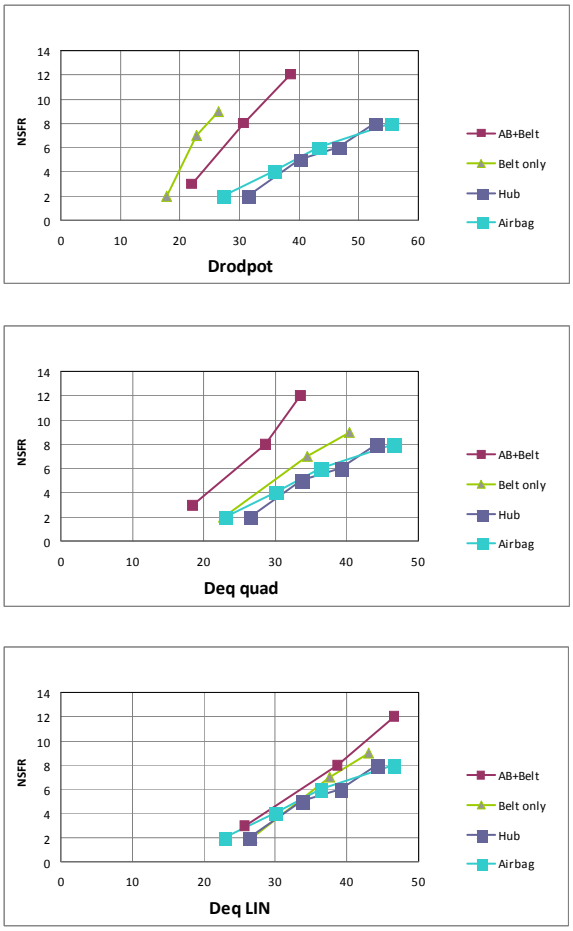

Figure 4. HBM/HIII simulations.

Injury Risk Curve

The Deq IRC was constructed using Foret-Bruno sample because it is a large sample, based on living subjects and representative of the crash situations. The risk, as a function of Deq and age is defined in Equation 11.

The quality index of this IRC is presented in Table 4. It demonstrates a good to fair ability to predict the risk.

$$Risk_{50th}(AIS3+) = 1-\exp\left[-\exp\left(\frac{\ln(Deq)-4.99+0.0174\times age}{0.246}\right)\right]$$

Eq. 11

Table 4.
Quality index of the IRC for Deq

	5%	25%	50%
45 y/o	Good	Good	Fair
60 y/o	Fair	Good	Good

HIII 5th

There is not enough 5th percentile PMHS tests allowing to build injury risk curves as a function of the Deq. However, the principle of the Deq thoracic injury criterion is also applicable to the Hybrid III 5th dummy, given some correspondences are done between the Hybrid III 50th and 5th. The values to be used for the different parameters have to be checked in order to adapt the Deq to the small female.

Thoracic response under localized loading
Linear stiffness and damping were calculated on a sample of Hybrid III 5th tests with belt only restraint (Table A 3). These tests were collected in the NHTSA Biomechanics Test Database.

The stiffness and damping were compared to those determined for the Hybrid III 50th. Figure 5 and Figure 6 show that the values found for the Hybrid III 5th are consistent with those found for Hybrid III 50th. Therefore the same coefficients were used to calculate the localized deflection from the shoulder belt force.

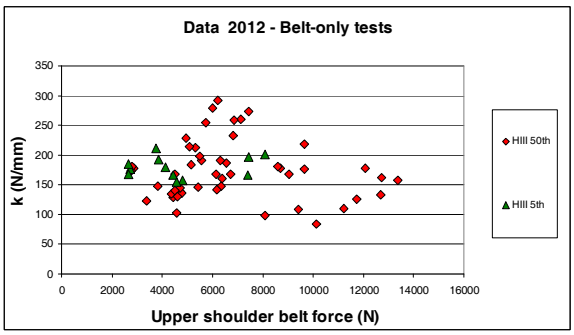

Figure 5. Comparison of the relationship between the upper shoulder belt load and the stiffness for the Hybrid III 50th and 5th.

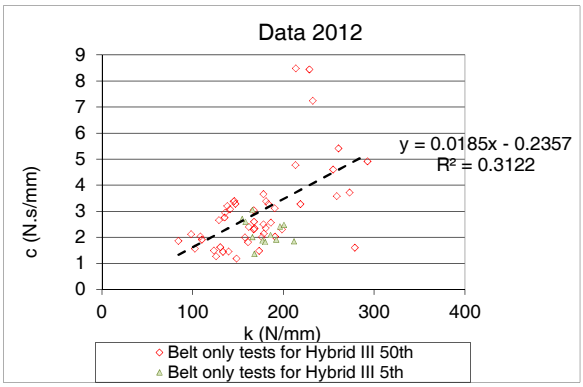

Figure 6. Comparison of the relationship between the damping and the stiffness for the Hybrid III 50th and 5th.

Thoracic response under distributed loading
The stiffness of the thorax should also be compared between the Hybrid III 50th and 5th for an impactor

test. This should be done for impactor test with a scaled impactor mass and impactor surface. Unfortunately, the only impactor tests available with the Hybrid III 5th are certification tests performed with a scaled impactor mass (13.98 kg) but with the same impactor surface as for the Hybrid III 50th (152.4 mm).
The stiffness ratio found based on the certification test corridors is close to 1 (Figure 7).

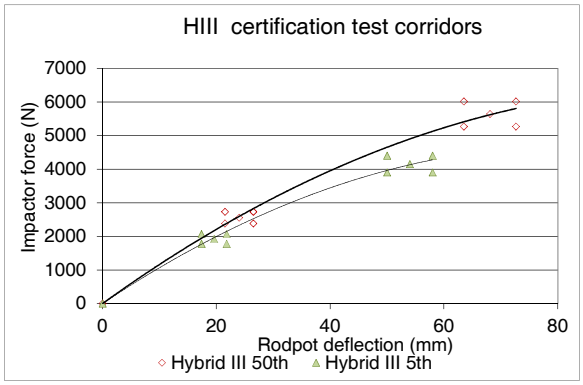

Figure 7. Comparison of the thoracic stiffness under distributed loading for the Hybrid III 50th and Hybrid III 5th.

Maximum upper shoulder belt load and upper shoulder belt load at the time of maximum deflection

Figure 8 shows that the relationship between the maximum upper shoulder belt load and the upper shoulder belt load at the time of maximum deflection was very consistent for the Hybrid III 50th and 5th.

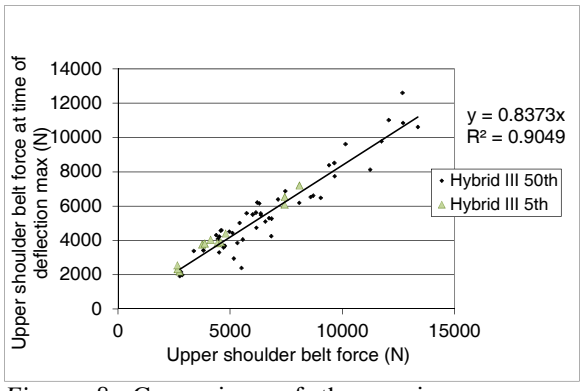

Figure 8. Comparison of the maximum upper shoulder belt load and of the upper shoulder belt load at the time of maximum deflection for the Hybrid III 50th and Hybrid III 5th.

The behaviour of the HIII 5th female being close enough to the HIII 50th male, it was considered that the same formula should be applied for the Deq calculation.

IRC for the Hybrid III 5th

Identically, the injury risk curve described in Equation 11 can be used for the prediction of the risk as a function of the Deq scaled to the Hybrid III 5th percentile.
The Deq scaled to the HIII 5th is the Deq divided by the length ratio. The length ration is the ratio of the chest depth of the Hybrid III 5th (182.9 mm) and the chest depth of the Hybrid III 50th (221 mm). It equals 0.83.
Therefore, Equation 12 defines the IRC for the HIII 5th female.

$$Risk_{5th}(AIS3+) = 1-\exp\left[-\exp\left(\frac{\ln(Deq/0.83)-4.99+0.0174\times age}{0.246}\right)\right]$$

Eq. 12

DISCUSSION

Upper shoulder belt force measurement

Belt force transducers are not conventional and concerns were raised about the calibration of these transducers and their ability to provide accurate measurements.

A calibration procedure is required and is under development at ISO TC22/SC12/WG3. The following steps are necessary:

- Linearization (as rodpot)
- Calibration with an harmonized standard belt strap

A round robin is in progress and ISO expects a range of +/- 5%.

As a comparison, the deflection measured by the rodpot in calibration tests has to fall in a range of +/- 10% at low severity (Figure 9).

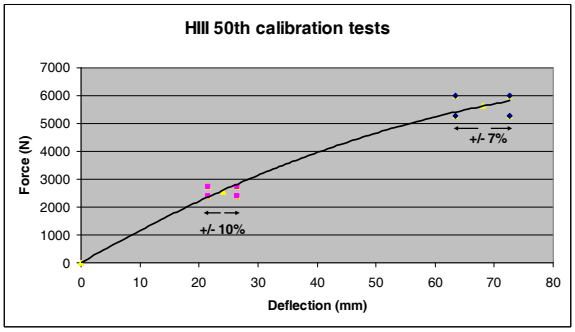

Figure 9. HIII 50th calibration tests.

Speed sensitivity and effect of the lower body restraint

Another concern about Deq was its sensitivity to the test speed and its ability to detect changes in the pelvis retraint. The rational of this objection was that the Deq is highly driven by the upper shoulder belt force which is often limited. This was true with

the 2003 version and the 2012 version was modified to account for this concern. In particular, the use of a linear form of the Deq, by providing a higher contribution of the distributed deflection, increased the speed sensitivity and the effect of the pelvis restraint. However, the need to take this latest effect is not fully validated.

Simulations performed by LAB on Humos2Lab / HIII (Table 5) show that:

- HIII simulations are not very sensitive to pelvis restraint
- Rodpot variations are often opposite to Humos2Lab injury outcome
- Both Drodpot, Deq quad and Deq LIN are sensitive to the velocity

Table 5.
Humos2Lab injuries and HIII measurements at different velocities

Velocity	Drodpot	USBF	LSBF	Deq	Deq LIN	NFR
40	38.5	4.1	3.1	33.5	46.6	2.0
45	40.6	4.1	3.4	35.7	49.7	4.0
60	45.0	4.2	4.0	38.2	53.6	12.0
45/40	6%	0%	11%	7%	7%	100%
60/40	17%	2%	30%	14%	15%	500%

Geometry sensitivity

It was said that Deq may be insensitive to the restraint geometry, in opposite to the injury outcome.
Simulations performed by LAB on Humos2Lab / HIII with different anchorage geometries (Table 6) show that:

- Deq Lin and Rodpot increase while injuries remain the same.
- Deq quad is less sensitive to the geometry

Table 6.
Humos2Lab injuries and HIII measurements for different geometries

Configuration	Drodpot	USBF	LSBF	Deq	Deq LIN	NFR
base	40.1	4.1	3.7	36	49.8	5
lower B3	46.2	4.1	3.7	38.7	54.6	5
Lower & rear B3	47.9	4.1	3.8	40.1	56.5	5

Effect of the Rodpot deflection and the upper shoulder belt force

In order to better understand the contributions of the rodpot deflection and the upper shoulder belt force, the Deq formula was simplified. The viscous component was removed and only the relationship between Fbelt_max and Fmax at the time of maximum deflection was kept. The stiffness was considered as constant over Fbelt (the value was chosen at Fbelt = 5 kN).

Deq = dlocalized + Fn * ddistributed

Dlocalized was replaced by (Fshoulder* λ_F)/kl
Ddistributed was replaced by Drodpot-(Fshoulder* λ_F)/klr
With λ_F =Fbelt@dmax/Fbelt_max

Deq LIN = 6.6*USBF(kN) + 0.84*(Rodpot(mm) - 3.7*USBF(kN))

Then Deq can be written as a linear combination of Fshoulder and Drodpot.

Deq LIN = 3.5*USBF(kN) + 0.84*Rodpot(mm)

The smaller the shoulder belt force is, the higher the rodpot deflection can be for the same risk.

This simplified version of the Deq is illustrated in Figure 10. It gives the iso-Deq in terms of Rodpot deflection as a function of the Shoulder belt force.
The airbag limit (in black) is the limit under which the rodpot does not measure properly the deflection. This figure illustrates the fact that the DEQ IRC has nothing to do with the Rodpot IRC, because the Deq accounts for the maximum deflection and generally not the rodpot. For instance for a belt-only restraint, 5kN of Shoulder belt force generate a rodpot deflection of 22 mm as a mean. In that case, the Deq is equal to 36, which is much higher than the rodpot deflection.

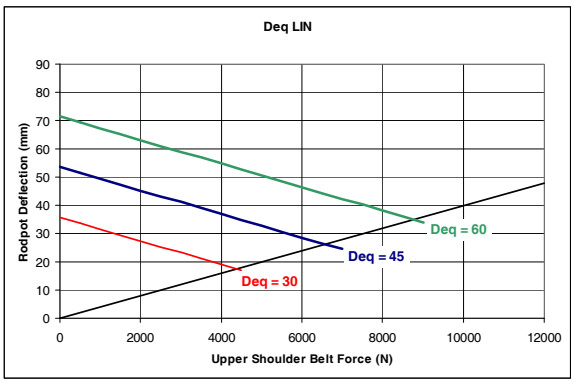

Figure 10. Iso-Deq curves.

This simplified version of Deq allows getting a good approximation of the final result, within a margin of generally 1 or 2 points, sometimes up to 5 points of Deq. This is the reason why a more sophisticated routine for the Deq calculation is needed, which takes into account the viscous component of the chest.

Deq versus Deflection

The Rodpot deflection is known to be a criterion which depends on the restraining system. An injury risk curve based on the rodpot is therefore only valid for a given contribution of the belt and the airbag. Mertz et al. (2003) proposed a curve for distributed loading and another one for belt loading. Laituri et al. (2005) mixed all kind of loading systems and therefore proposed a curve for an undefined balance of belt and airbag. Consequently, the same rodpot deflection gives different risks, depending on the belt force (Figure 11):

- 5% Laituri goes from 0.3% to 15% risk
- 50% Laituri goes from 15% to 90% risk

When looking at some equivalence between the rodpot and the Deq, it is then necessary to define at which shoulder belt force the risk should be equal.

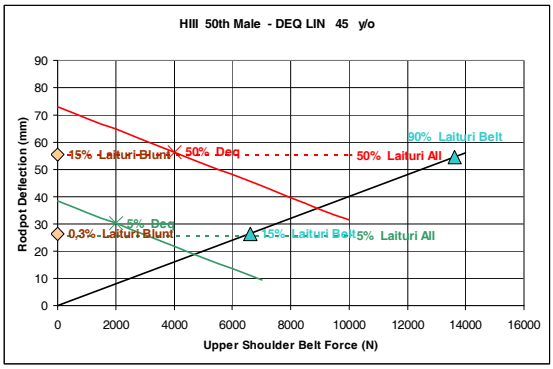

Figure 11. Risks associated with Rodpot deflection compared to Deq.

Deq limits

The risks used to calculate Deq limits should be calculated in order to promote load limitation and give enough room for airbag loading.

A strategy should be to define the upper performance limit for the 5th female and the lower performance limit for the 50% male, the existing limits as defined by EuroNCAP (Rodpot @ 18mm for the 5% female as an upper limit and 50mm for the 50th male as a lower limit) being defined for instance at 4.5kN and 5.5 kN respectively (5.5kN scaled for the small female gives 4.5 kN). This would mean that systems at 4.5 kN of load limitation would be evaluated identically with the rodpot and the Deq for the small female and systems at 5.5 kN Load limitation would be evaluated identically with the rodpot and the Deq for the mid male. Then lower load limitation would be encouraged while higher load limitation would be discouraged. This would be an improvement for the elderly.

Following this strategy, the limits for Deq at 45 y/o would be set at 10% and 50% of risk.

The upper limit (10% risk @ 45 y/o for a 5th female) would correspond to 37% risk at 65 y/o for a 5th female.

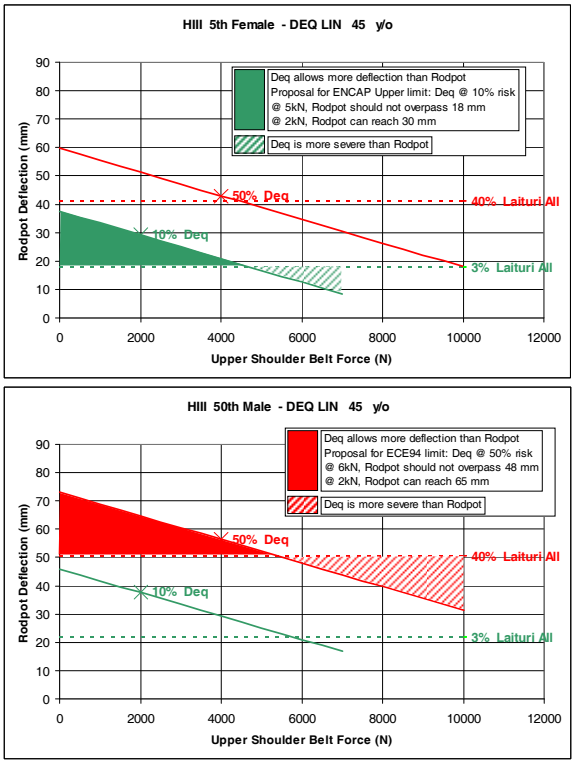

Figure 12. Deq limits compared to Rodpot limits.

CONCLUSIONS

What we know

- The only proven effect on the injury outcome is the belt load limitation, especially for elderly
- The limitation is made possible by means of the combination with an airbag

What DEQ is NOT

- A universal criterion (apply only to belt and airbag systems)
- A perfect criterion (does not solve all HIII concerns)

What is DEQ

- A way to better balance belt and airbag contributions
  - Lower belt loads
  - Higher bag loads, but limited
- The only criterion on HIII that take into account the effect of belt load limitation
- An interim solution, waiting for THOR dummy with associated criteria

REFERENCES

Abbreviated Injury Scale 2005, Editors: Gennarelli, T.A., Wodzin, E., Association for the Advancement of Automotive Medecine.

Foret-Bruno, J-Y, Trosseille, X, Le Coz,, J-Y, Bendjellal, F, Steyer, C. (1998). Thoracic Injury Risk in Frontal Car Crashes with Occupant Restrained with Belt Load Limiter. SAE Paper No.983166, Proceedings of 42nd Stapp Car Crash Conference.

Forman, J., Lessley, D., Shaw, G., Evan, J., Kent, R., Rouhana, S.W., Prasad, P. (2006) Thoracic Response of Belted PMHS, the Hybrid III, and the THOR-NT Mid-Sized Male Surrogates in Low Speed, Frontal Crashes. Stapp Car Crash Journal, Vol. 50, pp. 191-215.

Forman, J., Lopez-Valdes, F., Lessley, D., Kindig, M., Kent, R. (2009) Rear Seat Occupant Safety: An Investigation of a Progressive Force-Limiting, Pretensioning 3-point Belt System Using Adult PMHS in Frontal Sled Tests, Stapp Car Crash Journal, Vol. 53, pp 49-74

Humos (2000) Work Package 4: Experimentation on PMHS, PMHS Tests and Analysis

Kent, R., Bolton, J., Crandall, J., Prasad, P., Nusholtz, G., Mertz, H., Kallieris, D. (2001) Restrained Hybrid III Dummy-Based Criteria For Thoracic Hard-Tissue Injury Prediction, Proc. 2001 International IRCOBI Conference on the Biomechanics of Impact, pp215-232. IRCOBI, Bron, France.

Kent, R., Lessley, D., Shaw, G., and Crandall, J. (2003) The utility of H-III and THOR chest deflection for discriminating between standard and force-limiting belt systems. Stapp Car Crash Journal 47: 267-297.

Kroell, C.K., Schneider, D.C, Nahum, A.M. (1971) Impact Tolerance and Response of the Human Thorax. Proc. 15th Stapp Car Crash Conference, pp84-134. Society of Automotive Engineers, Warrendale, PA.

Kroell, C.K., Schneider, D.C, Nahum, A.M. (1974) Impact Tolerance and Response of the Human Thorax II. Proc. 18th Stapp Car Crash Conference, pp383-412. Society of Automotive Engineers, Warrendale, PA.

Laituri, T.R., Prasad, P., Sullivan, K., Frankstein, M., Thomas, R.S. (2005) Derivation and Evaluation of a Provisionel, Age-Dependant, AIS3+ Thoracic Risk Curve for Belted Adults in Frontal Impacts, SAE paper 2005-01-0297.

Lebarbé, M., Potier, P., Baudrit, P., Petit, P., Trosseille, X., Vallancien, G. (2005) Thoracic Injury Investigation using PMHS in Frontal Airbag Out-of-Position Situations, Stapp Car Crash Journal, Vol. 49, pp. 323-342.

Mertz, H.J., Irwin, A.L., Prasad, P. (2003) Biomechanical and Scaling Bases for Frontal and Side Impact Injury Assessment Reference Values, Stapp Car Crash Journal, Vol. 47, pp. 155-188.

NHTSA Biomechanics Test Database: http://www-nrd.nhtsa.dot.gov/database/aspx/biodb/querytesttable.aspx

Petitjean, A., Baudrit, P., Trosseille, X. (2003) Thoracic injury criterion for frontal crash applicable to all restraint systems, Stapp Car Crash Journal, Vol. 47

Petitjean, A., Trosseille, X. (2011) Statistical simulations to evaluate the methods of the construction of injury risk curves. Stapp Car Crash Journal, Vol. 55

Song, E. Lecuyer, E., Trosseille, X. (2011) Development of injury criteria for frontal impact using a human body FE model, ESV paper number 11-0330

Table A 1.
PMHS impactor tests (Kroell et al. (1971, 1974)) used in the 2012 update for the construction of the injury risk curve for the distributed deflection

PMHS test number	Chest compression	PMHS age	Rib fractures	Impactor mass (kg)	Impactor velocity (m/s)	Hybrid III rodpot deflection (mm)
12FF	0.42	67	22	22.86	7.24	83.2
13FM	0.44	81	21	22.86	7.42	88.7
14FF	0.44	76	7	22.86	7.33	86.6
15FM	0.39	80	13	23.59	6.88	77.0
18FM	0.42	78	14	23.59	6.70	82.7
19FM	0.38	19	1	23.59	6.70	72.9
20FM	0.35	29	0	23.59	6.70	67.2
21FF	0.56	45	18	23.59	6.84	115.5
22FM	0.42	72	17	23.59	6.70	82.5
23FF	0.43	58	23	19.50	7.73	85.0
31FM	0.46	51	14	23.04	10.19	92.1
32FM	0.46	75	20	22.86	9.92	91.8
34FM	0.45	64	13	18.96	8.22	89.6
36FM	0.35	52	7	18.96	7.20	66.2
37FM	0.33	48	9	22.86	9.83	62.0
42FM	0.32	61	0	22.86	4.87	60.5
45FM	0.32	64	10	23.00	5.05	59.1
46FM	0.31	46	0	19.28	7.33	58.0
53FM	0.26	75	3	22.95	5.23	45.9
54FF	0.41	49	7	19.55	9.92	80.1
55FF	0.41	46	8	19.55	9.92	80.4
60FM	0.27	66	9	22.95	4.34	48.6
63FM	0.37	53	4	23.00	6.93	72.2
64FM	0.37	72	6	23.00	6.93	72.0

Table A 2.
PMHS tests performed with different restraints used of the validation of the Deq in the 2012 update

PMHS test number	Source	HIII test number	Restraint type	PMHS age	Number of rib fractures	USBF (N)	Defl (mm)	Deq LIN
1386	Forman et al. (2009)	1316, 1317, 1318	Lap and Shoulder Belt, Dual stage load limiter	67	12	4446	22.9	36.1
1387	Forman et al. (2009)		Lap and Shoulder Belt, Dual stage load limiter	69	2	4446	22.9	36.1
1389	Forman et al. (2009)		Lap and Shoulder Belt, Dual stage load limiter	72	17	4446	22.9	36.1
Humos 3	Humos (2000)	Dummy 3, Dummy 4	Lap and Shoulder Belt, shoulder load limiter	58	19	4457	15.6	37.0
Humos 4	Humos (2000)		Lap and Shoulder Belt, shoulder load limiter	70	9	4457	15.6	37.0
Humos 1	Humos (2000)	Dummy 1, Dummy 2	Lap and Shoulder Belt, shoulder load limiter	76	26	6126	25.9	48.7
Humos 2	Humos (2000)		Lap and Shoulder Belt, shoulder load	66	24	6126	25.9	48.7

PMHS test number	Source	HIII test number	Restraint type	PMHS age	Number of rib fractures	USBF (N)	Defl (mm)	Deq LIN
			limiter					
C17	Petitjean et al. (2002)	C11, C12, C19, C21	Lap and Shoulder Belt, shoulder load limiter	76	25	6557	20.6	48.6
C23	Petitjean et al. (2002)		Lap and Shoulder Belt, shoulder load limiter	75	18	6557	20.6	48.6
1262	Forman et al. (2009)	1210, 1211, 1212	Lap and Shoulder belt	51	13	8774	32.8	59.5
1263	Forman et al. (2009)		Lap and Shoulder belt	57	29	8774	32.8	59.5
1264	Forman et al. (2009)		Lap and Shoulder belt	57	13	8774	32.8	59.5
102	Kent et al. (2001)	101	Shoulder belt	60	19	9405	56.7	81.8
9013	Kent et al. (2001)	9002D	Lap and Shoulder belt	34	0	9661	28.3	65.7
114	Kent et al. (2001)	112	Shoulder belt	60	27	10141	75.3	102.3
227	Kent et al. (2001)	226	Shoulder belt	53	12	11747	63.4	95.8
228	Kent et al. (2001)		Shoulder belt	47	16	11747	63.4	95.8
1094	Forman et al. (2006)	1023, 1024, 1025	Lap and Shoulder belt	49	0	4722	23.3	36.0
1095	Forman et al. (2006)		Lap and Shoulder belt	44	0	4722	23.3	36.0
1096	Forman et al. (2006)		Lap and Shoulder belt	39	0	4722	23.3	36.0
1110	Forman et al. (2006)	1108, 1109	Lap and Shoulder belt	44	0	6262	30.3	48.3
577P	Kent et al. (2001)	571P, 572P, 576P	Lap and Shoulder Belt, shoulder load limiter, airbag	57	0	5318	29.2	45.7
580P	Kent et al. (2001)		Lap and Shoulder Belt, shoulder load limiter, airbag	57	0	5318	29.2	45.7
665P	Kent et al. (2001)	663P, 664P	Lap and Shoulder Belt, airbag	55	3	7979	39.8	63.3
666P	Kent et al. (2001)		Lap and Shoulder Belt, airbag	69	3	7979	39.8	63.3
667P	Kent et al. (2001)		Lap and Shoulder Belt, airbag	59	13	7979	39.8	63.3
668P	Kent et al. (2001)		Lap and Shoulder Belt, airbag	54	23	7979	39.8	63.3
C05	Petitjean et al. (2002)	C03, C13, C18, C20	Lap and Shoulder Belt, shoulder load limiter, airbag	78	6	3988	25.0	35.9
C22	Petitjean et al. (2002)		Lap and Shoulder Belt, shoulder load limiter, airbag	81	19	3988	25.0	35.9
651P	Kent et al. (2001)	648P, 649P	Lap belt, airbag	70	0	0	19.4	16.3
652P	Kent et al. (2001)		Lap belt, airbag	46	0	0	19.4	16.3
9014C	Kent et al. (2001)	9003D	Airbag	31	0	0	12.6	10.6
9207C	Kent et al. (2001)		Airbag	25	0	0	12.6	10.6
9212C	Kent et al. (2001)		Airbag	38	0	0	12.6	10.6
554-M13-PCH1597	Lebarbé et al. (2005)	PCH1640, PCH1641	Airbag	76	15	0	45.2	38.0
555-M13-PCH1598	Lebarbé et al. (2005)		Airbag	67	15	0	45.2	38.0
559-M78-PCH1624	Lebarbé et al. (2005)	PCH1628, PCH1629	Airbag	73	11	0	37.3	31.3
561-M78-PCH1658	Lebarbé et al. (2005)		Airbag	72	0	0	37.3	31.3
594-M78-SEB144	Lebarbé et al. (2005)		Airbag	78	3	0	37.3	31.3
560-M128-PCH1625	Lebarbé et al. (2005)	PCH1627, PCH1643	Airbag	74	0	0	27.7	23.2

Table A 3.
Hybrid III 5th belt tests of the sample used to determine the relation between the belt load and the sternal deflection

HIII 5th test number	Source of the tests	Type of belt restraint	Maximal upper shoulder belt load (N)	Optimised stiffness (N/mm)	Optimised damping (N,s/mm)	Upper shoulder belt load at the time of maximal rodpot deflection (N)
UVA1218	NHTSA b09319	Lap and shoulder	4429	166	3,0	3823
UVA1219	NHTSA b09320		4794	158	2,6	4383
UVA1220	NHTSA b09321		4581	155	2,7	3880
UVA1221	NHTSA b09322		7419	166	2,0	6072
UVA1222	NHTSA b09323		7429	196	2,4	6515
UVA1223	NHTSA b09324		8089	201	2,5	7187
UVA1297	NHTSA b10008	Lap and Shoulder, Shoulder Dual Force limiter	2738	177	1,9	2167
UVA1298	NHTSA b10009		2652	186	2,1	2306
UVA1299	NHTSA b10010		2644	168	1,4	2533
UVA1300	NHTSA b10011		3744	212	1,8	3740
UVA1301	NHTSA b10012		4124	180	1,8	4028
UVA1302	NHTSA b10013		3859	192	1,9	3800

Deq calculation process

For the belt deflection calculation

- the stiffness and damping are calculated as follow:
  - k1 = 135.78 – 0.0018*Max_Upper_Shoulder_Belt_Force
  - c1 = 0.0185*k1 – 0.2357
- The belt deflection (Dbelt) is calculated by solving the differential equation
  - USBF = k1*Dbelt + c1*dDbelt/dt

For the airbag deflection calculation

- the initial stiffness and damping are calculated as follow:
  - ki = 238.14 – 0.0023* Max_Upper_Shoulder_Belt_Force
  - ci = 0.0185*k1-0.2357
- The belt deflection is calculated by solving the differential equation
  - USBF = ki*Dbelt + ci*dDbelt/dt
- The airbag deflection (Defl_airbag) is calculated by substracting the belt deflection from the rodpot deflection
- Then the stiffness is increased until the difference between the localized calculated deflection and the measured sternal deflection is less than 5mm at any time,

DEQ is calculated as follows:

- DEQ LIN = Defl_belt + (Fn*Defl_airbag)
- With Fn =0.84

The risks for M50 and F05 are calculated with the following formulas:

- Risk DEQ M50 = (1-exp(-exp((log(DEQ_max)-intercept-fage*age)/scale)))*100
- Risk DEQ F05 = (1-exp(-exp((log(DEQ_max/F05)-intercept-fage*age)/scale)))*100
  - With scale=0.246
  - intercept=4.9908
  - fage=-0.0174
  - F05=0.83

MECHANISM OF REDUCING THORACIC DEFLECTIONS AND RIB STRAINS USING SUPPLEMENTAL SHOULDER BELTS DURING FRONTAL IMPACTS

Ola Bostrom
Autoliv Research
Sweden
Yasuki Motozawa
Honda R&D
Japan
Shinsuke Oda
Autoliv
Japan
Yuichi Ito
Honda R&D
Japan
Krystoffer Mroz
Autoliv Research
Sweden

Paper number 13-0372

ABSTRACT

With an ageing population with increased needs of mobility, special attention to the safety of senior car occupants is becoming more important. As seniors in fatal crashes primarily die of chest injuries there is need of understanding how to reduce the risk of rib fractures. Recently new types of belts have been introduced on the market including inflatable and supplemental.

It has been suggested, one key to protect more ribs in frontal impacts is by optimizing the force distribution. In this study the role of kinematics or more specifically the orientation of the torso in relation to the belt loading, is evaluated.

The aim of this paper was to further understand the protection role of a supplementary belt. The hypothesis was that the upper body rotation, the twisting of the torso is critical in saving ribs. We conducted simulated frontal tests in three configurations by using a human FE model (THUMS) representative of an American 50 percentile male adult. The three configurations were a reference 4 kN three point belt and a driver airbag, an added 1 kN two point shoulder belt restraining the shoulder not restrained by the three point belt (the single) and two added 0.5 kN two point belts restraining each shoulder (the double).We compared the kinematics of the upper torso with the chest deflections and rib strains.

Adding a 1 kN belt load, single or double, resulted in reduced chest deflection and excursion as well as rib strain. The single belt as opposed to the double reduced the upper body rotation considerably. The greatest chest deflection reductions were found at the lower part of the chest for the single belt and at the upper for the double.

As a conclusion, the kinematics of the occupant may contribute to the loading on the chest. The paper is relevant for understanding how to optimize belt systems for minimal occupant loading and excursion.

INTRODUCTION

The three point belt is doubtless a practical way to distribute the restraining forces on the occupant body during a frontal impact. Not only is the usage rate high, 97.5% in European cars with seat belt reminders according to Lie et al [2008], the overall lifesaving effectiveness is also high (61% according to Cummings et al [2003]). Still the performance can be enhanced. While belt load limiters and pretensioners have become more or less a standard for the front seats, four-point belts in the form of a V have been suggested and evaluated by Rouhana et al [2003]. Moreover inflatable belts have been introduced in Ford Explorer, Lexus LFA and this year in Mercedes S-class ; although they are intended to enhance the performance in conventional three-points seatbelts geometry, their implementation is currently limited due to the complexity of the system. Also, four point belts in the form of a supplementary belt have been introduced in the Renault Twizy. The extra belt sometimes called the rucksack belt was first

described by Bostrom et al [2008]. The belt was shown to have a considerable protective effect in far side impacts and rollovers.

The protective effect of belt force limiting and pretensioning, V-shaped four point belt and inflatable shoulder part of the belt have been proved by means of PHMS in particular types of frontal impacts [Forman et al 2009, Rouhana et al 2003]. It has been suggested that by distributing the forces on a larger area and engaging additional bony structures such as the other clavicle, the load on the ribs is reduced in general.

Rib fractures after a car crash are not necessarily life threatening. However, the situation for seniors (elderly) is different compared to the younger. When young people tend to die from head injuries seniors tend to die from chest injuries [Kent et al 2005]. According to a study by Kent et al [2008] seniors ending up at a hospital after a car crash may die from only a few rib fractures. As the ageing population and requirements of mobility is increasing around the world, rib fracture countermeasures for seniors are becoming more and more important.

In this paper a new hypothesis of rib fracture reduction, the twisting theory, is suggested and tested in a simplified way. During a frontal impact the thorax is twisting and thereby changing the load distribution and the direction. The twisting hypothesis can be formulated such that reduction of twisting is beneficial regarding braking of ribs.

The aim of this paper was to further understand the protection role of a supplementary belt. More specifically, the aim was to understand the importance of changed kinematics versus changed force distribution. The method used was numerical human body model simulations.

METHOD

The set-up of the simulations is described in detail by Mroz et al [2010]. The crash pulse used was a 56km/h full frontal (USNCAP 2006 Honda Civic). The mid-sized male human body model THUMS [Iwamoto et al. 2002] was used as the occupant on the driver side of a generic vehicle interior model of typical mid-sized sedan. For this study the material model of the THUMS rib cortical bone was simplified by using an elasto-plastic material model without any fracture failure criterion and strain-rate dependency. The total number of elements for this modified version of THUMS was app. 158000.

The occupant was, as a reference, restrained by a three point pretensioned belt with a 4 kN load limiter and a symmetric driver airbag. In addition to the 1) reference configuration simulations were performed with 2) a supplemental two-point belt with a 1 kN load limiting and 3) two symmetrical two-point belts with each 0,5 kN load limiting levels. The supplemental belts were not pretensioned.

Torso twisting was analyzed by calculating the rotation of a thought line between the shoulder blades, see Figure 1.

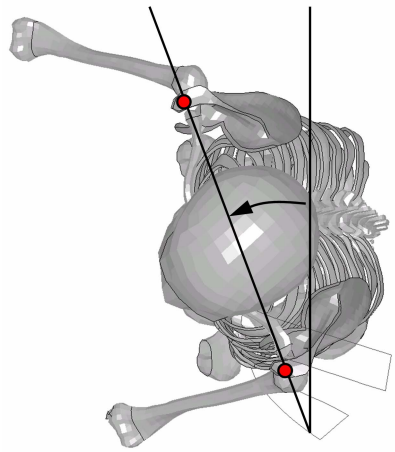

Figure 1 – Twisting of the torso was analyzed by calculating the rotation of a line through the shoulder blades.

To evaluate the risk of rib fractures, chest deflections and rib strains were chosen as measurements. Chest deflections were measured at mid-sternum and at left and right hand side of the ribs 3 to 7. See Figure 2. Regarding rib strain, the strain levels were divided into the discrete values of 0, 0.5, 1, 1.5, 2% and so on. If at least one element on a rib exceeded say 1% but not 1.5% the rib was considered as a rib with rib strain 1%.

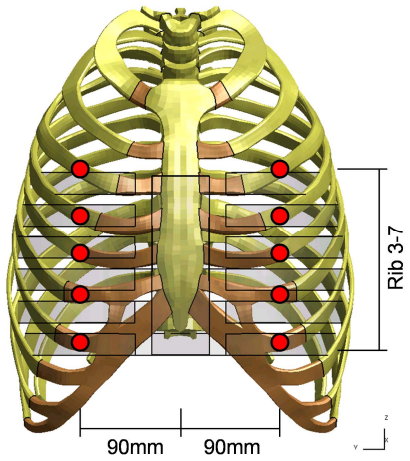

Figure 2. The location of the 11 points where chest deflections were evaluated.

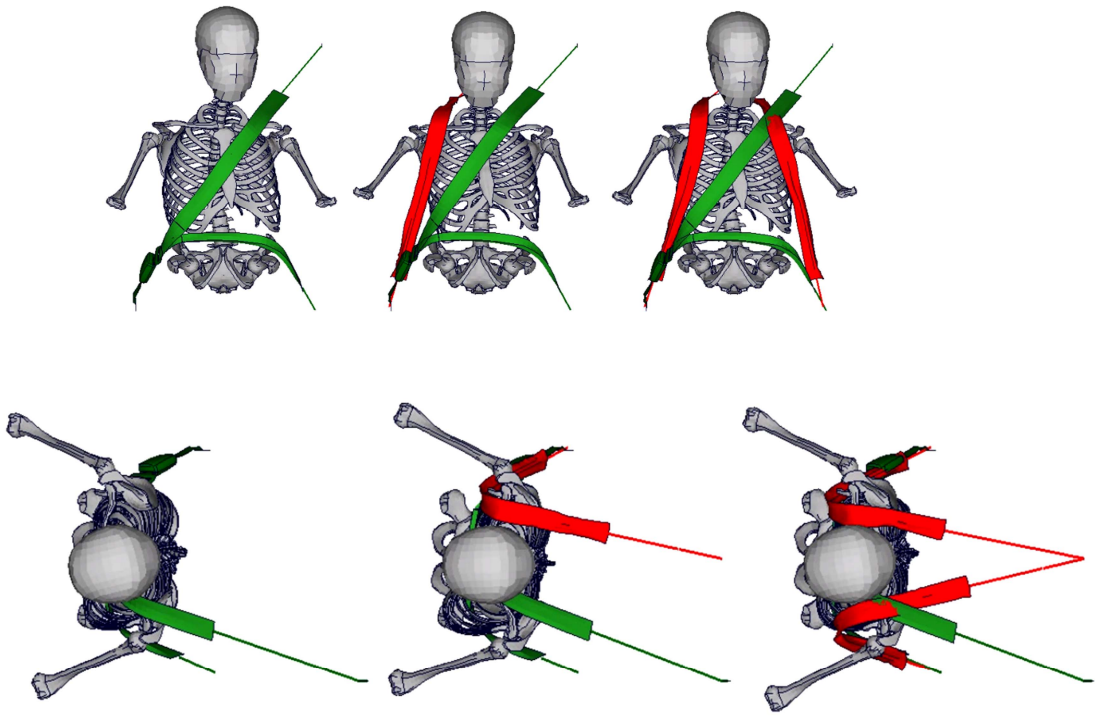

Figure 3. Front and top view, 80 ms into a 56km/h full frontal frontal impact for the three belt configurations.

RESULTS

Adding 1 kN of belt load resulted in 36 (single) and 35 (double) mm less peak chest excursion (279 compared to 242 and 243 mm). In addition the upper body rotation (the twisting), the mid sternum chest deflection and the rib strain decreased.

The top and side views 80 ms into the crash are shown in Figure 3.

The upper body rotation, the torso twisting, during the impact is shown in Figure 4.

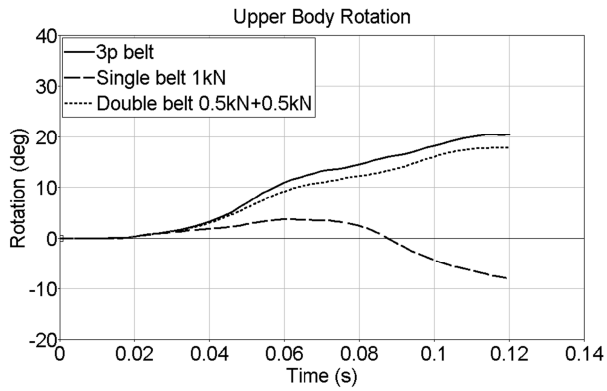

Figure 4 The upper body rotation, or torso twisting, for the three configurations during the impact.

The mid-sternum deflections are shown in Figure 5. The lowest deflections were obtained for the single followed by the double extra belts.

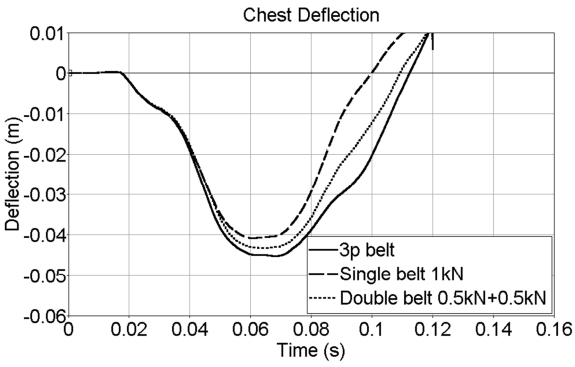

Figure 5. Mid sternum chest deflection for the three configurations.

The distribution of the peak chest deflections for the 5 left and right locations are shown in Figure 6. The deflections follow the belt route with the highest deflections in the lower part of the thorax. The greatest reduction was found at rib level 7 for the single belt and at rib level 3 for the double belt.

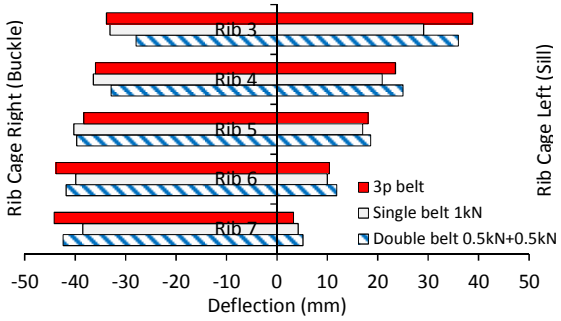

Figure 6. Distribution of the chest deflection at the 5 right and 5 left locations defined in Figure 2.

The strain distribution is shown in Figure 7. For levels up to 3% the added belts produced the smallest strains.

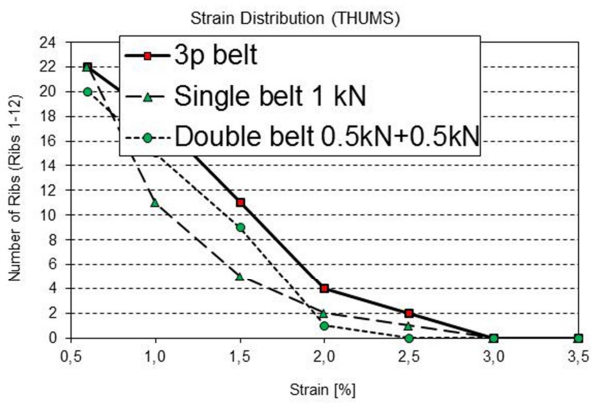

Figure 7. Number of ribs with the discrete values of 0, 0.5%, 1% and so on for the three configurations.

DISCUSSION

Previous studies have shown that blunt loading is more effective than belt loading. It has been explained as an effect of distribution i.e. reduction of pressure on the thorax. Recently a supplemental shoulder belt system was proposed to enhance chest protection. In the present study, we focused on the mechanism of its effect. Major limitations are the unpractical (however theoretically ideal) usage of the double belt configuration as well as the usage of chest deflection and rib strain as indicators of rib fractures.

According to the results of this paper, reducing the twisting of the torso by restraining the shoulder not directly restrained by the three point belt, does reduce chest excursion and deflection and rib strain. By distributing the extra load of 1 kN on both shoulders (0.5 kN on each) the twisting is more or less the same as without extra belts and still the chest excursion and deflection and rib strain is reduced. That is reducing the twisting seems related to reduction of chest load (in terms of deflection and rib strain) however not necessarily.

In a recent paper, Forman et al [2012] described a causal probabilistic framework to predict rib fracture risk based on strains observed in human-body FE models. Distribution of crash speeds, critical rib strain levels and known age dependent risks of dying due to rib fractures were used in order to evaluate differences between restraint systems. This framework, although beneficial for the present purpose, was not used in this study.

In the present study the ribs of the THUMS were not allowed to fracture. The greatest reduction, thanks to the extra belts, occurred for levels of around 1.5%. Five ribs had strain levels above 1.5% for the single belt. The double belt reduced the chest deflection in the upper part of the thorax while the single in the lower part. In order to further understand the role of the twisting a fracture model need to be incorporated.

CONCLUSION

The consequence of adding two types of extra belt, the single and the double, to a human body model (THUMS) restrained by a 4 kN three point belt and a driver airbag in a 56 km/h full frontal crash test was evaluated in this study. The two types of extra belts were designed to distribute the force on the chest differently. Adding a 1 kN belt load, single or double, resulted in lower chest deflection and excursion as well as rib strain. The single belt as opposed to the double reduced the upper body rotation considerably. The greatest chest deflection

reductions were found at the lower part of the chest for the single belt and at the upper for the double.

As a conclusion, the kinematics of the occupant may contribute to the load of the chest. The paper is relevant for understanding how to optimize belt systems for minimal occupant loading and excursion.

ACKNOWLEDGEMENT

The authors are thankful to Associate Professor Bengt Pipkorn at Autoliv Research for the discussions related to this paper.

REFERENCES

Bostrom, O., H. C. Gabler, K. Digges, B. Fildes and C.Sunnevang (2008). "Injury reduction opportunities of far side impact countermeasures." Annu Proc Assoc Adv Automot Med 52: 289-300.

Cummings P, Wells JD, Rivara FP (2003) Estimating seat belt effectiveness using matched-pair cohort methods, Accident Anal Prev. Jan;35(1):143-9

Forman, J., Lopez-Valdes, F., Lessley, D., Kindig, M., Kent, R., Ridella, S., Bostrom, O., (2009). Rear seat occupant safety: an investigation of a progressive force-limiting, pretensioning 3-point belt system using adult PMHS in frontal sled tests. Stapp Car Crash Journal 53**,** 49-74.'

Forman J, Kent R, Mroz K, Pipkorn B, Bostrom O, Segui-Gomez M Predicting rib fracture risk with whole-body finite element models: Development and preliminary evaluation of a probabilistic analytical framework (2012) Association for the advancements of Automotive Medicine October, 56: 109-124

Iwamoto, M., Kisanuki, Y., Watanabe, I., Furusu, K., Miki, K., and Hasegawa, J. (2002) Development of a Finite Element Model of the Total Human Model for Safety (THUMS) and Application to Injury Reconstruction", IRCOBI.

Kent, R., Henary, B., Matsuoka, F., (2005). On the fatal crash experience of older drivers. Ann Adv Automot Med.

Kent, R., Woods, W., Bostrom, O., (2008). Fatality risk and the presence of rib fractures. Annals of Advances in Automotive Medicine 53, 73-84.

Lie A, Krafft M, Kullgren A, Tingvall C (2008) Intelligent seat belt reminders-do they change driver seat belt use in Europe? Traffic Injury Orev Oct 9 (5): 446-9

Mroz K, Bostrom O, Pipkorn B, Wisman J, Brolin K, “Comparison of Hybrid III and human body models in evaluating thoracic response for various seat belt and airbag loading conditions”, Ircobi2010.

Rouhana SW, Bedewi PG, Kankanala SV, Prasad P, Zwolinski JJ, Meduvsky AG, Rupp JD, Jeffreys TA, Schneider LW (2003) Biomechanics of 4-point seat belt systems in frontal impacts Stapp Car Crash Journal 2003; 47:367-99.

.